



ARALIYA MOSLEH

**AVALIAÇÃO DA VULNERABILIDADE SÍSMICA DE
PONTES RODOVIÁRIAS EXISTENTES DE BETÃO
ARMADO NO IRÃO**

**SEISMIC VULNERABILITY ASSESSMENT OF
EXISTING CONCRETE HIGHWAY IRANIAN BRIDGES**



ARALIYA MOSLEH

**AVALIAÇÃO DA VULNERABILIDADE SÍSMICA DE
PONTES RODOVIÁRIAS EXISTENTES DE BETÃO
ARMADO NO IRÃO**

This report is submitted to the rectory, University of Aveiro, as a PhD project research report, under the scientific supervision of Humberto Varum, Full Professor at the Civil Engineering Department of the University of Porto, co-supervision of José Jara, Full Professor at the Structural Engineering Department of the Universidad Michoacana San Nicolas de Hidalgo, Morelia, Mexico and Mehran Razzaghi, Assistant Professor at the Faculty of Civil Engineering, Islamic Azad University, Qazvin, Iran.

I wish to dedicate this thesis to my son Alireza. His enduring love and unconditional support and encouragement have been the real inspiration that I always felt during the course of this study.

I would like to thank my mother, who was an integral ear during the entire process and for her unwavering support in this endeavor.

You are both an inspiration to me on daily basis to be more than what I was the day before. No road is void of stumbling block and pot holes, but you always have been there to pull me up whenever I fell. I could not have completed this journey without either of you.

o júri

presidente

Prof. Doutor João Carlos de Oliveira Matias
professor catedrático da Universidade de Aveiro

Prof. Doutor Humberto Salazar Amorim Varum
professor catedrático da Faculdade de Engenharia da Universidade do Porto

Prof. Doutor Rui Manuel de Menezes e Carneiro de Barros
professor Associado com Agregação da Faculdade de Engenharia da Universidade do Porto

Prof. Doutor Miguel Nuno Lobato de Sousa Monteiro de Morais
Professor Auxilia Faculdade de Engenharia da Universidade de Aveiro

Prof. Doutor Hugo Filipe Pinheiro Rodrigues
professor Adjunto Escola Superior de Tecnologia e Gestão de Leiria Instituto Politécnico de Leiria

Prof. Doutor Pedro da Silva Delgado
professor Adjunto Escola Superior de Tecnologia e Gestão de Leiria Instituto Politécnico de Viana do Castelo

agradecimentos/ acknowledgements

At the end of every journey there lies a road behind, built and defined by those around us. My graduate tenure at Aveiro university has been no different. This has been a positive experience upon which I will often reflect with great fondness. I wish to express my sincere gratitude to the following persons, who have contributed to make this work possible and helped me growing.

I would like to express my sincere appreciation to my advisors, Professor Humberto Varum for his guidance, encouragement and continuous support through the course of this work. The extensive knowledge, vision, and creative thinking of Professor Varum have been the source of inspiration for me throughout this work.

I would like to express my sincere thanks and gratitude to my Co-supervisors Professor José Jara and Dr. Mehran Razzaghi who made the otherwise impossible task an easy one by providing me valuable materials, guidance and suggestions and thus built stairs of hope and confidence by which I was able to complete this research work.

I would also like to thank my thesis committee Professor Humberto Varum, Professor Rui Barros, Professor Miguel Morais, Professor Hugo Rodrigues and Professor Pedro Delgado for help and encouragement.

My sincere thanks also goes to Professor Steffen Marburg and Dr. Kheirolla Sepahvand, who provided me an opportunity to join their research group, access to the research facilities and also who made it possible for me to obtain a grant from the Deutscher Akademischer Austausch Dienst (DAAD). Without their precious support it would not be possible to conduct the last part of this research (chapter-7).

I would like to thank to Hugo Rodrigues who provided the support and equipment I have needed to produce and complete my thesis.

Finally, I would like to thank to all my colleagues from the PhD room in University of Aveiro for their suggestions and support.

palavras-chave

Curvas de fragilidade, Vulnerabilidade sísmica, Pontes de betão armado no Irão, Análise não-linear

resumo

Sismos recentes mostram que as pontes são uma das infraestruturas mais vulneráveis dos sistemas de transporte rodoviário, e comprovam a necessidade de avaliação da vulnerabilidade deste tipo de estruturas, especialmente as projetadas segundo a filosofia patente nos códigos antigos. A avaliação da vulnerabilidade sísmica das pontes rodoviárias localizadas em áreas de elevada perigosidade sísmica e a estimativa do seu desempenho sísmico representam tarefas importantes para a segurança dos sistemas de transporte.

Neste contexto, esta investigação tem como objetivo estudar a vulnerabilidade sísmica das pontes de betão armado existentes no Irão. O trabalho foca-se principalmente nas seguintes tarefas: desenvolvimento de análises estatísticas, classificação das pontes mais comuns no Irão, seleção da ação sísmica representativa, definição de estados de dano, estudo dos efeitos das práticas de construção e, finalmente, análise de curvas de fragilidade para avaliar a vulnerabilidade sísmica de pontes tipo representativas das obras existentes no Irão.

O primeiro capítulo resume trabalhos no domínio da caracterização da sismicidade na área geográfica em estudo, em função das diferentes placas tectónicas e da distribuição das zonas de rotura prováveis, com base em informação recolhida em sismos passados e uma revisão geral dos estudos anteriores e a pesquisa bibliográfica, nomeadamente em termos de curvas de fragilidade para as pontes com base em diferentes abordagens. O Capítulo 2 descreve os tipos de ponte mais comuns existentes no Irão e classifica-as de acordo com as suas características estruturais primárias.

Capítulo 3 explicar os modelos analíticos não lineares 3-D das estruturas de pontes amostra usando modelos analíticos detalhados para os seus componentes. O Capítulo 4 é dedicado à seleção de um conjunto de registos sísmicos reais que sejam representativos das diferentes fontes sísmicas. O Capítulo 5 é dedicado à definição de estados limite de dano. Neste capítulo, foi realizada uma revisão das propostas para a avaliação dos estados limite de dano disponíveis na literatura. Para isso, diferentes tipos de incertezas associadas a parâmetros que influenciam o comportamento das pontes foram consideradas, nomeadamente em termos de seção e altura dos pilares, presença da emenda da armadura longitudinal e vão. Além disso, a influência das propriedades dos materiais com base na resistência à compressão do betão e da resistência do aço são analisadas e os resultados são tratados em termos de curvas de fragilidade para cada classe de pontes considerada. O Capítulo 6 apresenta os principais resultados da análise sísmica tridimensional realizada sobre vários casos de estudo. Capítulos 7 indicam o estudo da resposta estocástica de pontes de betão considerando a incerteza na rigidez de rolamento e de encosto. Finalmente, no capítulo 8, as principais conclusões são tiradas a partir do trabalho desenvolvido no âmbito do presente estudo.

keywords

Fragility curves, Seismic vulnerability, Iranian Concrete bridges, Nonlinear analysis

abstract

Past earthquakes occurred in seismically active areas around the world show that bridges are one of the most vulnerable components of the highway transportation systems, and evidence the need to study the vulnerability of bridges, especially the ones designed with the old codes. Thus, the seismic vulnerability assessment of the highway bridges located in high seismic hazard areas and the assessment of the bridges' performance under seismic demands play an important role for the safety of transportation systems.

In this context, this research aimed to study the seismic vulnerability of existing old concrete bridges in Iran. The research work was mainly focused on the following tasks: identification of the most common bridges in Iran, ground motion selection, damage state definition, real construction practices and finally the analysis of fragility curves to assess the seismic vulnerability of common bridges in Iran.

The first chapter presents the study of seismicity in a geographical area of interest for this study, covered by different tectonic plates and distribution of probable rupture zones of past earthquakes and the general overview of previous studies and a literature survey developed to generate the bridge fragility curves based on different approaches. Chapter 2 describes the most common existing ordinary highway bridges and classifies them according to their primary structural characteristics. Chapter 3 explains the 3-D nonlinear analytical models of the sample bridge structures using detailed analytical models for its components. Chapter 4 is devoted to the procedure followed in the selection of earthquake ground motion records that are representative of the different seismic sources, based on ground motion intensity. Chapter 5 addresses aspects related with the definition of damage limit states. In this chapter, a review of the damage states definitions and strategies available in the literature is also made. For this, different types of bridges uncertainties, in terms of column height, superstructure type, lap splice and span length are investigated for the selected case studies. Also, the influence of material properties, namely the compressive strength of concrete and the yield strength of steel is described. In Chapter 6 the results are generated in terms of fragility curves for each bridges class. Chapter 7 indicates the study of the stochastic response of concrete bridges considering the uncertainty in the bearing and abutment stiffness. Finally in chapter 8, the main conclusions are drawn from the work developed within the present study.

TABLE OF CONTENTS

TABLE OF CONTENTS	I
LIST OF FIGURES	IV
LIST OF TABLES	VIII
SYMBOLOLOGY	X
CHAPTER 1.....	1
1 INTRODUCTION.....	1
1.1 Problem description and motivation	1
1.2 Research objectives	8
1.3 Approaches and methodology	9
1.4 Evolution in the development of fragility curves and theoretical background.....	11
1.5 Methods for fragility curves development.....	12
1.5.1 Judgmental methods	13
1.5.2 Empirical methods.....	14
1.5.3 Analytical methods:.....	15
1.5.4 Hybrid methods	18
1.6 Stochastic dynamic analysis of concrete bridges	18
1.7 Seismic regulations and construction practice.....	20
1.8 Organization of the thesis	21
CHAPTER 2.....	24
2 CLASSIFICATION OF BRIDGES.....	24
2.1 Previous research of bridge classifications.....	24
2.2 Description of Bridge Inventory	28
2.3 Parameters influencing the bridges response.....	30
2.3.1 Span number.....	31
2.3.2 Skew angle	31
2.3.3 Maximum and total span length	32

2.3.4	Column height and bent column number.....	33
2.3.5	Superstructure girder spacing.....	34
2.3.6	Bridge deck width.....	34
2.4	Major bridge classes.....	35
2.5	Bridge samples for the major bridge classes	39
CHAPTER 3.....	40
3	NUMERICAL ANALYSES.....	40
3.1	Modeling of bridge components	43
3.2	Material properties	44
3.3	Superstructure	47
3.4	Substructure	48
3.5	Abutment	51
3.6	Bearing	55
CHAPTER 4.....	56
4	GROUND MOTION SELECTION	56
4.1	Earthquake ground motion intensity measures.....	56
4.2	Geological and seismological feature of Iran	60
4.3	Selection of ground motion records	61
CHAPTER 5.....	70
5	SEISMIC DAMAGE LIMIT STATES AND UNCERTANITIES.....	70
5.1	Previous studies.....	70
5.2	Damage parameters	83
5.3	Damage states for RC column based on displacement ductility.....	85
5.4	Uncertainties	87
5.4.1	Uncertainties in span length and superstructure type	87
5.4.2	Uncertainties in column section and column height.....	89
5.4.3	Uncertainties in material	90
5.4.4	Uncertainties in connectivity between superstructure and substructure	91
5.4.5	Uncertainties in lap splice of the reinforcement.....	92

CHAPTER 6.....	96
6 DEVELOPMENT OF ANALYTICAL FRAGILITY CURVES	96
6.1 Seismic demand calculation of bridge components	96
6.2 Methodology used for fragility curves	97
6.3 Development of fragility curves	98
6.4 Fragility curves for major bridge classes.....	99
6.4.1 Span length.....	100
6.4.2 Column height	102
6.4.3 Material	104
6.4.4 Connectivity between superstructure and substructure	106
6.4.5 Present of lap splice	109
6.4.6 Fragility curves due to intensity measure	113
CHAPTER 7.....	116
7 STOCHASTIC COLLOCATION BASED ANALYSIS OF CONCRETE BRIDGES WITH UNCERTAIN PARAMETERS	116
7.1 Polynomial chaos discretization of random parameters.....	117
7.2 Spectral stochastic modelling for seismic analyses	118
7.3 Numerical Study	121
7.3.1 Representation of uncertain parameters.....	123
7.3.2 Unknown coefficients for uncertain parameters	123
7.3.3 Approximate polynomial model of the response	126
7.3.4 Determination of collocation points for the response.....	127
7.4 Spectral stochastic modelling of seismic analyses.....	128
CHAPTER 8.....	131
8 CONCLUSIONS AND FUTURE WORKS	131
8.1 Summary.....	131
8.2 Conclusions.....	132
8.3 Recommendations for future studies.....	135
REFERENCES.....	137

LIST OF FIGURES

Figure 1- 1: Topographic map of the Middle East region with plate boundaries, (http://www.see.leeds.ac.uk/structure/leb/tectonics/regional/regional.htm).....	2
Figure 1- 2: Seismicity of the Alpine-Himalayan belt, (15).....	3
Figure 1- 3: Population distribution of Iran in 2006 and 2011, (14).....	3
Figure 1- 4: (a) Seismic hazard map of Iran (http://earthquake.usgs.gov/earthquakes/world/iran/gshap.php),	4
Figure 1- 5: Examples of superstructure damages : (a) Loma Prieta earthquake (USA) - inadequate seat, (b) Chi Chi earthquake (Taiwan) - collapse of end spans due to ground failure and nearby fault rupture, (c) Varzaghan earthquake (Iran) - Displacement of the deck, (d) San Fernando earthquake (USA) - damage to truss support bearing shoe, e) Varzaghan earthquake (Iran) – sitting of abutment.....	6
Figure 1- 6: Examples of the substructure damages: (a) Manjil Earthquake (Iran) - Large lateral pier displacement of undamaged concrete bridge, (b) San Fernando earthquake (USA) - collapsed overpasses highway bridges, (c) San Fernando earthquake (USA) – Shear failure due to insufficient transverse reinforcement, (d) San Fernando earthquake (USA) - failure in flexure due to deficient anchorage of longitudinal reinforcement, (e) Loma Prieta earthquake (USA) - collapse of the bridge due to Joint shear failure (http://www.ngdc.noaa.gov/hazardimages/picture/list).....	7
Figure 1- 7: Flowchart to develop bridges’ fragility curves.....	10
Figure 1- 8: An example of a set of fragility curves for different damage limit states.....	10
Figure 1- 9: Probabilistic representation of capacity and demand spectra (77)	17
Figure 2- 1: General geometry of (a) simply supported bridge, (b) integral bridge, (c) transverse view of simply supported bridge and (d) transverse view of integral bridge	29
Figure 2- 2: Frequency distribution for the span number.....	31
Figure 2- 3: Frequency distribution for the skew angle	32
Figure 2- 4: Frequency distribution for (a) the maximum span length, (b) the total length.....	33
Figure 2- 5: Frequency distributions of (a) the columns height, (b) the number of columns per bent	34
Figure 2- 6: Frequency distribution of number of girders.....	34
Figure 2- 7: Frequency distribution of total deck width	35
Figure 2- 8: Frequency distribution for the columns cross section.....	36
Figure 2- 9: Frequency distribution of superstructure type and span length.....	38
Figure 2- 10: Characterization procedures and sampling, a) soil around the abutment to obtain the abutment dimension, b) longitudinal and transversal reinforcements, c) Facial reconstruction after the procedures.....	39

Figure 3- 1: Levels of modeling for seismic bridge analysis [108]	40
Figure 3- 2: (a): Picture of example highway bridge,(b): Longitudinal and transverse directions in the bridge modeling	42
Figure 3- 3: Three-dimensional finite-element model	44
Figure 3- 4: Steel Stress-Strain Model	45
Figure 3- 5: Material models for confined and unconfined concrete.....	46
Figure 3- 6: Concrete bridge bent model.....	49
Figure 3- 7: Moment-curvature diagram of columns.....	50
Figure 3- 8: Earth pressure type and their directions at the abutment	53
Figure 3- 9: Seat abutment's effective stiffness for highway bridges.....	54
Figure 3- 10: Typical elastomeric bearing of a highway bridge in Iran.....	55
Figure 4- 1: Definition of ASI	59
Figure 4- 2: (a) Strike-slip, (b) Reverse fault in Iran	61
Figure 4- 3: Mechanism of (a) strike slip fault, (b) reverse fault.....	61
Figure 4- 4: Final selection of ground motions for (a) reverse, and (b) strike slip faults	67
Figure 4- 5: Response spectra (5%) of the selected ground motions for reverse faults	68
Figure 4- 6: Response spectra (5%) of the selected ground motions for strike slip faults	69
Figure 5- 1: Previous research work and codes related to seismic vulnerability assessment of existing bridges (adapted from http://www.guardian.co.uk/environment/damian-carrington-blog/2011/oct/26/climate-change-developing-country-impacts-risk#)	71
Figure 5- 2: Schematic representation of limit states, (a) member limit state, (b) structure limit state (Priestley <i>et al.</i> (108)).....	75
Figure 5- 3: Damage states and damage limits on a force-deformation curve (Avsar and Yakut) (173).....	83
Figure 5- 4: Histogram for the number of limit states used by codes and researchers	83
Figure 5- 5: Histogram of limit states for different codes and researchers (a) Qualitative, and (b) quantitative	84
Figure 5- 6: Histogram for the approaches used to assess the bridge damages in previous studies	85
Figure 5- 7: Concrete bridge configuration	88
Figure 5- 8: Concrete bridge configuration for two bridge classification: simply support and integral	92

Figure 5- 9: The ration of $p/(f'_c \times A_g)$ versus ductility for (a) HCC-S, (b) SCC-S bridge classification.....	95
Figure 6- 1: Schematic representation of a fragility curve	98
Figure 6- 2: Fragility curves for different damage limit states (PGA) in terms of span length (SL) (a) Reverse & $20 \leq SL < 30$, (b) Strike slip & $SL \geq 20$, (c) Reverse & $SL \geq 30$, and (d) Strike slip & $SL \geq 30$	102
Figure 6- 3: Fragility curves for different damage limit states (PGA) in terms of column height (SCC-S) without lap splice, (a) Revers, and (b) Strike slip	103
Figure 6- 4: Fragility curves for different damage limit states (PGA) in terms of column height (HCC-S) without lap splice, (a) Revers, and (b) Strike slip	103
Figure 6- 5: Fragility curves subjected to reverse and strike slip fault for different damage limit states (PGA) in terms of column height without lap splice, (a) SCC-S, and (b) HCC-S	104
Figure 6- 6: Fragility curves based on different f'_c , (a) LS-1, (b) LS-2, (c) LS-3, and (d): LS-3	105
Figure 6- 7: Fragility curves based on different f_y , (a) LS-1, (b) LS-2, (c) LS-3, and (d): LS-3	106
Figure 6- 8: Fragility curves for different damage limit states in terms of PGA and ASI subjected to reverse and strike-slip faults.....	108
Figure 6- 9: Response spectra of the selected ground motions (5% damping) for (a) reverse and (b) strike-slip faults.....	108
Figure 6- 10: Fragility curves subjected to reverse and strike-slip fault for different damage limit states in terms of PGA for (a) CC-S and (b) CC-I bridge classification	109
Figure 6- 11: Fragility curves for different damage limit states (PGA) in terms of column height (HCC-S) with lap splice, (a) Revers, and (b) Strike slip	110
Figure 6- 12: Fragility curves for different damage limit states (PGA) in function of the presence or not of lap splice in columns for HCC-S, (a) LS3-reverse fault, (b) LS3-strike slip fault, (c) LS4-reverse fault, and (d) LS4-strike slip fault.....	111
Figure 6- 13: Fragility curves for different damage limit states (PGA) as a function of the presence or not of lap splice in columns for two groups of classification, (a) CC-S-LS3&LS4-reverse fault, (b) CC-S-LS3&LS4-strike-slip fault, (c) CC-I-LS3&LS4-reverse fault, and (d): CC-I-LS3&LS4-strike-slip fault.....	113
Figure 6- 14: Comparison between jaggedly varing points and smooth fragility curve for CC-I bridge classification due to slight limit state based on (a): PGA and (b):ASI intensity measures.....	115
Figure 7- 1: The geometric characteristics of the bridge	122
Figure 7- 2: Reconstruction of the PDF of the uncertain parameters K_{si} , K_{vi} , K_{li} and K_{ti} with the gPC (dashed) compared with the theoretical PDF (bold lines). The dotted vertical lines indicate the mean values	125

Figure 7- 3: Time history of the gPC expansion coefficients 127

Figure 7- 4: Comparison of probability distributions of the maximum displacement quantities
obtained using gPC expansion and the MC simulation 128

Figure 7- 5: Comparison (a) mean value, and (b) standard deviation value of the displacement
quantities obtained using gPC expansion and the MC simulation 130

LIST OF TABLES

Table 1- 1: General data on the most important earthquakes in Iran (19, 20).....	5
Table 1- 2: Description of bridge damage states, adapted from HAZUS (53).....	13
Table 1- 3: Damage matrix for the 1994 Northridge earthquake in terms of PGA (1).....	15
Table 1- 4: Damage matrix for the 1995 Kobe earthquake in terms of PGA (60)	15
Table 2- 1: Description of bridge sub-categories employed by Basöz and Kiremidjian [1].....	25
Table 2- 2: Some construction material and construction types according to the NBI [99]	26
Table 2- 3: Bridge classification scheme based on HAZUS (FEMA, 2003) [37].....	27
Table 2- 4: Bridge classes defined by Nielsen [100]	27
Table 2- 5: Bridge classes defined by Avsar <i>et al.</i> [101]	28
Table 2- 6: Structural attributes for the bridge samples for each major bridge class in terms of section	36
Table 2- 7: Two major bridge classes in terms of superstructure type	36
Table 2- 8: Definition of the bridge classes in terms of the column height	37
Table 2- 9: Structural attributes for the bridge samples for each major bridge class in terms of span length	38
Table 2- 10: Material properties for the bridge samples for each major bridge class.....	38
Table 4- 1: Elastic fundamental periods of the major bridges.....	60
Table 4- 2: Ground motion selection for reverse fault.....	64
Table 4- 3: Ground motion selection for strike-slip fault.....	65
Table 4- 4: Some important parameters of the selected earthquake ground motions (reverse)	68
Table 4- 5: Some important parameters of the selected earthquake ground motions (strike-slip) 69	
Table 5- 1: Summary of previous researches and codes	72
Table 5- 2: Drift and displacement limits for each damage state (Basöz and Mander) (77).....	76
Table 5- 3: Quantitative damage limit state definitions (Kowalsky) (150).....	76
Table 5- 4: Bridge damage assessment (Hose <i>et al.</i>) (152).....	77
Table 5- 5: Bridge performance assessment (Hose <i>et al.</i>) (152)	77
Table 5- 6: Seismic damage assessment criteria for columns in flexure (Hwang <i>et al.</i>) (67).....	78

Table 5- 7: Bridge damage states by displacement ductility ratios (Hwang <i>et al.</i>) (67).....	79
Table 5- 8: Definitions of damage states by HAZUS (FEMA, 2003) (37).....	79
Table 5- 9: Damage state description for bridge components (Liao and Loh) (155)	80
Table 5- 10: Ductility and displacement limits for each damage state (Liao and Loh) (155).....	80
Table 5- 11: Definition of damage states for bridge components (Elnashai <i>et al.</i>) (56).....	81
Table 5- 12: Definition of damage states for bridge components (Choi <i>et al.</i>) (69).....	82
Table 5- 13: Structural attributes for the bridge samples for each major bridge class in terms of span length	89
Table 5- 14: Concrete reinforcing layout for each case study in terms of span length.....	89
Table 5- 15: Structural attributes for the bridge samples for each major bridge class in terms of column height.....	90
Table 5- 16: Geometric characteristics for each case study in terms of span length	90
Table 5- 17: Structural attributes for the bridge samples for each major bridge class in terms of material properties	91
Table 5- 18: Structural attributes for the bridge samples for each major bridge classes in terms of superstructure connectivity	92
Table 5- 19: Geometric characteristics for each case study in terms of superstructure connectivity	92
Table 5- 20: Limit states for simply support bridges (HCC-S)	94
Table 5- 21: Limit states for simply support bridges (SCC-S).....	94
Table 5- 22: Limit states for integral bridges (CC-I).....	95
Table 6- 1: Fragility curve parameters for different damage limit states in terms of span length	101
Table 6- 2: Fragility curve parameters for the material properties in terms of compressive concrete strength and steel yield stress	105
Table 6- 3: Fragility curve parameters of the HCC-S.....	114
Table 6- 4: Fragility curve parameters of the CC-S and CC-I bridge classes	115
Table 7- 1: Material properties of concrete bridge	122
Table 7- 2: The gPC-coefficients of the uncertain parameters.....	124
Table 7- 3: Bearing and abutments stiffness as input parameter for 9 sets of analyses.....	126

Symbology

A – gross rubber area

A_e – effective abutment wall area

A_g – cross section

A_h – cross-sectional area of transverse reinforcement

C – damping matrix

d_{bl} – diameter of the longitudinal reinforcing bars

d_s – diameter of spiral

D' – diameter of the confined concrete core

E_c – modulus of elasticity for concrete

f'_c – compressive strength of concrete

f'_{cc} – compressive strength of the confined concrete

f'_l – effective lateral confining stress

f_{su} – ultimate strength of longitudinal bars

f_{ye} – yield strength of the longitudinal bars

f_{yh} – yield strength of the transverse reinforcement

F_r – fragility function

G – shear modulus of rubber

G_c – shear modulus

h – total rubber height

h_a – height of the back-wall for seat abutments

h_{bw} – effective abutment height

K – stiffness matrix

k_e – confinement coefficient

K_{eff} – effective abutment's stiffness

k_i – deterministic unknown coefficients matrix

K – rubber bulk modulus

K_{al} – stiffness of abutment in longitudinal direction

K_{at} – stiffness of abutment in transvers direction

K_i – initial abutment's stiffness

K_v – vertical stiffness of the bearings
 K_s – vertical stiffness of the bearings
 L – distance from the plastic hinge to the point of contra-flexure
 L_p – plastic hinge length
 M – mass matrix
 M_{max} – degradation moment in pier
 M_n – nominal moment capacity
 M_w – moment magnitude
 M_y – moment at yielding of a vertical reinforcing bar
 M_l – moment at first yielding of a vertical reinforcing bar
 p – axial load
 P_{bw} – passive pressure force of the abutment
 R – distance from the epicenter
 R^2 – coefficient of determination
 s – longitudinal spacing of hoops or spirals
 S – shape factor.
 S_c – structural capacity
 S_d – structural demand
 S_m – *earthquake severity measure*
 T_i – initial period are used to calculate ASI
 T_f – final period are used to calculate ASI
 \mathbf{u} – nodal displacement
 u_i – unknown coefficient
 $\dot{\mathbf{u}}$ – velocity vector
 $\ddot{\mathbf{u}}$ – acceleration vector
 $\ddot{\mathbf{u}}g$ – vector of support motion
 $\mathbf{u}(t, \xi)$ – unknown displacement vector
 U – random variable
 V_s – shear wave velocity
 w_a – width of the back-wall for seat abutments
 w_{bw} – effective abutment width
 α – mass proportional damping coefficient
 β – stiffness proportional damping coefficient

Δ_i – relative displacement at the top of a column at the corresponding limit state i
 Δ_1 – relative displacement of a column when the longitudinal reinforcing bars reach the first yield
 Δ_3 – relative displacement of a column corresponded to third displacement ductility
 ε_c – compressive strain of the concrete column
 ε_{cc} – strain at peak stress for confined concrete
 ε_{cu} – ultimate compression strain for confined concrete
 ε_{su} – ultimate tensile strain
 ε_y – nominal yield strain
 ε_{ye} – expected yield strain
 θ_p – plastic hinge rotation
 θ_{p2} – plastic hinge rotation when the strain at the end of the column is equal to 0.002
 θ_{p4} – plastic hinge rotation when the strain at the end of the column is equal to 0.004
 μ – mean value
 μ_d – displacement ductility
 μ_i – ductility demand at the i^{th} damage state
 μ_y – yield displacement ductility ratio
 μ_1 – first limit state corresponded to slight damage
 μ_2 – second limit state corresponded to moderate damage
 μ_3 – third limit state corresponded to extensive damage
 $\mu_{3,2}$ – third damage state corresponded to extensive damage when $\varepsilon_c = 0.002$
 $\mu_{3,4}$ – third damage state corresponded to extensive damage when $\varepsilon_c = 0.004$
 μ_4 – fourth limit state corresponded to collapse damage
 μ_φ – curvature ductility
 ν – poisson's ratio of concrete
 ξ – random vector
 ρ_{cc} – ratio of area of longitudinal reinforcement to area of core of the section
 ρ_s – volumetric ratio of confining steel
 σ^2 – variance
 φ – curvature at the column bottom
 φ_y – equivalent curvature at the bottom of the column
 φ_u – ultimate curvature at the bottom of the column

φ_1 – curvature correspondent to the relative displacement of a column when the vertical reinforcing bars at the bottom of the column reach the first yield

$\varphi_{3,2}$ – curvature corresponded to the relative displacement of a column when $\varepsilon_c = 0.002$

$\varphi_{3,4}$ – curvature corresponded to the relative displacement of a column when $\varepsilon_c = 0.004$

$\psi_i(\xi)$ –stochastic basis function

Ω – random space

AASHTO – American Association of State Highway and Transportation Officials

ABA – Iranian Concrete Code

ASI – Acceleration Spectral Intensity

ATC – Applied technology Council

BHRC – Building and Housing Research Center

Caltrans – California Department of Transportation

CC-I – Circular Column Integral

CC-S – Circular Column Simply Support

DI – Damage Index

COSMOC – Consortium of Organization for Strong Motion Observation System

FEM – Finite Element Method

FEMA – Federal Emergency Management Agency

FHWA – Federal Highway Administration

GIS – Geographical Information System

GPC – Generalized Polynomial Chaos

HCC-S – High Circular Column-Simply Support

IDA – Incremental Dynamic Analysis

IMs – Intensity Measurements

KL – Karhunen-Loeve

LS1 – Slight

LS2 – Moderate

LS3 – Extensive

LS4 – Collapse

MC – Monte Carlo

NBI – National Building Inventory

NLTHA – Nonlinear Time History Analysis

NRHA – Nonlinear Response History Analysis

PEER – Pacific Earthquake Engineering Research
PGA – Peak Ground Acceleration
PGD – Peak Ground Displacement
PGV – Peak Ground Velocity
PSPA – Probabilistic Seismic Performance Analysis
RC – Reinforce Concrete
SCC-S – Short Circular Column-Simply Support
SL – Span Length

Chapter 1

1 INTRODUCTION

1.1 Problem description and motivation

Seismic vulnerability assessment of the highway bridges located in areas of high seismic hazards plays an important role for the safety of transportation systems. One of the most critical issue in pre-earthquake planning, and post-earthquake response of the transportation system is qualitative and quantitative assessment of the seismic risk in the highway bridge systems. The action of earthquakes on highway infrastructure systems as a natural hazard has typically investigated by previous researches due to economic and human losses [1-6]. Such previous assessments have led to valuable knowledge about a number of important effects of earthquakes on the regions' economy, traffic disruption of the transportation system and post-earthquake response and recovery [7]. Nations' freight economy on highway bridges combined with awareness of the seismic hazard in the region and appropriate consideration of their seismic response and vulnerability, are the important issues in risk assessment of bridges.

Before the 1970's, many of the bridges were not designed to earthquakes. During the 1971 San Fernando earthquake in California several bridges suffered damages [8]. The Loma Prieta earthquake in 1989 caused noticeable damage to bridges. Following the Loma Prieta earthquake, substantial changes have been made to seismic design provisions of the bridges. Seven bridges collapsed during the 1994 Northridge earthquake and many others sustained damages without collapse [9]. Performance of pre-1990 bridges revealed that these structures are seismically vulnerable. Statistics show that more than 680000 people died in past earthquakes in the first decade of the 21th century. One of the main reasons for this high casualty due to past earthquakes is delay in rescue and relief operation. This delay is almost due to insufficient performance of bridges which are one of the most important parts of a transportation system. The importance of acceptable seismic behavior for bridges in transportation systems has emphasized the need for seismic safety evaluations of existing bridges. In some countries, there is a lack of detailed studies analyzing the seismic vulnerability of the pre-1990 bridges that allows conducting specific tasks to reduce economic losses in the future.

Historical records show that Iran faced large earthquakes along the past centuries. Major past earthquakes occurring in Iran, caused an important number of human life losses and widespread damage in structures [10-13]. Iran is located in a geographical area affected by different tectonic plates. In Iran the active faulting is a direct indicator of active crustal deformation, due to the convergence between the Arabian and the Eurasian plates, which occurs in the range of 2.1-2.5 cm/yr. Figure 1- 1 shows the topographic map of the Middle East region, marking in black the plate' boundaries, and the position of Iran in Alpine-Himalayan seismic belt presents in Figure 1- 2. This level of seismicity is a result of the present convergence of the Arabian and Eurasia plate in a continental collision (in the Zagros mountain range), which lead to sandwich the Iranian old micro-plate between Arabia and the main Eurasian continent that gives rise of several bands of seismicity, including the Alborz Mountains at the southern coasts of the Caspian Sea. Seismic hazard in Iran consequently is one of the subjects of many discussions among societies and scientific communities. With a more than 75 million population in 2011 [14] (Figure 1-3), most which live in cities close to seismic zones (Figure1- 3), careful study of Iranian seismic hazard is of utmost importance.

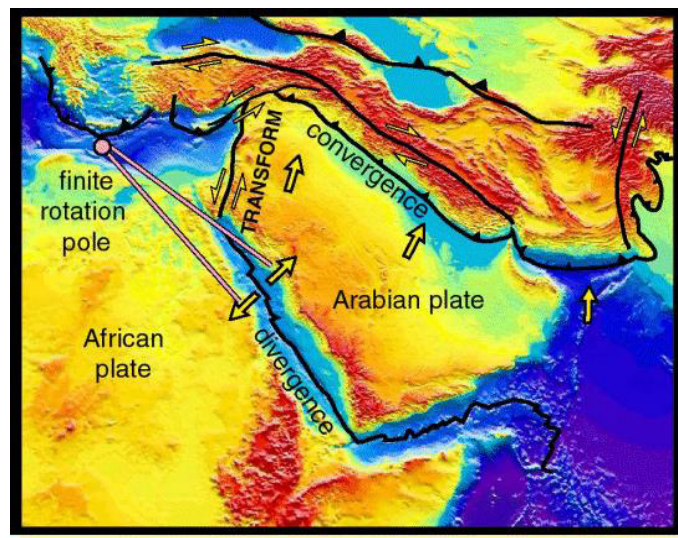


Figure 1- 1: Topographic map of the Middle East region with plate boundaries, (<http://www.see.leeds.ac.uk/structure/leb/tectonics/regional/regional.htm>)

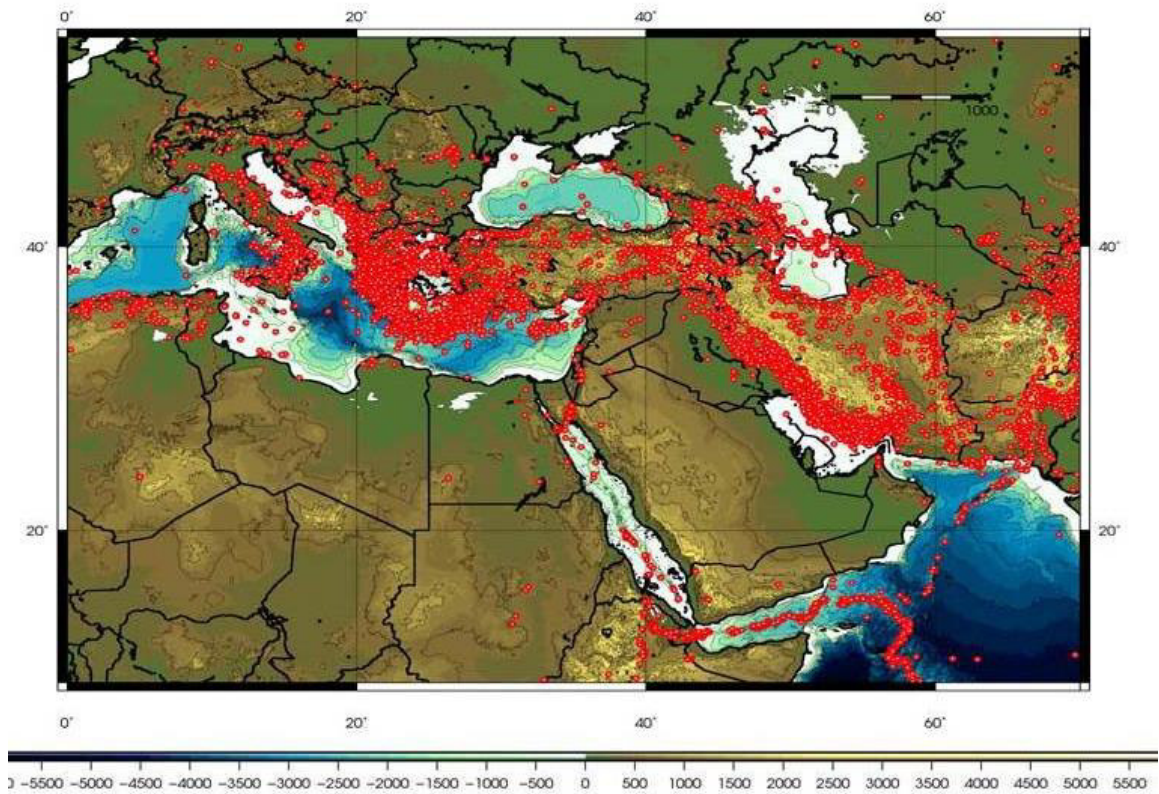


Figure 1- 2: Seismicity of the Alpine-Himalayan belt, [15]

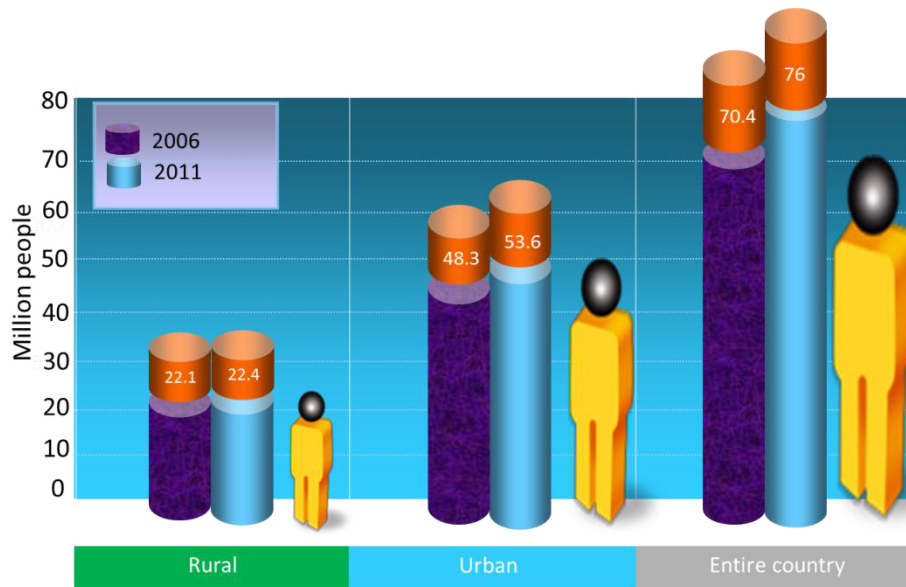


Figure 1- 3: Population distribution of Iran in 2006 and 2011, [14]

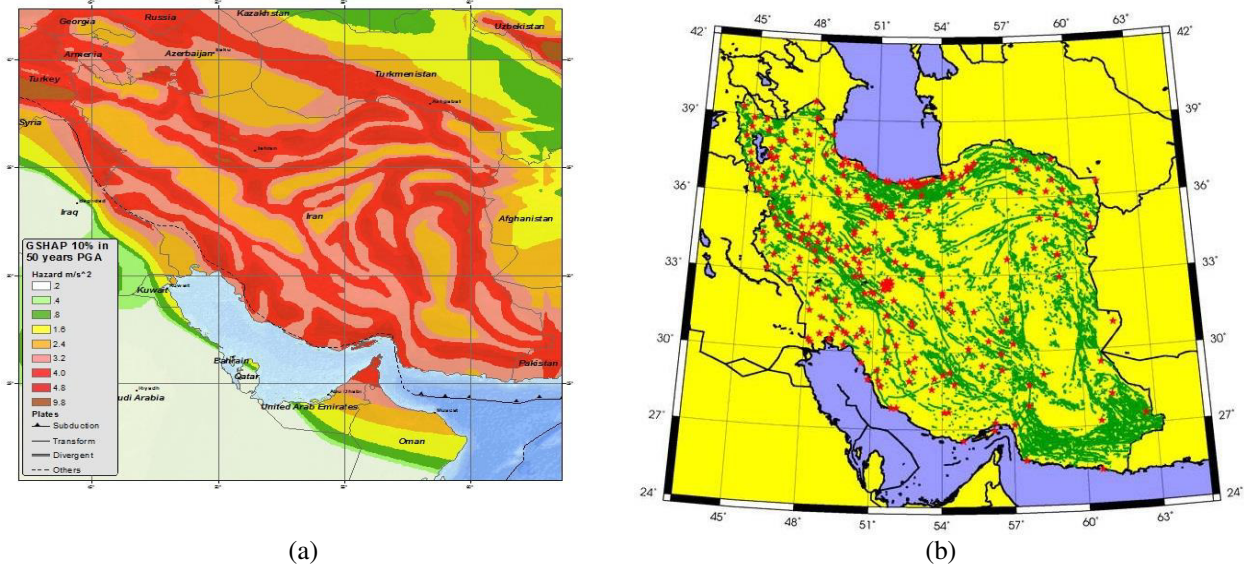


Figure 1- 4: (a) Seismic hazard map of Iran (<http://earthquake.usgs.gov/earthquakes/world/iran/gshap.php>), (b) Iranian Quaternary fault systems, [16]

A quick look on the data from figure 1- 4 shows that, the seismicity pattern in Iran in agreement with the positions of active faults in. From among 231 past seismic events along the period of 1900-2014, the event known as Tabas earthquake had the highest magnitude ($M_w = 7.4$), and occurred on September 16th, 1978. Death toll exceeded 20,000, and hundreds of people were injured; further, 15,000 structures were destroyed. The economic loss was estimated approximately to be 11 million U.S. dollars at that time [17]. Among other earthquakes in Iran is the one that occurred on December 26th, 2003, causing severe damages at the south area Iran. The earthquake destroyed major part of Bam city and the nearby villages. The official total number of people deaths reached 26,000, accompanied by 30,000 injured and 75,000 homeless people [17]. The Manjil earthquake with a magnitude 7.4 occurred on June 21th, 1990, in the provinces of Zanzan and Gilan located at the northwest of Iran. Around 40,000 fatalities were caused directly from the earthquake and the damaged area reported is larger than 10,000 km² [18]. Past records show evidence that Iran can expect earthquakes with magnitude in the range of 6.3 to 7.4, (Table1- 1). According to official records, over the past 35 years, more than 100,000 people have lost their lives as a result of earthquakes in Iran. Thus, it is difficult to estimate the level of damage and number of deaths or casualties that Iran will experience under the occurrence of high-intensity earthquakes. A comparison between this number and other loss figures in Iran, along with responsible, scientific considerations on the seismic hazard in the

country can lead to a valuable, realistic insight about the level of seriousness of the issue. In this study, we are going to address the above question on an introductory level.

Table 1- 1: General data on the most important earthquakes in Iran [19, 20]

Date	Location	M_w	Fatalities
1909	Borujerd	7.3	8,000
1930	Salmas	7.2	2,500
1953	Semnan	6.4	970
1962	Buyin-Zahra, western Iran	7.3	12,225
1968	Dasht-i Biyaz, eastern Iran	7.3	12,000
1972	Ghir (Qir), southern Iran	6.8	5,054
1976	Turkey:Muradiye (Turkey-Iran border region)	7.3	5,000
1978	Tabas, eastern Iran	7.4	20,000
1990	Manjil, northern Iran	7.4	40,000
1997	Ardekul, eastern Iran	7.3	1,572
2003	Bam, south eastern Iran	6.6	31,000
2005	Zarand, central Iran	6.4	612
2012	Ahar	6.4	500
2013	Bushehr	6.3	850

The seismically active areas around the world have exhibited the vulnerability of the structures under the occurrence of major past earthquakes; particularly in Iran, those events revealed that bridges are one of the vulnerable components of the transportation system. Further, there are records showing that most of the damaged bridges were designed according to old versions of the seismic codes [21]. The seismic vulnerability assessment for highway bridges located in areas of high seismic hazard plays an important role in the safety of the transportation network. Bridges damaged could lead to the interruption of road services, to prevent break downs of the bridge network, studies be led of the bridges' seismic vulnerability to define the seismic risk of the whole road transportation system in order to take preventive actions. Therefore, due to the above mentioned reasons, a study of the seismic vulnerability of Iran's bridges is needed, especially for bridges located in highly seismic zone. A proper design tends to reduce the amount of damage and ensures bridge better performance. More strict recommendations made by current guidelines and codes suggest methodologies to avoid severe damages during earthquakes. In the past decades, several bridges have been damaged by earthquakes [21-24]. Recently, researchers have developed different approaches to assess the seismic vulnerability of bridges in the deterministic and probabilistic domains using linear and nonlinear analyses [25-28]. Low ductility and inadequate resistance of the columns led to severe damages in past earthquakes. In addition, insufficient splice length splices of the longitudinal reinforcement, in the potential

plastic hinge region, and premature shear failures have also been investigated by several researchers [29-33]. After specifying the seismic levels to which bridges can be exposed along their lifetime and using probabilistic approaches, fragility curves can be used to perform the seismic vulnerability assessment. Figures 1- 5 and 1- 6 show some pictures of damaged bridges under earthquakes.

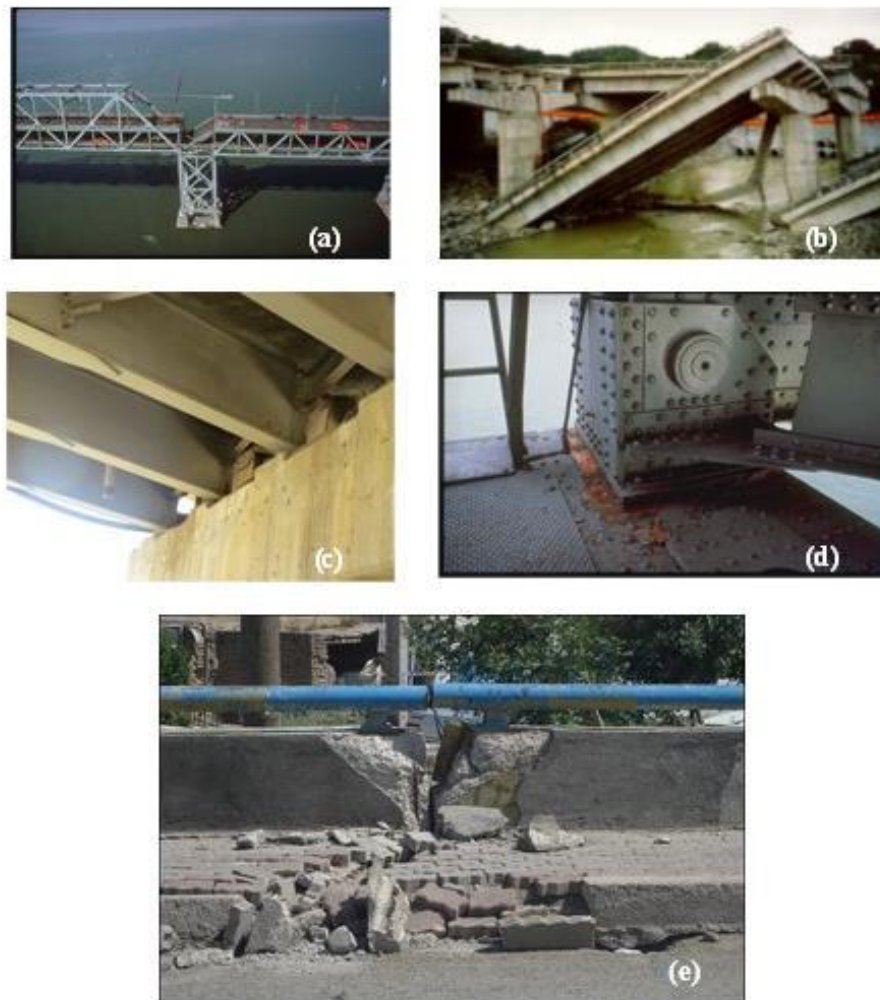


Figure 1- 5: Examples of superstructure damages : (a) Loma Prieta earthquake (USA) - inadequate seat, (b) Chi Chi earthquake (Taiwan) - collapse of end spans due to ground failure and nearby fault rupture, (c) Varzaghan earthquake (Iran) - Displacement of the deck, (d) San Fernando earthquake (USA) - damage to truss support bearing shoe, e) Varzaghan earthquake (Iran) – sitting of abutment

<http://www.ngdc.noaa.gov/hazardimages/picture/list>



Figure 1- 6: Examples of the substructure damages: (a) Manjil Earthquake (Iran) - Large lateral pier displacement of undamaged concrete bridge, (b) San Fernando earthquake (USA) - collapsed overpasses highway bridges, (c) San Fernando earthquake (USA) – Shear failure due to insufficient transverse reinforcement, (d) San Fernando earthquake (USA) - failure in flexure due to deficient anchorage of longitudinal reinforcement, (e) Loma Prieta earthquake (USA) - collapse of the bridge due to Joint shear failure
<http://www.ngdc.noaa.gov/hazardimages/picture/list>

This research aimed to study the seismic vulnerability of bridges in Iran, with the most common geometry that were designed and constructed based on recommendations of old seismic design construction codes. For this purpose, analytical methods are used to estimate the bridges' responses under various seismic scenarios characterized with earthquake ground motions for various intensities and from different seismic sources. At the end the results of the analytical models are exposed to compare the sampling (e.g., Monte Carlo simulation) and non-sampling

(e.g., collocation methodology). To achieve the main objective of the work, the overall study mainly consists of: (a) bridges classification into different groups based on similar dynamic behavior for seismic demands; (b) selection of the appropriate methodologies to lead the numerical analyses in order to estimate the bridges' seismic vulnerability; (c) generation of fragility curves for each bridge class accounting for different seismic sources and; (d) evaluation of the uncertainty in the stiffness properties and its contribution to the stochastic response of concrete bridges.

1.2 Research objectives

The main objective of the study is to develop fragility curves for the ordinary highway reinforce concrete (RC) bridges in Iran designed and constructed based on old design and construction practices, to assess their seismic vulnerability when subjected to seismic demands from different sources. Subsequently the results are compared with a sampling method such as Monte Carlo (MC) simulation and a non-sampling method such as the collocation method. For this purpose, the following specific objectives are proposed to be accomplished:

1. To study the seismicity in different geographical areas of Iran
2. To compile a general overview from previous studies
3. Classification of common bridges in Iran
4. Selection of earthquake ground motion records based on ground motion intensity
5. Definition of specific damage limit states
6. Development of seismic 3-D time history analyses
7. To estimate fragility curves
8. To evaluate the effect of uncertainty in the bearing and abutment stiffness properties and contribution to the stochastic response of concrete bridges.

1.3 Approaches and methodology

In order to achieve the mentioned specific objectives, the research work is arranged in different steps. First, the study of the seismicity in Iran and the analysis of the seismic hazard are conducted. Second, different type of common ordinary bridges in Iran are classified and selected for a detailed study. The more relevant types of bridges are selected from the inventory of the region according to their primary structural characteristics. 3-D analytical time history analyses are developed for each bridge sample to derive the nonlinear response under a selected set of ground motion earthquake records. Fragility curves can be developed for different ground motion intensity. However some of the intensity parameters can be easily determined through equations and some others are calculated from ground motion records. It is noticeable that in selecting the appropriate intensity measure, it must have certain level of correlation with the seismic damage of the bridges. Thus, the reliability of the bridge fragility curves depends on the selected intensity measure. Third, damage limit states are defined for each bridge class. Then, fragility curves are generated using nonlinear analysis and comparing the identified damage states and the seismic demands applied on the bridge. Figure 1- 7 presents the flow chart followed to the applied analytical method to generate the fragility curves. As depicted in Figure 1- 7, bridge structure sampling modeling, ground motion selection and damage state definition are three important items in the process of developing the fragility curves; the reliability of the analytically fragility curves determined is influenced by these three items. Finally, the effects on stochastic response analysis of concrete bridges, considering the uncertainty in the abutment and bearing stiffness, are investigated. A typical fragility curve for different damage states is presented in Figure 1- 8.

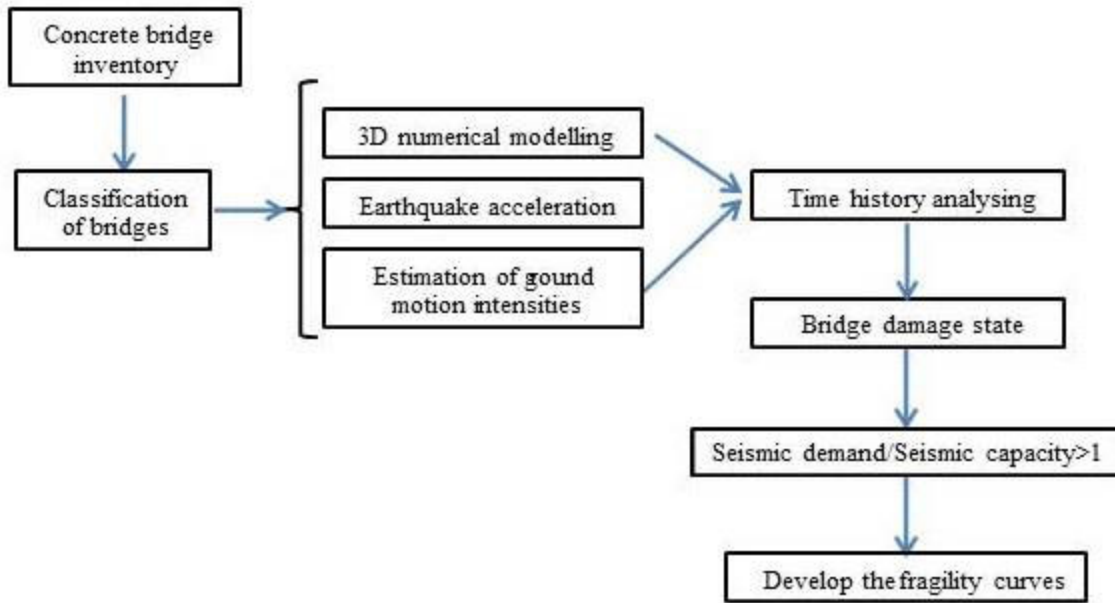


Figure 1- 7: Flowchart to develop bridges' fragility curves

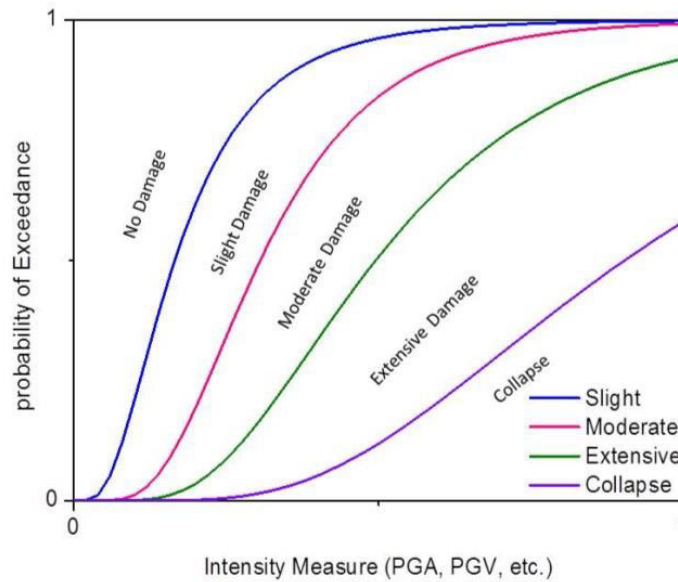


Figure 1- 8: An example of a set of fragility curves for different damage limit states

1.4 Evolution in the development of fragility curves and theoretical background

Fragility curves relate strong motion intensity to the probability of reaching or exceeding a certain limit state. These curves found widespread use in probabilistic seismic risk assessment of highway bridges. Peak ground acceleration (PGA) or spectral acceleration, by considering the root of the sum of the squares (SRSS) of the two horizontal components of the ground motions, are common seismic intensities. Fragility curves have a current and potential future to be employed as an application including: (a) emergency response such as priority in bridge inspection, (b) design support and performance based earthquake engineering and (c) Planning support like traffic impacts from scenario earthquakes, or cost effectiveness of alternative bridge retrofit strategies and additional seismic retrofit needs.

The use of fragility curves to assess the seismic vulnerability of structures can be traced back to 1975, when the seismic risk assessment method was formalized by Whitman *et al.* [34]. In 1991, the Applied Technology Council (ATC) introduced the concept of fragility function in the ATC 25 report [35]. Subsequently, in 1997 a risk assessment software package [36] based on the geographical information system (GIS) was presented by the Federal Emergency Management Agency (FEMA). The more recent version, HAZUS [37], is capable of assessing potential risk and losses from earthquakes. In the last two decades, the safety of structures and infrastructures has been assessed by using fragility curves as an efficient and useful tool.

In the past decades, important research efforts had been focused on the estimation of fragility functions for buildings [38-43] whereas less attention had been paid to investigate the vulnerability of bridges. Studies have shown that a great number of highway bridges around the world do not meet the seismic-detailing requirements recommended in current codes and guidelines [44]; for example, after the Kobe earthquake, Kawashima *et al.* [45] suggested that the bridges' failure of structures designed before 1980 was governed by shear, while bridge piers designed after 1980 failed mostly in flexure. Kim and Shinozuka [46] selected nonlinear time history analysis (NLTHA) to study the effect of steel jacketed column retrofits on the performance of bridges. Incremental dynamic analysis (IDA) are utilized by Mander *et al.* [47] in a performance-based earthquake engineering to study the expected seismic damage and the

associated financial loss from highway bridges. Zhang and Huo [48] used NLTHA and IDA to develop fragility curves for conventionally designed and base isolated bridges to assess the optimum design parameters of isolation devices. Huang *et al.* [49] considered the effect of near-field ground motions and effects from soil characteristics for typical California reinforced concrete bridges with single column bents.

A fundamental requirement for estimating the seismic performance of a particular structure is the ability to quantify the potential for damage as a function of earthquake intensity (e.g., Peak Ground Acceleration, PGA). A probabilistic seismic performance analysis (PSPA) based on fragility curves provides a framework to estimate the seismic performance and reliability of the structures [50-52]. Fragility functions relate the probability that the demand on a particular structure exceeds its capacity to an earthquake severity measure; this can be expressed as follows:

$$Fr = P[(S_d \geq S_c | SM)] \quad (1.1)$$

where Fr = fragility function, S_d = structural demand, S_c = structural capacity and SM = earthquake severity measure. The structural demand was estimated by conducting nonlinear time history analyses. There are various approaches for establishing damage limit states. HAZUS [53] provides five qualitative damage states varying from no damage to structure collapse, based on the column damages and bridges' serviceability state (Table 1- 2). There are different ways to generate the fragility curves once is determined the bridge response data. Each data source has associated advantages and disadvantages. The following sections provide an overview of some methods to perform the assessment of the seismic vulnerability of highway bridges.

1.5 Methods for fragility curves development

Researchers have developed different approaches to assess the seismic fragility of bridges, such as judgmental, empirical, analytical and hybrid methods. In the following section a brief outline of each method is described where the advantages and disadvantages are highlighted.

Table 1- 2: Description of bridge damage states, adapted from HAZUS [53]

Damage states	Description
No damage (N)	No damage to a bridge.
Slight/minor damage (S)	Minor cracking and spalling to the abutment, cracks in shear keys at abutments, minor spalling and cracks at hinges, minor spalling at the column (damage requires no more than cosmetic repair) or minor cracking to the deck.
Moderate damage (M)	Any column experiencing moderate cracking and spalling (column structurally still sound), any connection having cracked shear keys or bent bolts, or moderate settlement of the approach.
Extensive damage (E)	Any column degrading without collapse (column structurally unsafe), any connection losing some bearing support, or major settlement of the approach.
Complete damage (C)	Any column collapsing and connection losing all bearing support, which may lead to imminent deck collapse.

1.5.1 Judgmental methods

One of the oldest and simplest methods to obtain fragility curves is a judgmental or expert-based fragility curve that is based on the bridge response data obtained from experts' opinion. This method could be a good selection to trust on subjective information obtained from the expert engineers' opinion when the available information in terms of recorded data is not sufficient. In this process some questions based on various components of a typical highway bridge are asked to experts panels with expertise in the field of earthquake engineering. Based on this information, the estimation of the probability distribution of damage due to earthquakes with different intensities is assessed [28]. Then, the probability distribution function presents damage level for different ground motion intensities based on expert opinion. This method largely depends on panel expertise and the questions asked can be extremely subjective [19]. In the USA, the Applied Technology Council applied this method and presented the results by the report entitle: ATC-13 [54]. In the mentioned report, earthquake damages to the facilities in California were estimated. In this report, 70 senior level experts in earthquake engineering were organized to estimate the probable damage distribution for several components of a typical Californian infrastructure based on different seismic intensities. The questions answered by the experts on the probability of a bridge to fail due to one of the seven damage limit states for a given Modified-Mercalli Intensity (MMI) were provided for two classes of bridges according to the

total length. Finally, the results were reported in the ATC-13 as the bridges' damage probability. Since these curves depend on the individual experience of the experts consulted, the reliability curves obtained with this method are questionable. This method has some disadvantages when comparing to other methods because the results are based on the expertise's opinion, the uncertainty in the structural response and the randomness of the ground motion.

1.5.2 Empirical methods

Another way to develop fragility curves is the use of damage distribution functions determined based on post-earthquakes field observations or reconnaissance reports. This method is the most realistic approach since existing damage states are described in detail on the analytical model when considering all components of bridge after earthquake, such as structural and nonstructural. Also in this method is implemented the observation damage data to perform the fragility curves, therefore the subjectivity involved decreases when the reliability curves are estimated. Hence, the result from the process of inspection led to evaluate the bridge's damage, is different from one inspector to another, this is due to physical condition and the experience of the inspector. Another drawback to perform fragility curves using an empirical method is the contradiction and the disagreement among the bridge damage limit state definitions provided by different inspection teams. Moreover, in this method the damage states, the number of damaged bridges and their structural variability, the seismicity of the bridge local site and other important components needed to develop the fragility curves are limited due to the damaged bridges in the region affected by earthquake. Therefore the curves obtained by this method are highly explicit for a specific region. Note that the result from an empirical method is highly influenced by inadequate number of field observations and insufficient information, due to the bridges damaged distribution under an earthquake. Therefore it is noticeable the very limited application of the empirical fragility curves.

Several other researchers developed empirical fragility curves based on the post-earthquake damage data and observations [55-59]. Basoz and Kiremidjian [1] present a logistic regression analysis to generate empirical fragility curves for the Northridge earthquake bridges damaged data, while Shinozuka *et al.* [58] used the parameters of a lognormal probability distribution estimated by the Maximum Likelihood Method for Kobe earthquake data. Similar procedures are

employed by other researchers to develop fragility curves using as intensity measure the PGA for the highway bridges damage matrix. Table 1- 3 present the bridge damage matrix in terms of PGA for the 1994 Northridge earthquake [1] and Table 1- 4 shows the damage matrix for 1995 Kobe earthquake [60], respectively.

Table 1- 3: Damage matrix for the 1994 Northridge earthquake in terms of PGA [1]

Observed damage	0.15-0.2	0.2-0.3	0.3-0.4	0.4-0.5	0.5-0.6	0.6-0.7	0.7-0.8	0.8-0.9	0.9-1.0	> 1.0	Total
None	318	502	234	50	34	29	24	29	16	16	1252
Minor	2	10	25	2	6	4	6	1	7	3	66
Moderate	1	15	13	11	10	9	5	4	9	4	81
Major	0	10	2	6	7	3	2	5	11	1	47
Collapse	0	0	1	0	0	0	0	2	2	1	6

Table 1- 4: Damage matrix for the 1995 Kobe earthquake in terms of PGA [60]

Observed damage	0.15-0.2	0.2-0.3	0.3-0.4	0.4-0.5	0.5-0.6	0.6-0.7	0.7-0.8	0.8-0.9	0.9-1.0	> 1.0	Total
None	80	34	23	28	12	3	3	1	0	0	184
Minor	0	0	2	1	0	4	0	1	0	0	8
Moderate	0	0	1	3	3	6	0	0	0	0	13
Major	0	0	0	1	0	5	1	0	0	0	7
Collapse	0	0	0	2	0	2	0	0	0	0	4

By utilizing a damage matrix, empirical fragility curves and damage probability matrix can be developed based on appropriate distribution. However if there are considered the drawbacks mentioned before, a good correlation between the collected data and the fragility function is impossible to reach because the data is going to be fitted by a lognormal or normal distribution. Therefore the accuracy of the fragility curves obtained through this method needs to be supplemented by analytical simulation. Even if the empirical fragility curves reveal a more realistic curve than the judgmental criteria, it is influenced by some uncertainties such as discrepancy in observation between different inspection teams, or by inconsistency of different damage states definition.

1.5.3 Analytical methods

In the lack of adequate damage data or expert opinion, analytical fragility curves are the best choice to assess the seismic performance of highway bridges. Bridge models in 2-D or 3-D are formed in this method, and ground motions with different intensity levels are applied to each bridge model, leading to perform several analyses. Finally, the fragility curves are derived as the

probability of exceeding a specified damage limit state under specific ground motion intensity. The curves can be developed by a variety of analytical methods, such as elastic spectral method [61], nonlinear static analysis [62-66], nonlinear time history analysis (NLTHA) [56, 67-73] and (IDA) [27]. In the following, a brief overview of each methodology used to develop fragility curves is explained:

Elastic spectral analysis

The elastic spectral method is one of the least time consuming and simplest methods for developing bridge' fragility curves. Hwang *et al.* [61] employed this method to develop fragility curves for the Memphis bridges. The capacity/demand ratios for each bridge component which have the potential to be damaged under an earthquake are determined according to FHWA [74]. Subsequently, the seismic demand is evaluated based on an elastic spectral analysis according to the specified method as recommended in the AASHTO code [75]. Then, the capacity and demand for each bridge component are calculated. This method has several disadvantages, even though it is one of the simplest to use. It should be noted that this method is selected for the bridges expected to remain in elastic range of behavior. If the bridge response undergo into the nonlinear range, the method fails to accurately predict the demand which in turn makes questionable the reliability of derived fragility function.

Nonlinear static analysis

The limitations of the elastic spectral method can be decreased by using the nonlinear static analysis method [62-66]. The benefit of this procedure is the consideration of the nonlinearity in the computational model. In this method, the nonlinear static pushover analysis is used to calculate the bridge capacity whereas the demand is estimated by scaling a response spectrum. Then by placing the two mentioned curves in the same plot and determining the intersection of the capacity and demand curves, the maximum response of the structure can be determined as shown in Figure 1- 9. The probability of failure is determined for the specific intensity level accounting for uncertainty through a distribution plot over the capacity and demand curves. The fragility curves can be performed by increasing the level of ground motion and associating the response to different damage states. This method is based on the recommendation of the ATC 40 [76] which is developed for buildings. Therefore, the limitation of this method is static analysis,

the lack of information in defining the bridge structure type, and how to use the effect of hysteric damping.

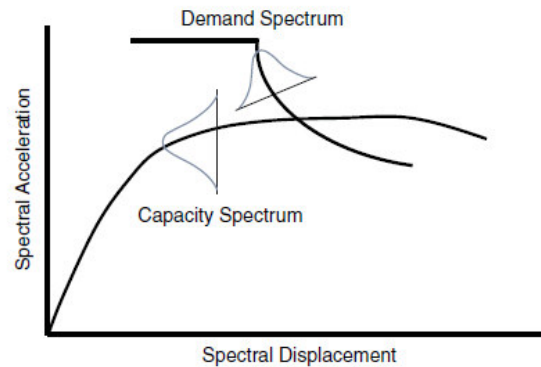


Figure 1- 9: Probabilistic representation of capacity and demand spectra [77]

Nonlinear time history analysis

Nonlinear response history analysis (NRHA) is the most reliable method to develop fragility curves. Although this method has been known as the most computationally expensive method, however fragility curves which are performed with this method are believed to have a better reliability in comparison to the other mentioned methods [57]. This method is popular among previous studies that developed fragility curves [56, 67-73]. First, the major bridge classes are selected as a representative of the most common type of bridges in a specific area. Then, an appropriate suite of earthquake ground motion records is selected. The reliability of the fragility curves largely depends on the selected ground motion records which are used for the time history analyses. Also the selected ground motion should cover all levels of intensities for the selected intensity measure. Then, the nonlinear time history analyses are performed for each bridge sample and for the several ground motions scenarios. Maximum responses of critical components, such as columns which are most important elements in the seismic performance of a bridge, are recorded. Moreover, it can be defined other limit states when considering the seismic response of other critical bridge components. One of the essential parts to develop fragility curves is the definition of the damage limit states that would have a direct impact on reliability of the fragility curves. From this point, expert judgment, experimental data, or analytical models are utilized to define the damage limit states for each bridge components. Finally, analytical fragility curves are performed by using nonlinear response time history

analyses under an important number of seismic scenarios which results allow to estimate each damage limit states accounting for several levels of uncertainty.

Incremental dynamic analysis (IDA)

IDA is a specific type of nonlinear time history analysis that increases incrementally the ground motion amplitudes in order to reproduce the elastic and inelastic bridges behavior. This approach is used aiming to reduce the required several ground motions to generate the fragility curves based on time history analysis. The drawbacks of this method are related to the ground motion in terms of: selection, number, and scale. The selection of these parameters could cause over or under estimations in the estimation of fragility curves.

1.5.4 Hybrid methods

The above mentioned approaches for the development of fragility curves have their own advantages and disadvantages. When combining the advantages of several of these methods that can reasonable work together, we get a reasonable way for the construction of fragility curves. The hybrid method attempts to compensate the drawbacks of other methods such as: subjectivity of judgmental data, inadequate damage data related to past earthquakes, as well as modeling and uncertainties deficiencies of the analytical procedures induced when combining data from different sources [19].

As mentioned before one of the main objectives of this research is to assess the seismic vulnerability of concrete bridges in Iran. One analytical method (e.g., fragility curves) is proposed to obtain the aim of this dissertation. To complete the goal of this study another method which name is non-sampling method based on stochastic analyses is proposed. To clarify the issue instead of considering several non-linear samples, only by utilizing a few samples and selecting appropriate mathematic functions can achieve the same results.

1.6 Stochastic dynamic analysis of concrete bridges

The stochastic theory was developed by several researchers and was applied in different areas of science. The randomness of the seismic action and structural parameters, such as material

properties and boundary conditions of different structures under a stochastic earthquake has been reported by several researchers. Saha *et al.* [78] presented a stochastic response of base-isolated liquid tanks by considering uncertainty in the characteristic isolator parameters under random base excitation. The stochastic response of base-isolated buildings, considering the uncertainty in the characteristics of the earthquakes, was investigated by Jacob *et al.* [79]. In the work of Carrera [80], several numerical examples were investigated by considering a cantilever beam subjected to a tip force with material uncertainty. In this research, a linear oscillator with uncertainties in stiffness and damping subjected to a Gaussian stochastic process was solved using the random vibration theory.

The stochastic seismic response of bridges has been examined by several researchers by considering the uncertainty in earthquake parameters as well as in the system properties. Feng *et al.* [81] proposed stochastic seismic vulnerability analysis and seismic risk evaluation for a super-large cable-stayed bridge, by considering the randomness of the material properties. The analytic hierarchy process was performed by Dabous and Alkass [82] to evaluate the structural importance factors of various bridge elements. The spectral analysis of beam vibration with uncertain parameters under a random train of moving forces, forming a filtered Poisson process is presented by Gladysz *et al.* [83]. In this research, the uncertainties in the natural frequencies of the bridge beam were modelled with fuzzy numbers. Sgambi *et al.* [84] conducted an approach to evaluate the seismic analysis of a long span bridge using Monte Carlo (MC) simulation.

The stochastic probabilistic analyses are categorized into two distinct groups: sampling and non-sampling methods. In comparison to sampling methods, for example the MC simulation, polynomial chaos expansion is a non-sampling approach [85]. Although the results obtained through the MC simulation have a reasonable agreement with the analytical solutions, this method has some limitations. Hence, a large number of simulations are required to achieve reasonable results, which is extremely expensive and time consuming that becomes insufferable when complex systems such as bridges are investigated. Therefore, the sampling stochastic methods, such as the MC simulation techniques, are very expensive from a computational point of view, particularly for huge structure models. Over the last decade, the development of non-sampling stochastic techniques appears to be most widespread due to their strong mathematical basis and capability to produce functional representations of stochastic variability. The

generalized polynomial chaos (gPC) expansion plays a major role in these methods with uncertain parameters, and the structure responses can be characterized by a linear combination of random orthogonal bases. It was first introduced as homogeneous chaos by Wiener [86]. However, the application of the expansion in applied engineering problems was first reported by Ghanem and Spanos [87]. Later the mentioned method was widely applied in the engineering and physical fields [88-91]. Recent works present the advantage of the gPC expansion compared to other methods [e.g., MC simulation, perturbation techniques, Karhunen-Loeve (KL) expansion] for the stochastic finite element approach in uncertainty modelling [92-95]. From the literature review, there is a need for stochastic formulation of bridges under random excitation and uncertain response parameters. As mentioned before, the use of the non-sampling methods in structural analysis has been reported in many works. However, the application of the method for seismic analysis of bridges is very limited.

1.7 Seismic regulations and construction practice

The first seismic design Iranian regulation “Seismic Safety Code for Building” can be traced back to 1967; it was published by the Ministry of Housing and Reclamation after Buein-Zahra earthquake, which killed more than 12000 people. Subsequently, the Planning and Budget Organization published the seismic load calculation procedures for the mentioned code as “Standard No. 519, minimum loads for buildings”. Later, in 1988, the Building and Housing Research Centre (BHRC) published the first edition of the current code namely: Iranian Code of practice for Seismic Resistant Design of Buildings, Standard 2800". Lessons learned from different earthquakes around the world, including Iran, revealed the importance to maintain updated the design code of practice for seismic resistant design of buildings. Later, in 1989, the Ministry of Housing and Urban Planning was bounded by the Iran's government to make a continuous revision of the "Iranian code of practice for seismic resistant design of buildings" every five years. In 1999, the second edition of the Iranian's code was published which had more technical issues and standard safety levels in comparison to the first one [96]. However, the third edition started on December 12th, 2000, and it was published in 2007 [97], while recently the 4th edition has been published. Over the year the officials have worked on the "standard 2800" up to

date a significant development has achieved the most recent version adopted as the official document for the seismic design in Iran.

In 1990, the Iranian Concrete Code of practice for Analysis and Design of building structures, namely: "ABA", was published by the State Management and Planning Organization, publication No. 120, it has been reviewed only once since that date. The ABA code covers all aspects of concrete structures. It has been a goal with special features for other types of structures that have been published as appendices to this code. However, the main focus of the code is buildings. One of the purposes of this code was to publish in appendices certain structural features. The appendix named: "The Code of Practice for the Analysis and Design of Concrete Bridges" was included to the ABA in 2009 under the title of publication No. 389. The code consists of twenty chapters. The first nine chapters explain the general content for the analysis and design as well as material properties, similar to the ABA. Therefore, general issues can be found in the first nine chapters of the ABA whereas the particularities for the bridges are in the remaining eleven chapters (No. 389) [98]. It is desired that the new edition of the Code of Practice would be useful, and it would affect the design and construction practices. The main objective of the recent updates is to avoid disasters and irreparable damages caused by the occurrence of severe earthquakes, like the once happened in Bam and Zarand, Iran. It is noteworthy that old bridges were designed according to the codes used in those dates and regulations whereas the evolution of the Iran regulations started recently to be, therefore the seismic vulnerability of bridges in Iran especially those designed with old codes seems to be necessary.

1.8 Organization of the thesis

This thesis is composed of eight main chapters with the brief contents given as follows:

The first chapter presents the study of the seismicity in a geographical area of interest for this study; it is covered with the different tectonic plates and distribution of probable rupture zones of past earthquakes. The general overview of previous studies and a literature survey developed to generate the bridge fragility curves based on different approaches is described in this chapter as well.

Chapter 2 describes the most common existing ordinary highway bridges and classifies them according to their primary structural characteristics. First of all the review of bridge classification is described due to previous researchers, then the description of bridge inventory and parameters influencing the bridge response are discussed in this chapter.

Chapter 3 explains the 3-D nonlinear analytical models of the sample bridge structures using detailed analytical models for its components. Numerical analyses by considering material properties, detail modeling in superstructure and substructure with taking into account bearing and abutment modelling are described in this chapter.

Chapter 4 is devoted to describe the procedure followed for the selection of earthquake ground motion records that are representative of the different seismic sources.

Chapter 5 addresses aspects related with the definition of damage limit states. In this chapter, a review of the damage states definitions and strategies available in the literature is also made. For this, different types of bridges uncertainties, in terms of column height, lap splice for simply support and integral bridge classification, Connectivity between superstructure substructure, and span length are investigated for the selected case studies. Also, the influence of material properties, namely the compressive strength of concrete and the yield strength of steel is described.

Chapter 6 presents the seismic demands from 3-D nonlinear time history analysis. In this chapter the methodology used to generate the fragility curves are described. The seismic demand is calculated and the results are generated in terms of fragility curves for each bridges class in terms of span length, column height, material properties, connectivity between superstructure and substructure, present of lap splice. Finally fragility curves are developed due to different intensity measures.

Chapter 7 is devoted to assess the stochastic response of a concrete bridge with uncertainty in the parameters of the vertical and shear stiffness for bearings and the longitudinal and transverse stiffness for abutments. The results are compared with sampling method such as Monte-Carlo simulation and non-sampling method such as the collocation method.

Finally, in chapter 8 the main conclusions from the work developed within the present study are drawn.

Chapter 2

2 CLASSIFICATION OF BRIDGES

This study estimates fragility curves for ordinary highway bridges in Iran constructed after the 1980s in order to assess the bridges seismic vulnerability. To achieve the goal, it is necessary to understand the general characteristics of ordinary highway bridges built in Iran according to old design codes. We refer as general characteristics the bridges' geometry in plan and elevation, as well as the structural elements properties since these parameters directly influence the bridges' seismic behavior, these parameters are essential for to estimate fragility curves. When considering a large number of bridges to obtain fragility curves is neither practical nor feasible to do it for each individual bridge since each bridge has its own dynamic properties requiring an important amount of time to lead nonlinear dynamic analyses. Hence, it is difficult to evaluate in detail the seismic performance of each bridge in a large inventory due to all the aleatory variables that affect the problem. Although each bridge has its own structural characteristics, they also have similarities that enable us to group them and with this to reduce the time required for the analyses. Based on this, the bridges in this study are grouped into different classes in terms of their structural characteristics, which are expected to have similar seismic response. Bridge classification allows developing a more refined analytical model for each group bridge of the inventory in order to get a more realistic behavior of the bridges' behavior. It is worth noting that it is not practical to consider every bridge's structural characteristic to classify them because it leads to a large number of bridge classes. The bridge classes not only need to cover every bridge sample in the bridge inventory data, but also must be as small as possible according to the most important variables. Hence, the bridge classes must cover as many bridges as possible and it must be as simple as possible in order to be easily manageable and applicable. The following sections describe in detail the associated bridge inventory data:

2.1 Previous research of bridge classifications

To classify the bridges, structural features that have direct impact on the bridges seismic response have been used as the parameters to characterize the bridge inventory. Previous studies classified the bridges according to different structural properties. In the study of Basöz and

Kiremidjian [1] bridges are classified based on span number, type of superstructure and substructure, material, span continuity and abutment type. For each of the bridge classification empirical damage probability, and consequently fragility curves, were developed based on damage data from the Northridge and Loma Prieta earthquakes [1]. Table 2- 1 presents the bridge classification defined for the study of Basöz and Kiremidjian.

Table 2- 1: Description of bridge sub-categories employed by Basöz and Kiremidjian [1]

Bridge Sub-Category	Abutment Type	Column Bent Type	Span Continuity
Single Span Bridges			
C1S1	Monolithic	Not applicable	Not applicable
C1S2	Non-monolithic	Not applicable	Not applicable
C1S3	Partial integrity	Not applicable	Not applicable
Multiple Span Bridges			
C1M1	Monolithic	Multiple	Continuous
C1M2	Monolithic	Multiple	Discontinuous
C1M3	Monolithic	Single	Continuous
C1M4	Monolithic	Single	Discontinuous
C1M5	Monolithic	Pier wall	Continuous
C1M6	Monolithic	Pier wall	Discontinuous
C1M7	Non-monolithic	Multiple	Continuous
C1M8	Non-monolithic	Multiple	Discontinuous
C1M9	Non-monolithic	Single	Continuous
C1M10	Non-monolithic	Single	Discontinuous
C1M11	Non-monolithic	Pier wall	Continuous
C1M12	Non-monolithic	Pier wall	Discontinuous
C1M13	Partial integrity	Multiple	Continuous
C1M14	Partial integrity	Multiple	Discontinuous
C1M15	Partial integrity	Single	Continuous
C1M16	Partial integrity	Single	Discontinuous
C1M17	Partial integrity	Pier wall	Continuous
C1M18	Partial integrity	Pier wall	Discontinuous

The ATC-13 [54] has a bridge classification as function of the total bridge length, however in the classification developed by the Federal Highway Administration (FHWA) [99], bridges are grouped based on the superstructure type, material and the continuity at supports. Table 2- 2 presents some possible construction types and materials based on the National Building Inventory (NBI) in US.

Table 2- 2: Some construction material and construction types according to the NBI [99]

Construction Material	Construction Type
Concrete	Slab
Concrete Continuous	Stringer/Multi-beam or Girder
Steel	Girder and Floor beam System
Steel Continuous	Tee Beam
Pre-stressed Concrete	Box Beam or Girders –Multiple
Pre-stressed Concrete Continuous	Box Beam or Girders –Single or Spread
Timber	Frame
Masonry	Orthotropic
Aluminum, Wrought Iron, or Cast Iron	Truss – Deck
Other	Truss – Thru
	Arch – Deck
	Arch – Thru
	Suspension
	Stayed Girder
	Movable – Lift
	Movable – Bascule
	Movable – Swing
	Tunnel
	Culvert
	Mixed Types(applicable only to approach spans)
	Segmental Box Girder
	Channel Beam
	Other

HAZUS (FEMA, 2003) [37] considers a bridge classification in terms of the span number, abutment type, bearing type, pier type and seismic design strategy. Several parameters that have a direct impact on the damage quantification, used to estimate the fragility curves, are considered in the mentioned classification. Defining a total of 20 bridge classes (HWB1 through HWB20) described in Table 2- 3. In the classification developed by Nielson [100], 11 bridge classes are considered based on construction type, construction material and the span number (Table 2- 4). However, Avsar *et al.* [101] proposed 4 major bridge classes in terms of column bent number and skew angle (Table 2- 5).

Table 2- 3: Bridge classification scheme based on HAZUS (FEMA, 2003) [37]

Class	State	Year Built	Design	Description
HWB1	Non-CA	< 1990	Conventional	Major Bridge - Length > 150m
HWB1	CA	< 1975	Conventional	Major Bridge - Length > 150m
HWB2	Non-CA	≥ 1990	Seismic	Major Bridge - Length > 150m
HWB2	CA	< 1990	Seismic	Major Bridge - Length > 150m
HWB3	Non-CA	< 1990	Conventional	Single Span
HWB3	CA	< 1975	Conventional	Single Span
HWB4	Non-CA	≥ 1990	Seismic	Single Span
HWB4	CA	≥ 1975	Seismic	Single Span
HWB5	Non-CA	< 1990	Conventional	Multi-Col. Bent, Simple Support – Concrete
HWB6	CA	< 1975	Conventional	Multi-Col. Bent, Simple Support – Concrete
HWB7	Non-CA	≥ 1990	Seismic	Multi-Col. Bent, Simple Support – Concrete
HWB7	CA	≥ 1975	Seismic	Multi-Col. Bent, Simple Support – Concrete
HWB8	CA	< 1975	Conventional	Single Col. Box Girder - Continuous Concrete
HWB9	CA	≥ 1975	Seismic	Single Col. Box Girder - Continuous Concrete
HWB10	Non-CA	< 1990	Conventional	Continuous Concrete
HWB10	CA	< 1975	Conventional	Continuous Concrete
HWB11	Non-CA	≥ 1990	Seismic	Continuous Concrete
HWB11	CA	≥ 1975	Seismic	Continuous Concrete
HWB12	Non-CA	< 1990	Conventional	Multi-Col. Bent, Simple Support – Steel
HWB13	CA	< 1975	Conventional	Multi-Col. Bent, Simple Support – Steel
HWB14	Non-CA	≥ 1990	Seismic	Multi-Col. Bent, Simple Support – Steel
HWB14	CA	≥ 1975	Seismic	Multi-Col. Bent, Simple Support – Steel
HWB15	Non-CA	< 1990	Conventional	Continuous Steel
HWB15	CA	< 1975	Conventional	Continuous Steel
HWB16	Non-CA	≥ 1990	Seismic	Continuous Steel
HWB16	CA	≥ 1975	Seismic	Continuous Steel
HWB17	Non-CA	< 1990	Conventional	Multi-Col. Bent, Simple Support - Pre-stressed Concrete
HWB18	CA	< 1975	Conventional	Multi-Col. Bent, Simple Support – Pre-stressed Concrete
HWB19	Non-CA	≥ 1990	Seismic	Multi-Col. Bent, Simple Support – Pre-stressed Concrete
HWB19	CA	≥ 1975	Seismic	Multi-Col. Bent, Simple Support – Pre-stressed Concrete
HWB20	CA	≥ 1975	Conventional	Single Col., Box Girder – Pre-stressed Concrete

Table 2- 4: Bridge classes defined by Nielsen [100]

Bridge Class Name	Abbreviation
Multi-Span Continuous Concrete Girder	MSC Concrete
Multi-Span Continuous Steel Girder	MSC Steel
Multi-Span Continuous Slab	MSC Slab
Multi-Span Continuous Concrete Box Girder	MSC Concrete-Box
Multi-Span Simply Supported Concrete Girder	MSSS Concrete
Multi-Span Simply Supported Steel Girder	MSSS Steel
Multi-Span Simply Supported Slab	MSSS Slab
Multi-Span Simply Supported Concrete Box Girder	MSSS Concrete-Box
Single-Span Concrete Girder	SS Concrete
Single-Span Steel Girder	SS Steel
Others	

Table 2- 5: Bridge classes defined by Avsar *et al.* [101]

Bridge Class Name	Abbreviation
Multi span, multiple column, skew less than 30°	MS-MC-SL30
Multi span, multiple column, skew greater than 30°	MS-MC-SG30
Multi span, single column, skew less than 30°	MS-SC-SL30
Multi span, single column, skew greater than 30°	MS-SC-SG30

2.2 Description of Bridge Inventory

A list of the bridge inventory is needed in order to achieve the main goal of this work. However, detailed information for all the existing bridges such as material properties, structural type, location, year of construction, local soil site properties, is not available; therefore, the bridge inventory is built with 56 representative bridges built in Iran in the 1980s. Although the selected bridges in the inventory do not cover all the bridge types built in the country, they are representative bridges of the most common built in Iran. The selected 56 bridges are defined as Ordinary Standard Bridges according to Caltrans [44]:

- Span lengths smaller than 90m
- Constructed with normal weight concrete girder, and column or pier elements
- Horizontal members supported on conventional bearings
- There are no nonstandard components such as: dropped bent caps, outrigger bents; offset columns; isolation bearings or dampers
- Foundations supported on spread footing or pile cap with piles
- Soil that is not susceptible to liquefaction, lateral spreading, or scour

In this study, the bridges which do not cover the requirements defining the ordinary standard bridges according to Caltrans [44] are not considered, being out of the dissertation scope since their seismic response have important changes in comparison to the ordinary highway bridges, therefore they have to be considered individually. Figure 2- 1 shows schematic drawings of the

components of simply supported and integral bridges. All the selected bridges are assumed to be straight.

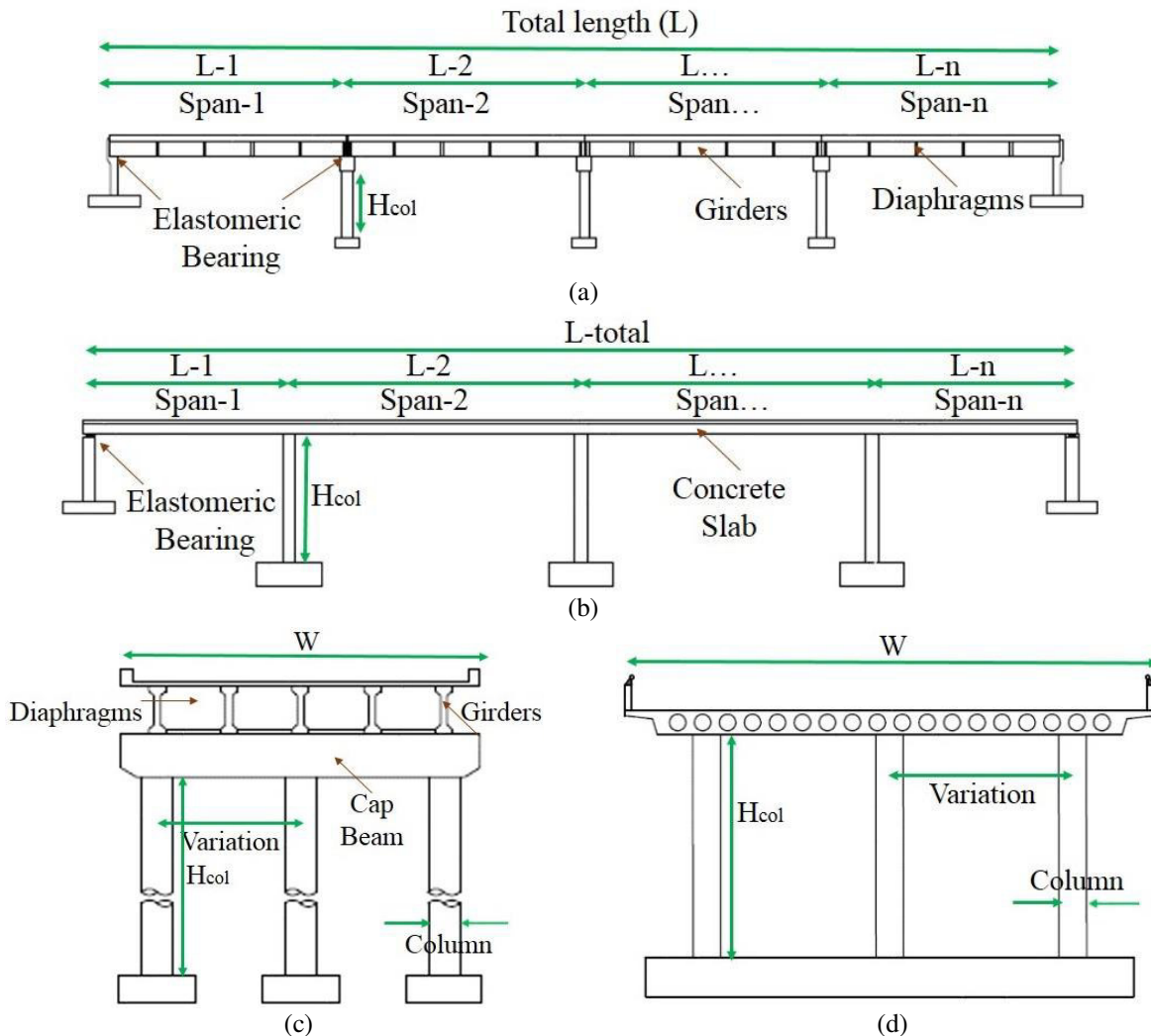


Figure 2- 1: General geometry of (a) simply supported bridge, (b) integral bridge, (c) transverse view of simply supported bridge and (d) transverse view of integral bridge

In the past decades, continuous bridges have become a popular alternative to common bridges designed with expansion joints [102]. Although the construction of integral bridges in recent decades is growing, the implementation of these bridges in some countries is limited due to technical issues and existing regulations [103]. Therefore, to achieve a better expected performance of the bridges at a variety of damage limit states, it is necessary to assess the seismic risk. One of the most important advantages of continuous bridges is the elimination of expansion joints, which reduces maintenance costs during the structure life. The installation and maintenance of the expansion joints are expensive and sometimes the replacement is even more

costly. Another advantage of continuous bridges is the avoidance of corrosion problems, which are frequently present in expansion joints and seals that permit salt-laden run-off water from the roadway surface to make contact with the substructure elements. Many problems may originate from leaky joints [104]. In addition, elastomeric glands can be filled up by trash, clods, and little stones and fail to function properly. Furthermore, steel bearings can be exposed to corrosion and elastomers can split or rupture due to sudden and unpredictable movements [105]. Hence, continuous bridge construction provides better durability performance and lower bridge operating costs. Moreover, the reduction of joints in bridge structures leads to substantial savings in the costs of construction and maintenance. In particular, the number of bearings in each pier is substantially reduced when compared with the case of simply supported multiple-span decks. It should be noted that greater demands may be transferred from superstructure to substructure in continuous systems [106].

Another advantage of continuous bridges is the elimination of the unseating superstructure problem. Moreover, the moment-resisting connection between superstructure and substructure offers enhanced redundancy in the bridge and the energy dissipation capability is increased by increasing the number of plastic hinges required to form a collapse mechanism. Previous researchers provide different approaches to evaluate the seismic performance of bridges with different types of superstructures [25, 69, 101]. Only a few studies have been carried out to compare the seismic performance of simply supported bridges with continuous structures subjected to different seismic sources [25, 72]. It is important to consider this comparison during the design and construction process of the bridges. Therefore in this research this type of bridges is selected and seismic vulnerability of integral bridges subjected to two seismic sources are considered.

2.3 Parameters influencing the bridges response

The statistical parameters for the most common bridges designed with old codes in Iran were determined. In the following subsection, a statistical analysis is presented through the construction of histograms for the structural characteristics of interest of this work.

2.3.1 Span number

All the bridges selected for this research are multiple-span simply supported and integral bridges. Since the single span bridges are seismically less vulnerable when compared to the multiple-span bridges, single span bridges are neglected and are not considered in this research [17, 74]. Figure 2- 2 shows that an almost uniform distribution can be considered to define the law variation for the span number. However, in this study only the bridges with 4 to 7 spans are considered.

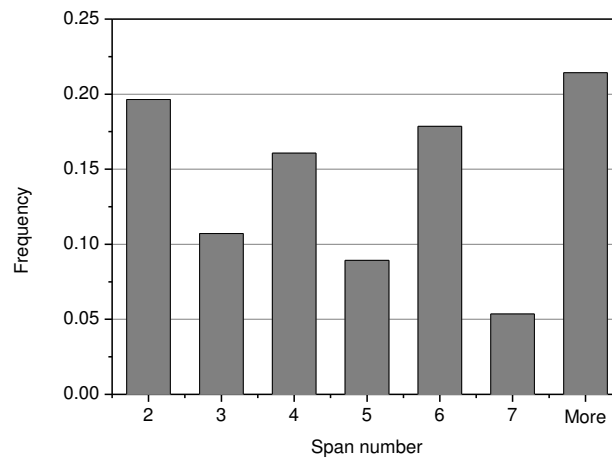


Figure 2- 2: Frequency distribution for the span number

2.3.2 Skew angle

Skew angle is the angle between the line perpendicular to the bridge center line and the center line of the bridge substructure. The effect of skewness on the seismic response of bridges is very significant, and it should be taken into consideration when estimating the actual seismic behavior of the highway bridges. In this bridge inventory, more than 50% of bridges have a skew angle less than 5° , as shown in Figure 2- 3. Therefore, the effect of skew angle can be neglected.

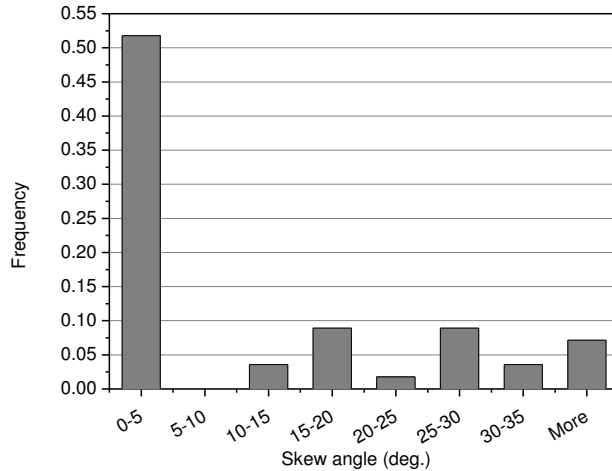


Figure 2- 3: Frequency distribution for the skew angle

2.3.3 Maximum and total span length

The maximum span length varies between 20 m to 40 m, as shown in Figure 2- 4 (a), since some of the bridges do not have a constant span length, maximum span length is obtained at the intermediate span. The superstructure mass is between the 85 to 90 percent of the total mass of the bridge. Because the mass and span length depends to each other, the dynamic behavior of the bridge systems is directly influenced by the maximum span length of the bridge. To accurately evaluate the seismic response of bridges, in this study, the variation of bridge characteristics are considered and divided in three in terms of the maximum span length: (a) bridges which have span length less than 20 m, (b) bridges which have span length between 20 m and 30 m, and (c) bridges which have span length larger than 30 m. The mentioned classification was considered due to the frequency distribution of the maximum span length, as well as superstructure type which is explained in detail in the following tasks. Figure 2- 4 (b) presents the variation of the total length of the bridges from 40 m to 240 m. However, the most important variation is in the range of 40 m to 140 m.

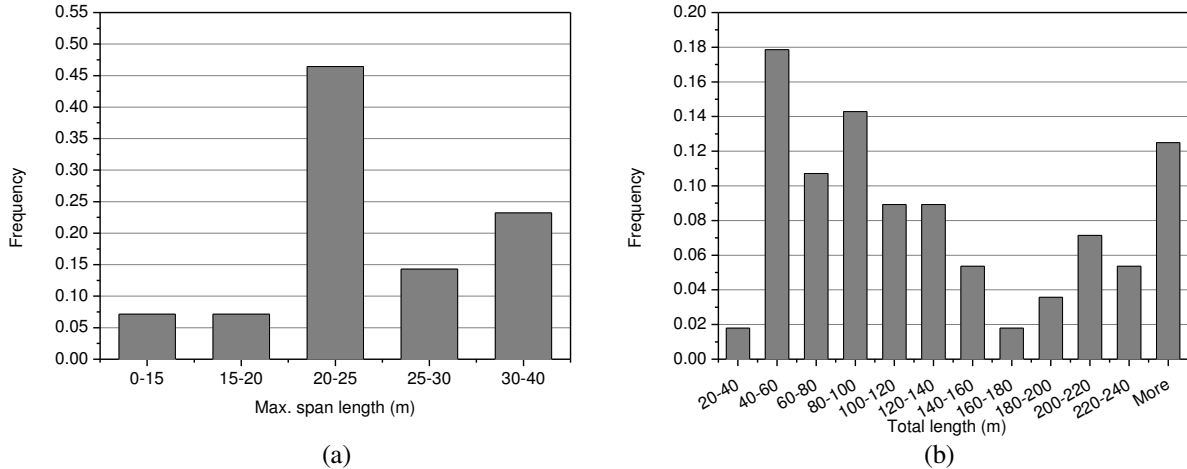


Figure 2- 4: Frequency distribution for (a) the maximum span length, (b) the total length

2.3.4 Column height and bent column number

Column height variation in the data is between 4 m to 22 m, as Figure 2- 5 (a) shows. Column height is determined from the top of the foundation or pile cap to the bottom surface of the cap beam. Most of the bridges have column height ranging between 4m to 12m and 18m to 20m. In addition, multi-column bents have different number of columns per bent. In Figure 2- 5 (b) is noticeable that the majority of bridges have 2 or 3 columns per bent. With respect to these variables, in this study, the bridges are classified according to the columns height as short columns and high columns and with have 2 or more columns per bent. A subdivision is made based on the superstructure type that is classified as simply or integral. In this classification, bridges are divided in several groups whose details are described in the following section.

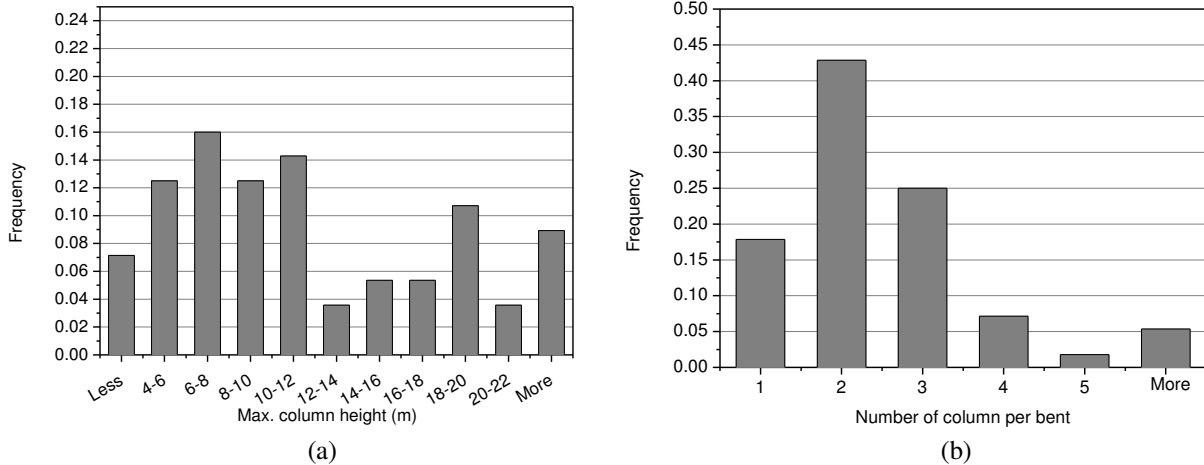


Figure 2- 5: Frequency distributions of (a) the columns height, (b) the number of columns per bent

2.3.5 Superstructure girder spacing

More than twenty five percent of bridges in the database compiled have 6 girders, as shown in Figure 2- 6. Diaphragms are located at the intermediate locations as well as at the end of the girders. The superstructure mass has an important contribution to the seismic response of the bridges, especially in this type of structures where an excessive number of the girders exist.

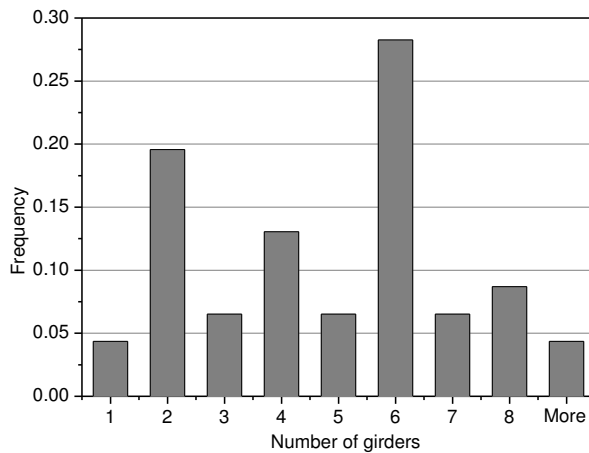


Figure 2- 6: Frequency distribution of number of girders

2.3.6 Bridge deck width

More than forty percent of the bridges have a total bridge deck of 10 m to 15 m and its distribution resembles a normal distribution, as Figure 2- 7 shows. The width of the bridge is function of the number of traffic lanes in the highway.

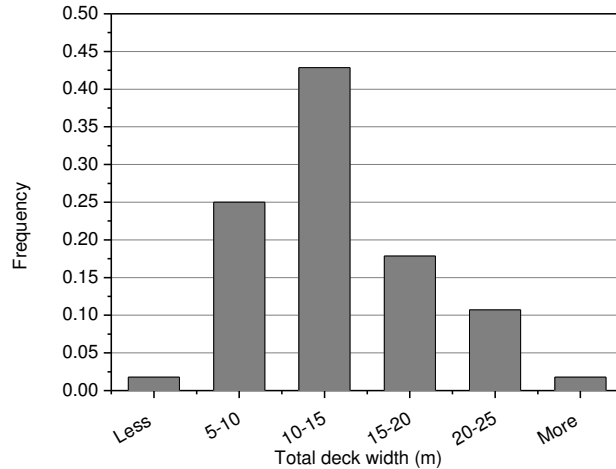


Figure 2- 7: Frequency distribution of total deck width

2.4 Major bridge classes

Important structural characteristics of the highway bridges are identified to select the major bridge classes. It is not proper to consider all the structural features for the selection of the major bridge classes, therefore most noteworthy bridge structural attributes that significantly affect the seismic response of the bridges have to be specified. As mentioned before, span and total length, superstructure types, bent column number and column height can be consider among the most important bridge structural attributes. Previous researchers such as Basöz and Kiremidjian, HAZUS (FEMA, 2003), and Nielson considered multi-span or single-span bridges [1, 37, 100]. As mentioned previously, single-span bridges are not taken into account in this study, all type of bridge classification are multi-span bridges. The frequency distribution of Figure 2- 8 shows that the majority of bridges have circular cross-section, based on this, in this study the fragility curves are developed for circular column bridges. Table 2-6, shows structural attributes for the bridge samples for each major bridge class in terms of section. In this study, since the 56 bridge inventory is not covered all existing bridges in Iran, also due to the importance of integral bridges, seismic vulnerability of simply support bridges and integral bridges are investigated. Also in Table 2- 7 bridges are classified in two major groups in terms of superstructure connectivity namely: circular column- integral bridge (CC-I) and circular column- simply supported (CC-S).

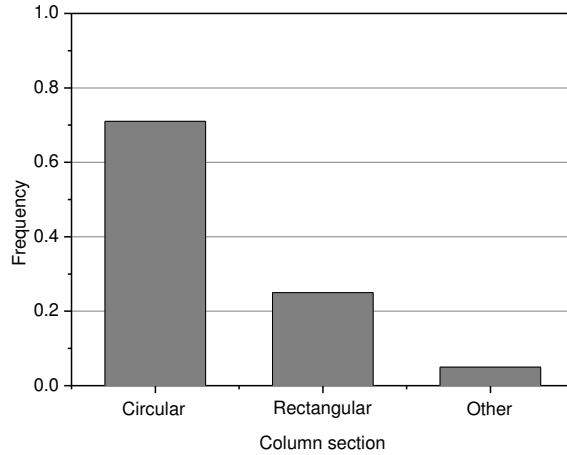


Figure 2- 8: Frequency distribution for the columns cross section

Table 2- 6: Structural attributes for the bridge samples for each major bridge class in terms of section

Bridges	Percentage (%)
Simply support-circular column	53
Simply support-rectangular column	8.4
Continues with bearing- circular column	8
Continues with bearing- rectangular column	6.3
Continues without bearing- circular column	9.5
Continues without bearing- rectangular column	8.7
Other	5

Table 2- 7: Two major bridge classes in terms of superstructure type

Bridge classes	Abbreviation
circular column- Integral	CC-I
circular column- simply supported	CC-S

In terms of column height, bridges are classified in two main groups: short column and high column. In the study of Avsar *et al.* [101] bridges are selected with height variation between 4 m to 10 m, however Nielson *et al.* [100] selected bridges with 3 m to 6 m. In this study, as can be seen in Figure 2- 5 (a) the column height ranges between 4 m and 12 m and between 18 m to 20 m, for what the range of column heights is selected as 4 m to 20 m. The mean value of column height is 11.6 m, thus, the bridges with column height shorter than 12 m are named short column and the bridges with column height higher than 12 m are named with high columns.

Table 2- 6 reveals that the majority of the bridges are simply supported with circular columns. Therefore, for the family of simply supported bridges, they are classified into 2 major groups in terms of column height as presented in Table 2- 8.

Table 2- 8: Definition of the bridge classes in terms of the column height

No.	Bridge classes	Abbreviation
1	Short circular column-simply supported	SCC-S
2	High circular column-simply supported	HCC-S

Depending on the superstructure type, the bridges are classified into different categories [25, 37, 69, 101]. As depicted in Figure 2- 9 most of the bridges with superstructure length less than 20 m are constructed with slab superstructure type, while bridges with SL between 20 m and 30 m have superstructure conformed by I-girders. Around 50% of the bridges that have span length larger than 30 m have a box girder type superstructure. In this work, bridges are classified in 3 different groups that consider the span length and the superstructure type that are defined as: with SL lower than 20 m and slab superstructure type, SL between 20 m and 30 m, and I-girder superstructure type and SL with more than 30 m with box girder superstructure as described in Table 2- 9. Three major bridge classes were determined based on the primary structural attributes mentioned above. Real bridges were selected as case studies, assuming for their selection the class type in terms of the span length. In this study bridges are classified in function of the: (a) superstructure connectivity as simply support or integral bridge, (b) column height: short column and high column, (c) span length and superstructure type. In the following chapter each of the classes will be described in detail. In this study the information collected from the considered surveys includes the compressive strength of concrete, steel yield stress, and ultimate stress of different components, are explained in Table 2- 9. For other cases, namely bridges without information on the material properties, we assume the average values. Figure 2- 10 shows characterization procedures and sampling.

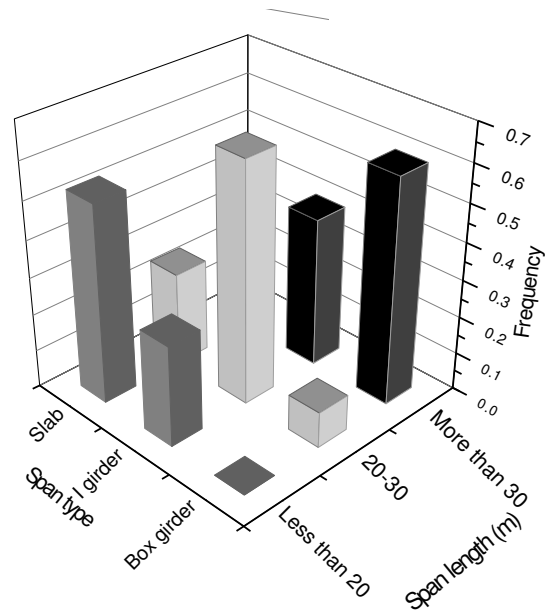


Figure 2- 9: Frequency distribution of superstructure type and span length

Table 2- 9: Structural attributes for the bridge samples for each major bridge class in terms of span length

No.	Bridge classes	Abbreviation
1	Multi span-span length less than 20 m	SL<20
2	Multi span-span length between 20 m and 30 m	20≤SL<30
3	Multi span-span length more than 30 m	SL≥30

Table 2- 10: Material properties for the bridge samples for each major bridge class

	f'_c (col) MPa	f'_c (cap beam) MPa	f'_c (girder) MPa	f_{ye} (bar) MPa	f_{su} (bar) MPa
Max	32	27	28	530	679
Min	19.5	24	16	252	344
Avg.	24.5	24.6	24.8	420	550

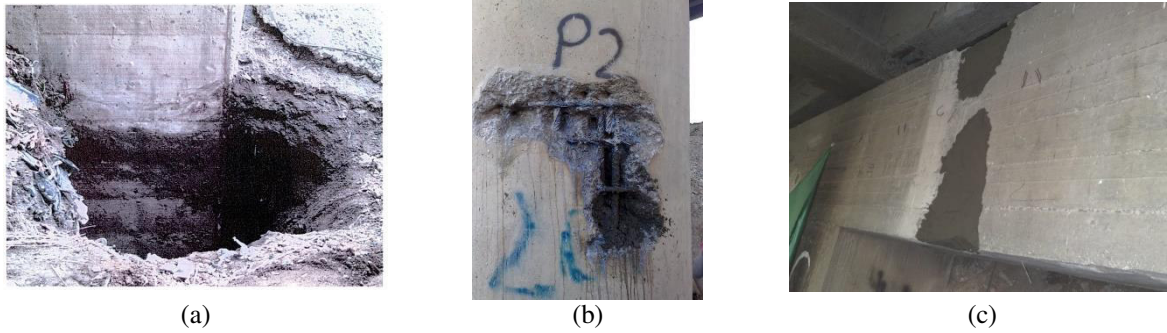


Figure 2- 10: Characterization procedures and sampling, a) soil around the abutment to obtain the abutment dimension, b) longitudinal and transversal reinforcements, c) Facial reconstruction after the procedures

2.5 Bridge samples for the major bridge classes

In this study fragility curves for different bridge classes will be generated. Fragility curves relate strong motion severity to the probability of reaching or exceeding a certain limit state [51]. The main objective of this study is to develop fragility curves for the ordinary highway bridges designed and constructed according to pre-1990 code regulations in Iran. It is noticeable that for the selected bridges, the fragility curves will represent the appropriate level of the structural variability. Therefore, the reliability of fragility curves depends on the selection of sample size and the structural variability. An insufficient sample size not only enhances the sensitivity of the fragility curves, but also leads to important modelling and computational efforts making the process complicated and time consuming. As in previous studies, for each major bridge class, different samples are generated. Shinozuka *et al.* [107] considered ten sample bridge classes, while six samples were analyzed by Choine *et. al* [72]. In the study of Banerjee and Shinozuka [62] only three cases of study were considered to develop the fragility curves. Nielson considered eight sample case studies for each bridge classification [100]. In this study, for each major bridge classification from three to four real bridges are considered as case studies.

Chapter 3

3 NUMERICAL ANALYSES

To perform analytical fragility curves, numerical analyses of the bridge samples are developed by considering a proper structural component model. The performance of individual components and the connectivity among them are of relevant importance on the seismic response of any highway bridge. Analytical analyses are performed by the consideration of certain assumptions and simplifications into the model that have a direct influence on the seismic response and on the reliability of the bridges fragility curves. Therefore, special attention is required on the process of modelling for the simplification of parameters. However, the consideration of a very detail and complicated bridge analytical model not is the best option because not only it is time consuming, but also it leads to an unrealistic analytical model that can be out of control. Hence, analytical models have to be as simple as the model can be represented, and the time required for analysis should not be excessive. Finally, it should be noted that the selection of the correct model to estimate the seismic response of a bridge is the most important criterion to define along the modeling process. Figure 3- 1 presents schematically different levels of modeling a bridge for seismic analysis [108], the models can be as simple as a single degree of freedom system, lumped-mass models, or as complicated as can be detailed finite-element models.

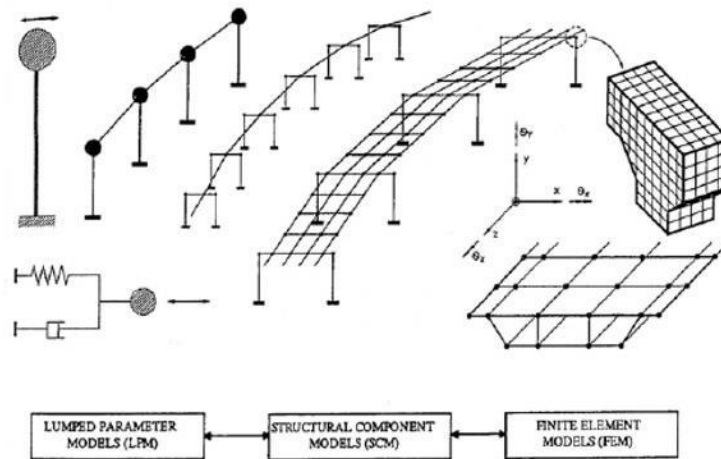
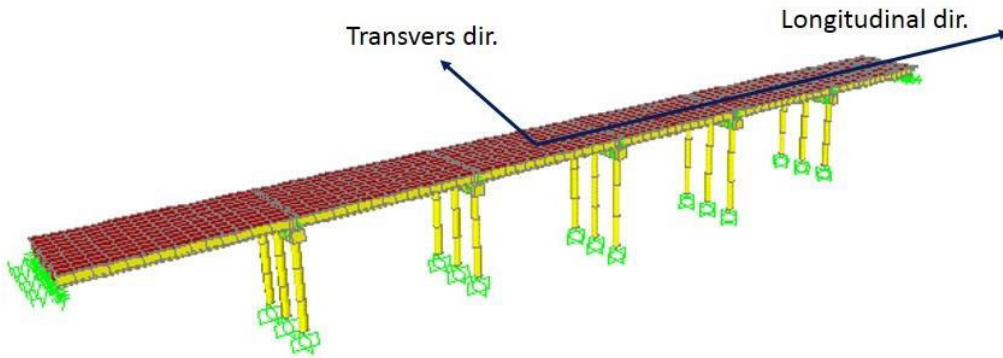


Figure 3- 1: Levels of modeling for seismic bridge analysis [108]

For the lumped-parameter models, structural properties such as stiffness, mass and damping are concentrated or lumped at specific locations. Although this type of models is simple in the fundamental concepts required it is important to remark that knowledge and experience are key elements to present the real seismic behavior of the bridges. A structure is discretized with a large number of small elements which are expected to perform according to their materials' constitutive laws. The geometric discretization and the time necessary for the structural analyses increase properly from the lumped-parameter models to the structural component models, and to the finite-element models. Although, the structural modelling needs extensive effort in terms of the characterization of individual members, significant definition and engineering judgment are required for the structural component and lumped-parameter models. To quantify the seismic response of bridges, numerical analysis computation effort and the time required depend on the analysis tool selected which ranges from linear elastic analyses to nonlinear dynamic time history analyses. The ATC-32 [109] classify the analyses into elastic static, elastic dynamic, inelastic static and inelastic dynamic analyses. Among the analyses, the nonlinear time history has some deficiencies such as converge problems, and require extensive amount of run time and post processing efforts, but it is considered as the most accurate simulation tool due to the nonlinear component characterization and seismic excitation. In this study, the nonlinear time history analysis is utilized for the structural system to estimate the seismic response of bridges. Figure 3- 2 presents one of the simply support bridges with 3-D analytical model of a bridge representative of a common simply support type of bridges in Iran by considering longitudinal and transvers directions.



(a)



(b)

Figure 3- 2: (a): Picture of example highway bridge,(b): Longitudinal and transverse directions in the bridge modeling

Previous studies mentioned that longitudinal direction is critical on the bridge seismic performance [110, 111], however other studies reported that seismic performance is often controlled by transverse direction [112, 113]. Damage in the bridge columns may occur due to large displacements in transverse direction, in the form of shear failures, plastic hinges or lap splice failures. To simulate the combined response of the bridge in longitudinal and transverse directions, 3-D models are required to capture the entire bridge system response and individual components under specific seismic demand characteristics [61, 100, 114]. In 3-D models, variations in the axial load at columns and the interaction between the responses in two orthogonal directions can be captured more accurately. This enables to a correct evaluation of the

capacity and ductility of the system under seismic loads or displacements applied along any given direction that not necessarily must be aligned with the principal axis of the bridge.

3.1 Modeling of bridge components

3-D analytical model of the bridges is performed by considering structural components. As mentioned before the seismic behavior response of highway bridges is influenced by the performance of individual components and the connectivity among them. Generally, superstructure and substructure can be considered as structural components. The superstructure is composed of cast-in place reinforced concrete girders whereas the bent system and abutments constitute the substructure of the bridge. Elastomeric bearings are located between the substructure and superstructure as an isolation unit. Figure 3- 3 presents the 3-D analytical model of a bridge representative of a common type of bridges in Iran. Link elements modelled as fixed springs are used to locate the exact position of the bearings. Rigid elements are utilized at the rigid zone of the cap beams, columns and superstructure ends connections. One of the important issues that should be considered is the selection of a realistic value for the stiffness of rigid members. If low stiffness values are assumed for rigid elements, these cannot represent accurately in the analytical models. If a large elastic stiffness is selected, the model can present numerical problems to converge. To minimize numerical problems, according to Wilson [115], the stiffness of rigid elements should not be 100 times over than adjacent elements. Therefore, stiffness of the rigid elements is specified accordingly. In the following sections, the analytical modelling for substructure and superstructure are described in detail.

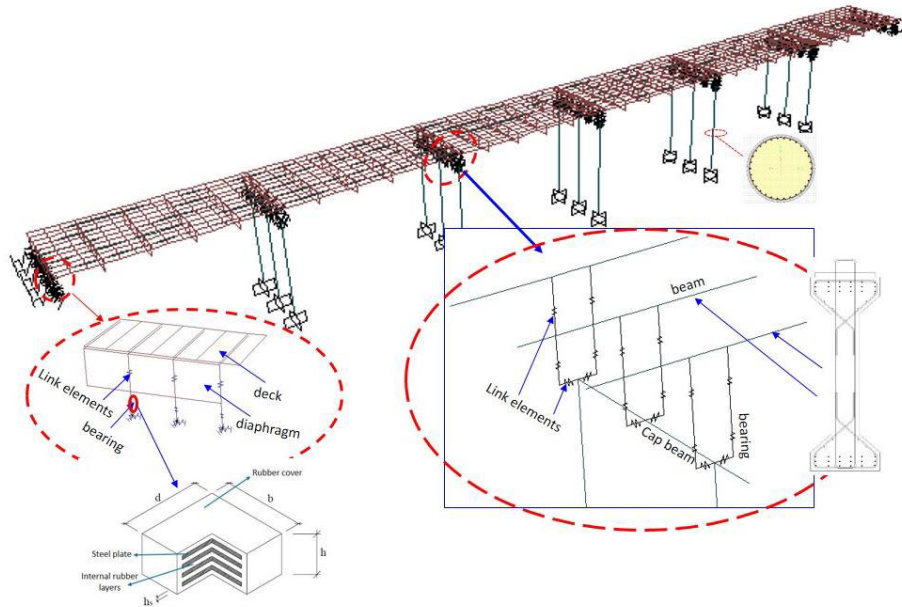


Figure 3- 3: Three-dimensional finite-element model

3.2 Material properties

The mechanical properties of the structural material play an important role in the seismic performance of bridges. Thus, variations in the mechanical properties of the materials should be considered during the fragility analysis. It is noted that the variations in material strengths have effects on both the strength and stiffness of a bridge [57]. The information collected during different surveys includes the compressive strength of concrete and the yield strength of longitudinal bars. Table 2- 10 presents the results from a statistical analysis of material properties.

It is important to remark that the nonlinear behavior of the structure is obtained directly from the nonlinear stress-strain relationship of concrete and steel, therefore the reliability of nonlinear bridge members depends on the accuracy of the material properties considered. Reinforcing steel bars are modeled utilizing bilinear steel material model with kinematic hardening behavior shown in Figure 3- 4, according to the Caltrans recommendation [44]. As mentioned before, for each real case of study, the yield and ultimate strength assumed correspond to real values measured from experimental tests reported in Table 2- 10. For the models which we do not have any information, average values are utilized. Modulus of elasticity is given as 200 GPa, nominal

yield strain (ϵ_y) and expected yield strain (ϵ_{ye}) are considered as 0.0021 and 0.0023, respectively, the ultimate tensile strain (ϵ_{su}) which is bar size dependent is determined as 0.12.

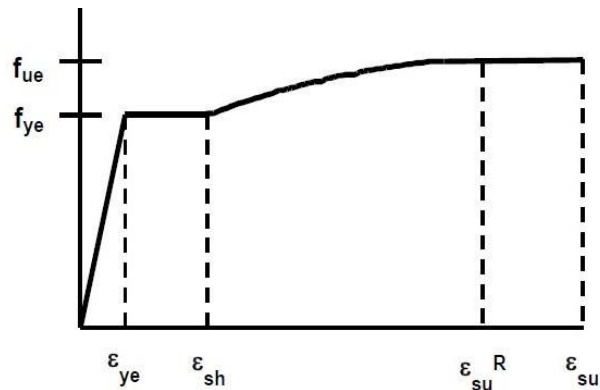


Figure 3- 4: Steel Stress-Strain Model

The effect of confinement is to enhance the compression strength and ultimate stress on concrete, as illustrated in Figure 3- 5. For the confined concrete, previous researchers developed different stress-strain relationships [116-119]. Some of the proposed methods have restriction in the range of condition (e.g., circular or rectangular sections), however the method suggested by Mander *et al.* [118] is applicable to all section shapes and all levels of confinement according to equations (3.1) – (3.6). Note that tensile strength of concrete members is neglected. In this study, for the columns the definition of confined and unconfined concrete strength parameters are estimated using the approach described by Mander *et al.* [118].

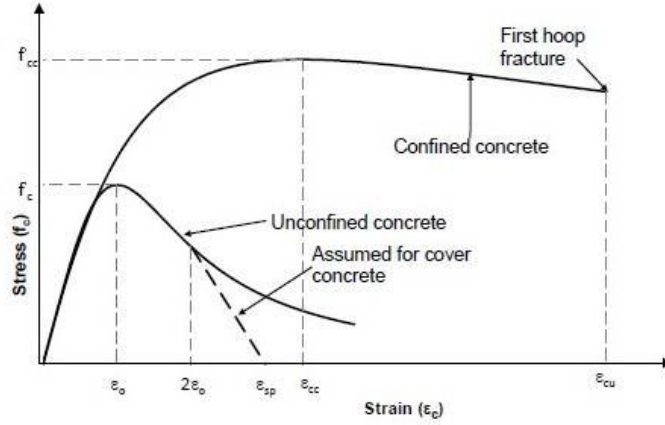


Figure 3- 5: Material models for confined and unconfined concrete

$$f'_{cc} = f'_c \left(2.254 \sqrt{1 + \frac{7.94 f'_l}{f'_c}} - \frac{2 f'_l}{f'_c} - 1.254 \right) \quad (3.1)$$

$$\varepsilon_{cc} = 0.002 \left(1 + 5 \frac{f'_{cc}}{f'_c} - 1 \right) \quad (3.2)$$

$$\varepsilon_{cu} = 0.004 + \frac{1.4 \rho_s f_{yh} \varepsilon_{su}}{f'_{cc}} \quad (3.3)$$

$$\rho_s = \frac{4 A_h}{D' s} \quad (3.4)$$

$$f'_l = \frac{1}{2} k_e \rho_s f_{yh} \quad (3.5)$$

Where f'_{cc} and ε_{cc} are concrete stress and strain at peak stress, f'_l is the effective lateral confining stress and ε_{cu} is the ultimate compression strain respectively. f_{yh} is the yield strength of the transverse reinforcement, ε_{su} is the steel strain at the maximum tensile stress, f'_{cc} is the compressive strength of the confined concrete, ρ_s is the volumetric ratio of confining steel, A_h is the cross-sectional area of transverse reinforcement, D' is the diameter of the confined concrete

core, k_e is confinement coefficient, ρ_{cc} is ratio of area of longitudinal reinforcement to area of core of the section, d_s is diameter of spiral, and s is the longitudinal spacing of hoops or spirals.

3.3 Superstructure

The mass of the bridges is provided from reinforce concrete girders, slab, diaphragms, parapets, and weight of asphalt and sidewalks. Truck loads are not taken into account in the bridges' seismic response calculations [120]. The superstructure is expected to remain in the elastic range without experiencing any seismic damage [47]. Frame elements with six degrees of freedom at each node are used to model the columns, bent caps, and girders; the deck and diaphragms are modelled with shell finite elements. Modulus of elasticity (E_c) for normal weight concrete and Shear modulus, G_c , for $\nu = 0.2$ are determined through equations (3.7) and (3.8) [75, 108].

$$E_c = 5000\sqrt{f_c} \text{ (MPa)} \quad (3.7)$$

$$G_c = \frac{E_c}{2(1 + \nu)} \quad (3.8)$$

From 85 to 90 percent of the bridge total mass is constituted by the superstructure mass [121]. To estimate the actual seismic behavior of the bridges, vertical rigid elements are defined between the superstructure mass and the substructure components in order to calculate accurately the superstructure mass. In addition, the mass of the asphalt cover is considered as 21.56 kN/m^3 . For modelling the mass distribution through the element length, the superstructure and the piers, the elements are divided into a sufficient number in small segments.

3.4 Substructure

Bents consist of cap beam and columns, or only columns, depending on the bent column number. The bent system is stiffer in transverse direction because of the frame action. Bents, columns, and cap beams are modelled with frame elements defined with six degrees of freedom at each node. The model accounts for the material nonlinearities in elements at columns and rigid links, defined at the rigid zones, as shown schematically in Figure 3- 6. The members correspond to the line elements passing through the cross section center of the members. The connections of the members are model through rigid elements in order to account for rigid end zone matter. About 10 to 15 percent of the total bridge mass corresponds to the mass of substructure components. The masses of cap beams and columns are assumed as lumped at their adjoining nodes according to their tributary area. According to Caltrans [44] concrete components such as cap beams and superstructures remain essentially elastic when the column reaches its over strength capacity, which is very beneficial and practical for the maintenance and retrofit purposes. Since in this study the column inertia ratio is less than the cap beams therefore cap beams assumed to be in elastic area. The effect of cap beam to column inertia ratio on the transverse response of multi column bridge bents has a considerable impact on the seismic behavior of the bridge [122]. When the columns are stronger than the cap beams, plastic hinges initiate at the cap beam. However in the case of weak-cap beam the plastic hinges place in cap beam before the column reaches its over strength capacity, therefore seismic damage can localize in the cap beam which lead to lower displacement ductility capacity in the transverse direction. On the other hand when the cap beam become rigid the yield displacement is the resulting from column flexibility, however cap beam flexibility increase the yield displacement, but will not influence in additional plastic displacement, because this is provided by column hinge rotation [108].

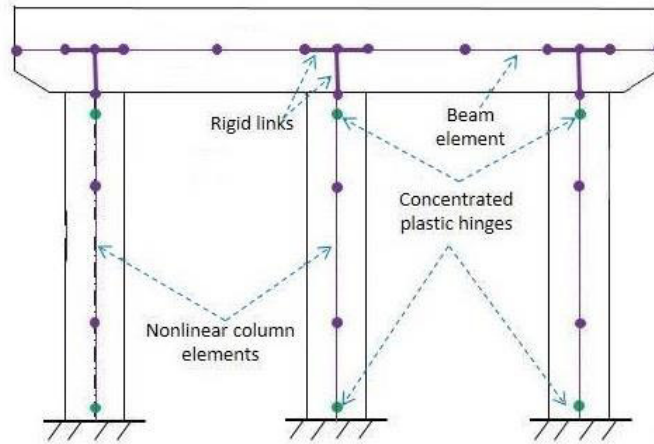


Figure 3- 6: Concrete bridge bent model

To consider the increase of the seismic demands at the columns, the model includes the P-delta effects. The Newmark's beta method is applied to solve the dynamic equations incrementally at each time step to calculate the deterministic response of the time history analysis. The mass- and stiffness-proportional Rayleigh damping coefficients are determined for the response-history analysis of the bridges considering the first two modal periods, and the hysteric damping is included. For each case study the number of modal analyses requires a minimum of 90% mass participation in both directions. To solve the error due to the convergence problem, the maximum sub-step is assumed as each time increment of the seismic records; the minimum sub-step considered is of $2E-7$. Nonlinear analyses with direct integration type in two orthogonal directions were conducted to evaluate the seismic vulnerability of the bridges. Multi-column bents in the longitudinal direction behave as a cantilever structural system, and thus plastic hinges can only form at the bottom of the columns. However, in the transverse direction, the columns and bent cap beam form a frame type system. In this case, plastic hinges can develop at both ends of columns, top and bottom of the columns. The plastic rotation and consequently ductility capacity depend on section properties and amount of transverse reinforcement distribution. This distribution provides the dual functions of confining the core concrete, which lead to enhance its compression strength and enable to sustain higher compression strains, and restraining the longitudinal compression against buckling. Figure 3- 7 shows a moment-curvature diagram, and the elastic-perfectly plastic idealization according to the software SAP2000 [123].

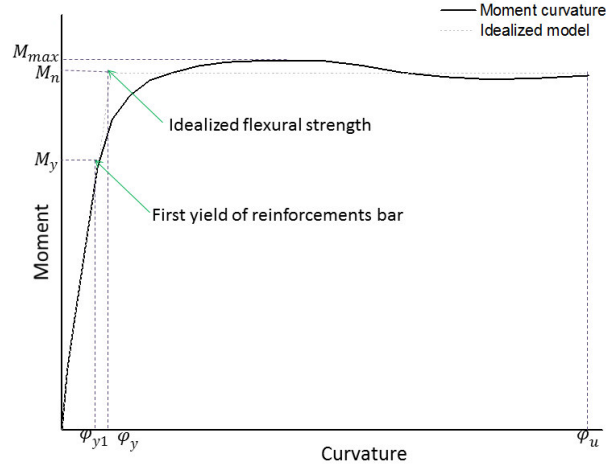


Figure 3- 7: Moment-curvature diagram of columns

The equivalent curvature (ϕ_y) corresponds to the relative displacement of the column when the vertical reinforcing bars at the bottom of the column reach the yield point. ϕ_y is obtained by extrapolating the line joining the origin and the point corresponding to the first yielding point of a reinforcing bar up to the nominal moment capacity M_n [108, 124]. Equation (3.9) gives the curvature ϕ_y , where M_y and ϕ_{y1} are the moment and curvature at first yielding of a vertical reinforcing bar. The curvature ϕ_y and M_y are the curvature and moment at yielding of a vertical reinforcing bar, given by Equation (3.10). Degradation in pier strength happens when the maximum moment M_{max} is reached. Finally, concrete crushing occurs at the ultimate curvature (ϕ_u) when the concrete strain is equal to ϵ_{cu} , Equation (3.11), where ϵ_{cu} is the compressive strain at the rupture of the transverse confining steel. The strain limit can be calculated utilizing the energy balance approach as defined by Mander *et al.* [118]. This has also been confirmed by more recent papers that are based on the analysis of energy balance of cross-sectional cores confined with transverse reinforcement (taking into account the fact that the increase in energy absorbed by confined core is closely related to the energy retained by transverse reinforcement up the limit of failure).

$$\phi_y = \frac{M_n}{M_y} \phi_{y1} \quad (3.9)$$

$$\varphi_y = \frac{M_n}{EI_e} \quad (3.10)$$

Since the gradient is small, a constant curvature along the length of the plastic hinge is assumed. Therefore the rotation angle can be calculated by Equation (3.11):

$$\theta_p = \varphi \times L_p \quad (3.11)$$

Different expressions exist to estimate the hinge length (L_p). In this study, we used the expression proposed by Priestley *et al.* [108], given by Equation (3.12):

$$L_p = 0.08L + 0.022f_{ye}d_{bl} \geq 0.044f_{ye}d_{bl} \quad (3.12)$$

where L is the distance from the plastic hinge to the point of contra-flexure, f_{ye} is the steel yield strength of the reinforcing bars and d_{bl} is the diameter of the longitudinal reinforcing bars. The nonlinear behavior of the columns is considered with a concentrated plasticity model by assigning plastic hinges at both column ends, as recommended in Caltrans code [125]. The moment-curvature describes the nonlinear behavior of plastic elements at the column ends in SAP2000. Outside the plastic hinge length, the behavior of the column is assumed to be linear.

3.5 Abutment

Abutments are one of the key components in the highway bridges which are influenced by the seismic response. Vertical support to the structure is provided by these elements, as well as lateral restraints due to load direction at the bridge ends. Inspection and statistical data show that seat abutment support with wing walls is one of the most common types in the inventory data. Since an abutment has interaction with the earth and fill behind the back wall, in the bridge modeling the soil-structure interaction is taken into consideration. Available models for abutments are based on geometric properties up to the consideration of actual abutment earthquake response data. Ventura *et al.* [126] obtained the abutment stiffness through field

vibration tests on highway bridges. An analytical model to calculate abutment transverse and vertical stiffness's based on soil properties of the earth embankment and cross-section dimensions is proposed by Wilson and Tan [127]. Goel and Chopra [128] reported a research on the stiffness and capacity for the abutment-soil system from the ground and bridge motion recorded during earthquakes. Although a multi-linear model for the force-deformation relationship of the abutments in different directions was investigated by Nielson [100], that study has some drawbacks. It is not completely clear how complex behavior of abutment-soil system is affected by nonlinear soil behavior and soil-structure interaction in analytical model. Complicated abutment models need huge computation efforts which lead to increase the numerical instabilities along the analysis. Moreover, based on the uncertainties in the abutment-soil systems, the unrealistic results could be increase. However, there is a lack of information in terms of backfill soil and abutment for each sample bridges, therefore the development of a detailed model suggested by other researchers is not appropriate. Taking into account the Caltrans recommendation [44], elastic springs in the longitudinal and transverse directions are utilized to model the abutments and backfill soil. The abutments are designed to provide unimpeded traffic access from the bridge and an economical means of resisting bridge inertial loads developed during ground excitations. Abutment walls are traditionally designed based on active and passive earth pressure theories presented in Figure 3- 8. However, under seismic events, when inertial loading from the massive bridge structure induces high passive earth pressure conditions, such pressure theories are invalid [129]. Post-earthquake reconnaissance reports have found that soil interaction, abutment behaviour, and embankment flexibility significantly influence the response of an entire bridge system under moderate to strong intensity ground motions.

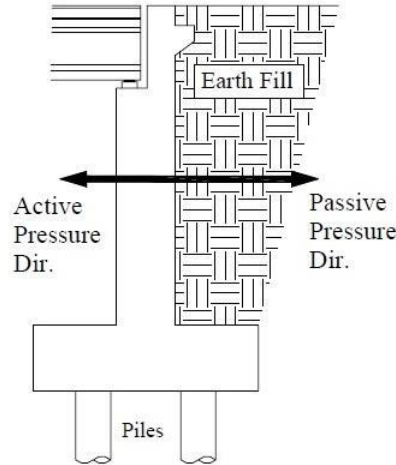


Figure 3- 8: Earth pressure type and their directions at the abutment

The resisting movement at the abutment is provided by backfill passive pressure force, and it depends on the material properties of the backfill. Abutment longitudinal response analysis could be explained by utilizing a bilinear approximation of the force–deformation relationship or the nonlinear force–deformation relationship [130]. The bilinear demand, which includes the effective abutment stiffness, is influenced by expansion gaps, and it includes a realistic value for the embankment fill response. Based on force deflection results from large-scale abutment testing [131-133] and passive earth pressure, the initial stiffness K_i is considered as 14.35 kN/mm/m according to the Caltrans recommendation [44]. The initial abutment’s stiffness could be adjusted proportionally to the back-wall height of the abutment through equation (3.13):

$$K_{abut} = K_i \times w_a \times \left(\frac{h_a}{1.7}\right) \quad (3.13)$$

where h_a and w_a are the height and width of the back-wall for seat abutments, respectively. For the abutments, the effective stiffness abutment (K_{eff}) is considered for the expansion hinge gaps as shown in Figure 3- 9.

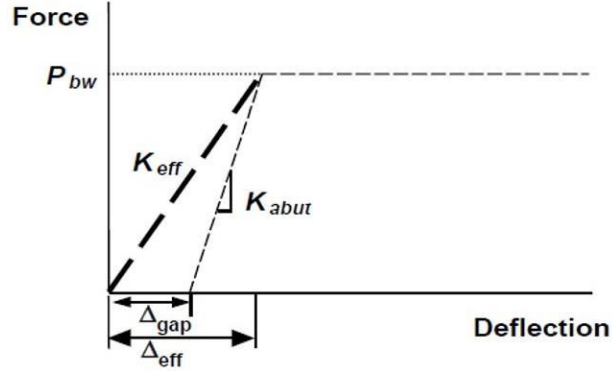


Figure 3- 9: Seat abutment's effective stiffness for highway bridges

Based on a bilinear idealization of the force–deformation relationship, the passive pressure force resisting the movement at the abutment (P_{bw}) is determined as follows:

$$P_{bw} = A_e \times 239 \text{ kPa} \times \left(\frac{h_{bw}}{1.7}\right)$$

$$A_e = h_{bw} \times w_{bw}$$

$$\Delta_{abut} = \frac{P_{bw}}{K_{abut}} \quad (3.14)$$

$$\Delta_{eff} = \Delta_{abut} + \Delta_{gap}$$

$$K_{eff} = \frac{P_{bw}}{\Delta_{eff}}$$

where A_e is the effective abutment wall area, and h_{bw} and w_{bw} are the effective abutment height and width respectively.

Previous researchers presented that in abutment's transverse direction, the response is characterized by the piles whereas the wing walls contribution is neglected [100], therefore in transverse direction the force-deformation relationship for piles is employed. However in this study the contribution of piles and abutments are not considered. Therefore, based on Caltrans recommendation [44], elastic springs are employed to model the abutment and backfill soil. The stiffness of these springs is equal to 50% of the transverse stiffness of the adjacent bent.

3.6 Bearing

Elastomeric bearings are located between the superstructure and substructure components, without any dowel or connecting device, as shown in Figure 3- 10. Bearings are located under each of the concrete girder of the superstructure. The vertical stiffness for each bearing is provided by the internal steel plates, referred to as shims, and reduced the lateral bulking of the bearing as well.

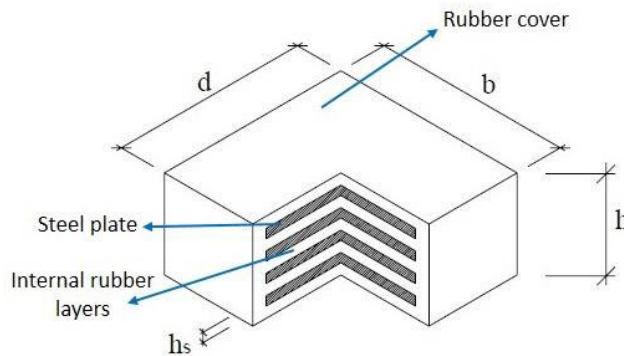


Figure 3- 10: Typical elastomeric bearing of a highway bridge in Iran

To model the vertical and lateral bearing stiffness's, spring elements are selected, using the functions proposed by Priestley *et al.* [108]:

$$K_v = \frac{G A}{h} \tag{3.15}$$

$$K_s = \frac{6GAKS^2}{(6GS^2 + K)h}$$

where K_v and K_s are the shear and vertical stiffness of the bearings respectively. G is the shear modulus of rubber and is taken as 1 MPa, A is the gross rubber area, and h is the total rubber height. K is the rubber bulk modulus and S is the shape factor. Column bents are assumed to be fixed for a continuous and single spread footing. The rotation should be considered in modelling the bridge foundation if uplift can occur, in this situation the rotational stiffness should be considered. However, in this study the soil–structure interaction is not considered.

Chapter 4

4 GROUND MOTION SELECTION

To develop fragility curves, one of the most needed components is the appropriate selection of the earthquake ground motions. As mentioned before, the reliability of the bridge fragility curves is influenced by the selected intensity measure. Among previous studies, Kwon and Elnashai [134] concluded that the effect of randomness in strong-motion characteristics is much more important than other uncertainties. The uncertainty in the seismic hazard is determined through the use of suites of earthquake ground motions that accurately represent the seismicity of the region where the bridges are located. Therefore, for reliable fragility curves the selection of suitable ground motions is crucial. There are different methods to select the appropriate ground motion data needed to lead the nonlinear time history analysis. However, the main goal in this part of the work is the selection of a wide range of earthquake database representative of different intensity levels, to lead the analytical models from the elastic behavior through the inelastic behavior up to the dynamic instability. The seismic hazard level of the earthquake ground motions can be represented by different ground motion intensity measures. The essential point in selecting the most suitable intensity measure could be the level of correlation with the seismic damage induced to the bridges. In this study, several ground motion are considered to generate the fragility curves.

4.1 Earthquake ground motion intensity measures

The intensity measure selected for the ground motion has effect on the fragility curves. The selection of the appropriate intensity measure is one of the most important parts of this study, actually, research still continues on this subject. There are not specific methods to select the optimal intensity measure to perform the fragility curves. There are several methods proposed to select the suitable intensity measure by different researchers, although there is a lack of agreement among them, to select the appropriate intensity measure to develop fragility curves.

Previous researchers presented the proficiency of different intensity measure (IM) to calculate the seismic damage. There are different methods of selecting the appropriate ground motion data

for the nonlinear time history analysis. Previous researchers used common intensity measurements (IMs) such as: PGA, peak ground velocity (PGV) or peak ground displacement (PGD). However optimal IMs selection can be supported by an examination of several characteristics of IMs, that have been discussed by several studies [20, 135, 136]. In the study of Zelaschi *et al.*[137] the analysis of RC bridges by providing a statistically sound comparison of analytical fragility curves due to traditional and innovative intensity measures of an extensive bridge is proposed. In the study of Buratti and Tavano [13] by utilizing the means of cloud analysis with a set of 40 recorded accelerograms, the sufficiency and efficiency of ground motion intensity is analyzed. In particular, the peak ground displacement was founded the most efficient and sufficient intensity measure. In the study of Bradley *et al.* [136] four methods were selected for dynamic seismic response analyses when the fundamental seismic hazard is quantified with ground motion simulation instead of empirical ground motion prediction equations. In that study PGA and S_a are considered as intensity measures. In the study of Avsar *et al.* [121] among the investigated ground motion intensity measures (ASI, PGV, PGA, and PGA/PGV) acceleration spectral intensity (ASI) and PGV appear to be the ones that have better correlation with the seismic damage of the bridge components. In the study of Padget *et al.* [135] it is noted that spectrally based quantities perform better correlation than PGA. However in this study PGA is utilized as a one of most common intensity measures for assessing bridge fragility curves. Dhakal *et al.* [138] proposed that in comparison with PGA, spectral acceleration is a more efficient intensity measure. Despite of utilizing PGA as the most common intensity measure, it has still some deficiencies when compared to other parameters. The implementation of the spectral acceleration as the intensity measure could give more confidence on the results, or it could lead to need less number of records to perform results with the same level of confidence.

In selecting the appropriate intensity measure, one of the most important principles is to account with the appropriate level of correlation between the hazard level of the ground motion and the degree of a constant seismic damage in the bridge. Therefore, the reliability of the fragility curves is proportional to the selected intensity measure and the level of correlation between the seismic damage. Existing ground motion intensities can be directly calculated from ground motion records, such as peak ground acceleration (PGA). In this method PGA can be obtained directly from earthquake record databases without any additional information. Another method to determine intensity measures is based on the use of the response spectrum of a ground motion,

such as spectral values and spectrum intensity parameters which can be calculated by utilizing response spectrum for certain periods, or specific equations are used for the calculations [139]. Since PGA is one parameter with common applications in earthquake engineering, it is considered as representative for the first method investigated. Also PGA is used by a large number of researchers as the intensity measure to develop fragility curves. The second method uses spectrum intensity parameters instead of considering a single period value, through this is possible to deal with a period range over the response spectra of the earthquake databases, this approach can be more realistic [37, 100].

From the elastic response spectrum of the ground motion, the maximum acceleration that the bridges can be subjected under an earthquake is measured through their fundamental periods. Therefore, to measure the seismic damage of the bridges is used the spectral acceleration at their fundamental period as a good intensity measure. Moreover, unrealistic acceleration values could be the result of being considered a single spectral acceleration without accounting for higher modes that effect the response, and the period elongation based on the inelastic response of the bridges. Therefore, it is more reasonable to consider a period range over the response spectra of the ground motion, instead of dealing with a single period value. It should be noted that it is not appropriate to consider a single period to determine the spectral acceleration. The area under the elastic response spectrum, defined by equation 4.1 with 5% damping between the boundary periods defined by T_i and T_f , is defined as acceleration spectrum intensity (ASI) [101, 140, 141]. In this study, ASI is considered as a representative of the second method as an intensity measure. An acceleration intensity spectrum is shown schematically in Figure 4- 1. In this graph, the initial and final periods which are used to calculate ASI are represented as T_i and T_f , respectively.

$$ASI = \int_{T_i}^{T_f} SA(T, \xi) dT \quad (4.1)$$

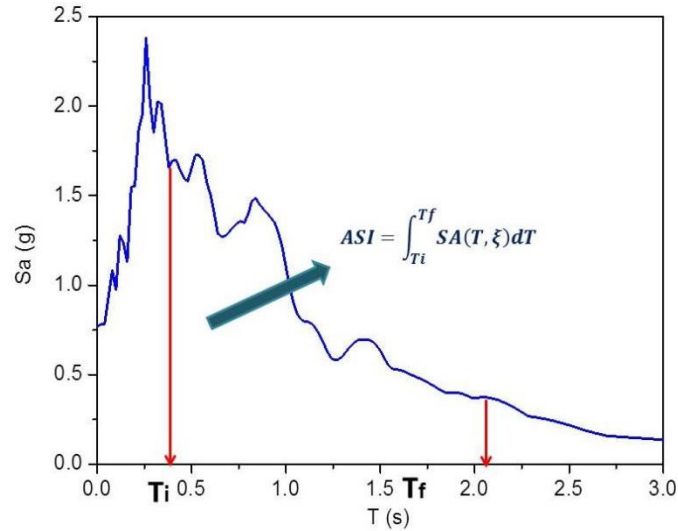


Figure 4- 1: Definition of ASI

In the seismic analysis of concrete dams with fundamental periods less than 0.5 s, ASI as the area under the elastic pseudoacceleration spectrum (5% damped) between the periods of $T_i = 0.1$ s and $T_f = 0.5$ s was selected as intensity measure. Yakut and Yılmaz [141] reported that in the period range between $T_i = 0.1$ s and $T_f = 2.0$ s, ASI has a better correlation with the response of building structures. It should be noted that the selection of period range between of T_i and T_f is highly influenced by the reliability of the ASI.

As mentioned before, bridges are classified in two groups in terms of the superstructure connectivity, namely simply support and integral bridges. However simply support bridges are classified in terms of column height, span length and superstructure type. For each major classification, due to the superstructure connectivity, the results of the modal analyses of sample bridges are presented in Table 4- 1. Fundamental period values of major bridge classes according to modal analyses are between 0.36 and 2.06 s. We select T_i and T_f periods of 0.3 and 2.12 s in order to consider the higher mode effects and cover the elongated period of the bridge structure due to nonlinear actions.

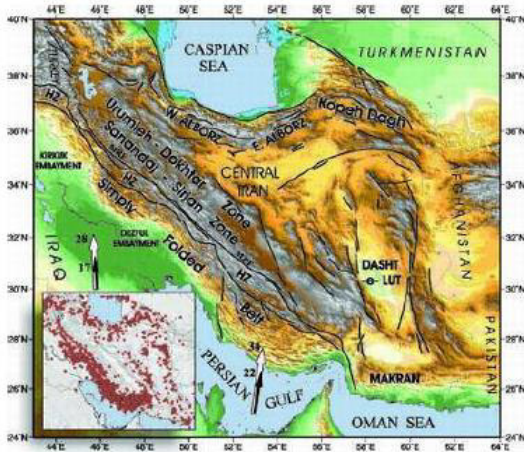
Table 4- 1: Elastic fundamental periods of the major bridges

Bridge classes	Modal analyses (s)	
	Min.	Max.
$20 \leq SL < 30$	0.997	1.88
$SL \geq 30$	1.34	2.06
SCC-S	0.99	1.51
HCC-S	1.7	2.06
CC-I	0.36	0.73
CC-S	0.99	1.38

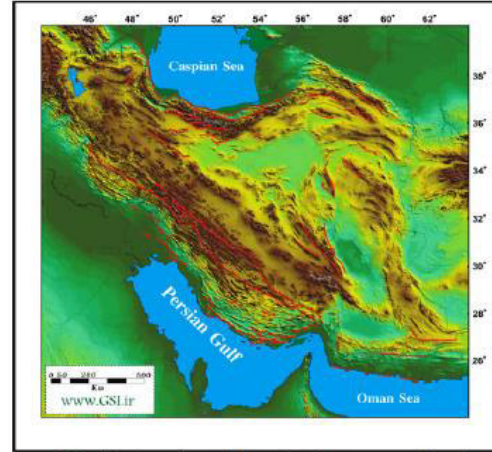
In the study of Baker and Cornell [142], for hazard analysis the geometric mean of the intensity measure of the two horizontal components of a ground motion is used. In this study, two horizontal orthogonal components are considered in the nonlinear time history analyses. On the other hand the intensity measure of each ground motion is determined through the SRSS of the intensity measures.

4.2 Geological and seismological feature of Iran

The Iranian plateau is located between the Arabian plate at the south, which moves at 2.1-2.5 cm/yr, and the Eurasian plate at the north. The study of earthquake mechanisms along the active fault systems in Iran includes dominance of strike-slip faulting and reverses faulting. Figure 4- 2 shows the distribution of reverse and strike-slip faults; particularly, in the south-western, the center and the northern regions of Iran. Figure 4- 3 shows the mechanism of strike slip and reverse faults, respectively. Due to the high density of active faults in Iran, and to the inaccuracy of the macro-seismic data of the area, the sources of some of the earthquakes have been related to more than one fault. Therefore, the development of studies on the seismic vulnerability of bridges based on different seismic sources seems to be necessary [143].

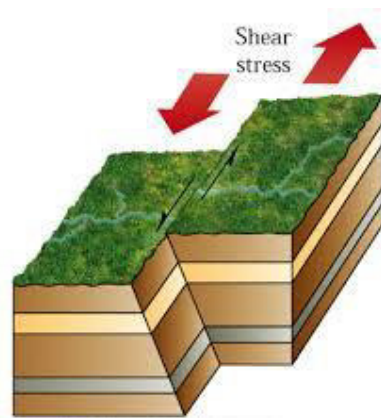


(a)

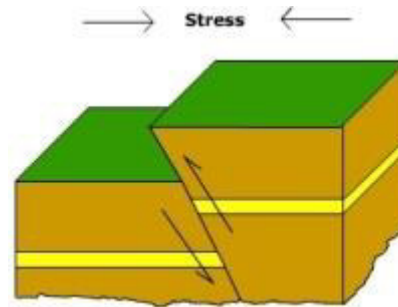


(b)

Figure 4- 2: (a) Strike-slip, (b) Reverse fault in Iran
<http://earthquake.usgs.gov/earthquakes/world/iran/gshap.php>



(a)



(b)

Figure 4- 3: Mechanism of (a) strike slip fault, (b) reverse fault

4.3 Selection of ground motion records

There are some important issues that should be considering in the selection of the ground motions. For the nonlinear response analysis, several earthquake ground motion records are considered, and appropriate number of these selected records is important to cover a wide range of seismic hazard levels what is desired in order to represent the seismic variability in the analytical fragility curves. Fragility curves present information about the probability of the seismic damage level based on several hazard levels expected in a certain region. Hence, the ground motion data, utilized in nonlinear analyses, should be selected from the earthquake

ground motions specific to the respective region. On the other hand, ground motion earthquake recorded for the specific region may not be sufficient in number. For this cases, other researchers used spectrum compatible synthetic ground motions which can be obtained by generating artificial spectrum that match the records through purpose programs, or by manipulating the existing ground motion records to have conformity with the design spectrum for the specific site [56, 100, 144]. To obtain ground motions at several levels of seismic hazard, even the synthetic records are very attractive, but it is highly possible to get ground motion records with unrealistic energy and frequency contents. Also Priestley *et al.* [145] noted that synthetic records typically have a longer duration when comparing with real earthquake ground motion data. Bommer and Acevedo [146] reported that the use of the real earthquake data bases as an input for the dynamic analysis of structures, is more realistic than the implementation of artificial records. Naeim and Lew [147] noted that there are several problems in terms of an uncontrolled use of synthetic records during the seismic design, that can lead to exaggerated displacement demands, energy input, and consciously mislead the expected performance of the structure. This study does not use synthetic in ground motions in order to avoid such type problems. Real earthquake ground motions are considered that show the seismic potential of the investigated region.

Most of the recorded ground motions in Iran with high potential of destruction are generated from the reverse and strike-slip faulting mechanisms. This cannot be extended for the whole country, however other recorded earthquake databases which have the same fault mechanism can be used with the aim to lead the time history analyses of the Iran highway bridges system. All bridges are considered recorded on hard soil, for what soil flexibility at the bridge foundations are not taken into account in the analytical models. Another factor which has effect on site condition is shear wave velocity. According to [148], firm soil site is assumed to be composed of at least dense soil or soft rock. This soil type is represented of the site category C, which has the lower limit for shear wave velocity (V_s) than 360 m/s. Hence, the ground motions from soil site having $V_s < 360$ m/s is not considered in this study. Since the ground motion with PGA less than 0.05g typically do not produce any damage in the bridge, the earthquake databases having $PGA < 0.05g$ are not considered. In light of the previous information, for the ground motion selection criteria 104 (which is shown in Tables 4- 2 and 4- 3) earthquake ground motions were selected satisfying the following conditions:

- All earthquake ground motions recorded in Iran
- Ground motions recorded from other regions but with the same seismic sources (strike-slip and reverse faulting mechanism)
- It is assumed that all bridges foundation are on hard soil, therefore ground motions recorded from soil sites having $V_s \geq 360$ m/s
- Ground motions having $PGA \geq 0.05$ g
- Moment magnitude, M_w , is greater than 5.2
- To avoid the effect of vertical component of earthquake ground motion far fault earthquakes are taking into account.
- Two horizontal orthogonal components are considered in the nonlinear time history analyses. The response spectrum of each ground motion is determined by taking the square root of the sum of the squares (SRSS) of the response spectrum of the two horizontal ground motion components.

Table 4- 2: Ground motion selection for reverse fault

Station	Year	R (KM)	M _w	PGD (cm)	PGV (cm/s)	PGA (g)	Earthquake	source
CWB 9999917 ENA	1999	113.5	7.62	1.09	5.5	0.0624	Chi-Chi	peer
CWB 99999 ILA050	1999	113.5	7.62	12.19	8.27	0.0671	Chi-Chi	peer
CWB 99999 NSK	1999	106.87	7.62	2.78	5.59	0.0682	Chi-Chi	peer
CWB 99999 TCU085	1999	106.87	7.62	11.01	7.48	0.0599	Chi-Chi	peer
CDMG 127 Lake Hughes #9	1994	44.77	6.69	3.31	9.02	0.169	Northridge	peer
USC 90017 LA - Wonderland Ave	1994	18.99	6.69	2.23	11.17	0.1343	Northridge	peer
CDMG 24399 Mt Wilson - CIT Seis Sta	1994	45.77	6.69	0.58	6.41	0.1678	Northridge	peer
CDMG 23595 Littlerock - Brainard Can	1994	61.26	6.69	1.13	4.93	0.0683	Northridge	peer
CDMG 23598 Rancho Cucamonga - Deer Can	1994	89.83	6.69	0.73	4.44	0.0645	Northridge	peer
USC 90019 San Gabriel - E Grand Ave	1994	44.32	6.69	2.27	10.23	0.2087	Northridge	peer
CDMG 127 Lake Hughes #9	1971	23.1	6.61	1.1	4.58	0.1395	San Fernando	peer
CDMG 24399 Mt Wilson - CIT Seis Sta	1987	19.5	5.99	0.3	3.96	0.1634	Whittier Narrows	peer
CDMG 24399 Mt Wilson - CIT Seis Sta	1987	18.74	5.99	0.27	4.85	0.1463	Whittier Narrows	peer
CDMG 89530 Shelter Cove Airport	1992	36.28	7.01	0.4	6.07	0.1954	Cape Mendocino	peer
CDMG 89324 Rio Dell Overpass - FF	1992	22.64	7.01	16.96	47.95	0.4244	Cape Mendocino	peer
CDMG 89509 Eureka - Myrtle & West	1992	53.34	7.01	8.29	24.99	0.1668	Cape Mendocino	peer
CWB 99999 HWA033	1999	69.11	7.62	8.7	18.35	0.1702	Chi-Chi	peer
CWB 9999917 ALS	1999	37.83	7.62	9.61	29.54	0.1748	Chi-Chi	peer
CWB 99999 CHY029	1999	39.7	7.62	20.73	33.11	0.2595	Chi-Chi	peer
CWB 99999 CHY042	1999	59.8	7.62	7.23	13.71	0.0823	Chi-Chi	peer
CWB 99999 CHY052	1999	70.51	7.62	7.04	11.51	0.1105	Chi-Chi	peer
CWB 99999 KAU054	1999	64.62	7.62	4.59	6.73	0.0787	Chi-Chi	peer
CWB 99999 TCU015	1999	101.62	7.62	31.58	37.47	0.1125	Chi-Chi	peer
CWB 99999 TCU029	1999	79.2	7.62	42.66	48.93	0.1771	Chi-Chi	peer
CWB 99999 TCU034	1999	87.88	7.62	28.34	38.04	0.1991	Chi-Chi	peer
CWB 99999 TCU047	1999	86.39	7.62	36.42	38.12	0.3643	Chi-Chi	peer
CWB 99999 TCU070	1999	47.86	7.62	51.04	56.45	0.2058	Chi-Chi	peer
CWB 99999 TCU095	1999	95.7	7.62	36.28	56.24	0.5283	Chi-Chi	peer
CDMG 24278 Castaic - Old Ridge Route	1994	40.68	6.69	13.57	46.51	0.4898	Northridge	peer
USC 90013 Beverly Hills - 14145 Mulhol	1994	13.39	6.69	12.06	54.22	0.4594	Northridge	peer
USC 90061 Big Tujunga, Angeles Nat F	1994	31.55	6.69	1.00	9.64	0.1999	Northridge	peer
USC 90021 LA - N Westmoreland	1994	27.29	6.69	2.97	22.05	0.3699	Northridge	peer
USC 90014 Beverly Hills - 12520 Mulhol	1994	16.27	6.69	6.67	32.82	0.5102	Northridge	peer
CDMG 24538 Santa Monica City Hall	1994	22.45	6.69	10.54	31.22	0.5908	Northridge	peer
USGS 5081 Topanga - Fire Sta	1994	14.19	6.69	3.13	13.76	0.2591	Northridge	peer
CDMG 24688 LA - UCLA Grounds	1994	18.62	6.69	5.11	22.41	0.3908	Northridge	peer
CDMG 24605 LA - Univ. Hospital	1994	36.47	6.69	2.38	19.39	0.3492	Northridge	peer
CDMG 24400 LA - Obregon Park	1994	39.39	6.69	2.05	21.79	0.4673	Northridge	peer
CDMG 24157 LA - Baldwin Hills	1994	28.2	6.69	5.36	17.19	0.2039	Northridge	peer
CDMG 24396 Malibu - Point Dume Sch	1994	31.21	6.69	1.93	8.63	0.1046	Northridge	peer
USC 90015 LA - Chalon Rd	1994	14.92	6.69	3.95	23.13	0.2148	Northridge	peer
USC 90059 Burbank - Howard Rd.	1994	23.18	6.69	2.05	9.09	0.1403	Northridge	peer
USC 90049 Pacific Palisades - Sunset	1994	18.22	6.69	5.99	22.65	0.3316	Northridge	peer
USC 90075 Whittier - S. Alta Dr	1994	52.81	6.69	0.85	4.91	0.0735	Northridge	peer
CDMG 24278 Castaic - Old Ridge Route	1971	25.36	6.61	3.29	19.83	0.2994	San Fernando	peer
USGS 128 Lake Hughes #12	1971	20.04	6.61	2.42	15.53	0.3297	San Fernando	peer
CDWR 269 Pearblossom Pump	1971	45.41	6.61	1.36	4.59	0.1387	San Fernando	peer
CDMG 24157 LA - Baldwin Hills	1987	26.21	5.99	1.01	8.36	0.1503	Whittier Narrows	peer
CDMG 14403 LA - 116th St School	1987	21.26	5.99	1.8	18.83	0.3408	Whittier Narrows	peer
CDMG 24088 Pacoima Kagel Canyon	1987	38.55	5.99	0.68	7.21	0.1564	Whittier Narrows	peer
CDMG 24157 LA - Baldwin Hills	1987	24.41	5.99	1.28	7.33	0.1079	Whittier Narrows	peer
CDMG 89486 Fortuna - Fortuna Blvd	1992	29.55	7.01	20	24.75	0.117g	Cape Mendocino	peer
CWB 99999 CHY080	1999	31.65	7.62	27.98	87.21	0.8199	Chi-Chi	peer
CWB 9999917 NSY	1999	63.29	7.62	38.09	47.16	0.1348	Chi-Chi	peer
CDMG 24087 Arleta - Nordhoff Fire Sta	1994	11.1	6.69	12.8	30.9	0.3298	Northridge	peer
CDMG 24461 Alhambra - Fremont School	1987	6.77	5.99	2.16	18.55	0.3880	Whittier Narrows	peer
CDMG 24400 LA - Obregon Park	1987	9.05	5.99	2.35	19.16	0.4242	Whittier Narrows	peer
9102 Dayhook	1978	20.63	7.38	9.03	28.24	0.3505	Tabas	peer
71 Ferdows	1978	117.66	7.38	7.18	7.08	0.1084	Tabas	peer
9101 Tabas	1978	55.24	7.38	62.15	98.2	0.8128	Tabas	peer
Maximum	1999	117.6	7.62	62.15	98.2	0.59		
Minimum	1971	6.77	5.99	0.27	3.96	0.05		
Average	1992	45.5	6.93	10.36	22.59	0.23		

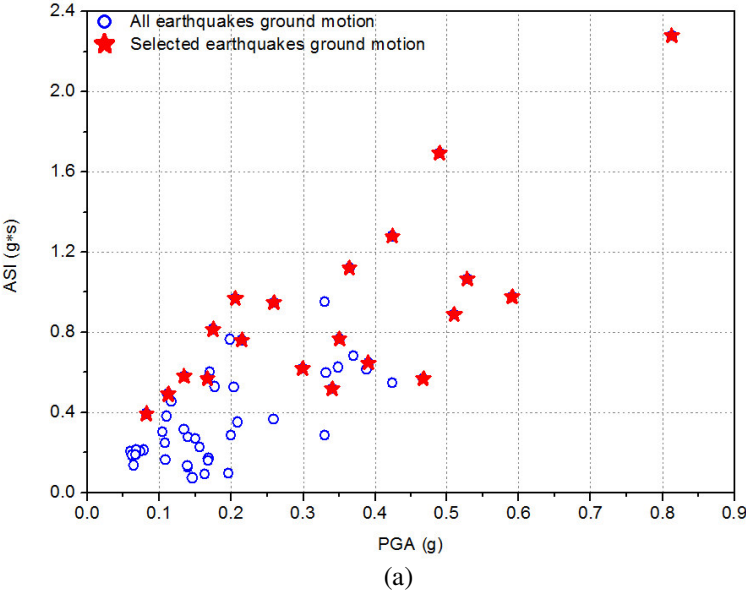
Table 4- 3: Ground motion selection for strike-slip fault

Station	Year	R (KM)	M _w	PGD (cm)	PGV (cm/s)	PGA (g)	Earthquake	source
ERD 99999 Gebze	1999	47.03	7.51	33.69	38.3	0.1833	Kocaeli	peer
CDMG 22161 Twenynine Palms	1992	44.1	7.28	2.93	4.34	0.07	Landers	peer
CDMG 47379 Gilroy Array #1	1984	38.63	6.19	1.12	2.86	0.0815	Morgan Hill	peer
LAMONT 1061 Lamont 1061	1999	31.56	7.14	8.1	12.85	0.1174	Duzce	peer
ITU 99999 Mecidiyekoy	1999	90.66	7.51	7.39	7.52	0.0567	Kocaeli	peer
KOERI 99999 Arcelik	1999	53.68	7.51	25.84	28.45	0.1741	Kocaeli	peer
CDMG 57007 Corralitos	1984	30.05	6.19	1.52	7.92	0.0983	Morgan Hill	peer
CDMG 47006 Gilroy - Gavilan Coll.	1984	38.73	6.19	0.93	3.44	0.1014	Morgan Hill	peer
CDMG 47315 SJB Overpass, Bent 3 g.l.	1979	23.91	5.74	0.79	6.9	0.1036	Coyote Lake	peer
UNAMUCSD 6604 Cerro Prieto	1979	24.82	6.53	5.84	14.04	0.176	Imperial Valley	peer
USGS 286 Superstition Mtn Camera	1979	59.54	6.53	2.41	6.7	0.1598	Imperial Valley	peer
CDMG 12149 Desert Hot Springs	1992	27.33	7.28	9.62	18.54	0.1407	Landers	peer
SCE 23 Coolwater	1992	82.12	7.28	12.81	34.64	0.3733	Landers	peer
CDMG 1438 Temblor pre-1969	1966	40.26	6.19	3.61	17.45	0.2934	Parkfield	peer
UNAMUCSD 6604 Cerro Prieto	1980	33.73	6.33	10.85	27.06	0.5722	Victoria	peer
CDMG 57383 Gilroy Array #6	1979	4.37	5.74	6.15	37.67	0.4038	Coyote Lake	peer
LAMONT 1058 Lamont 1058	1999	13.71	7.14	11.57	12.64	0.0917	Duzce	peer
USGS 5051 Parachute Test Site	1979	48.62	6.53	10.68	16.64	0.1661	Imperial Valley	peer
JMA 99999 KJMA	1995	18.27	6.9	18.87	77.83	0.7105	Kobe	peer
CDMG 57383 Gilroy Array #6	1984	36.34	6.19	3.85	23.53	0.2814	Morgan Hill	peer
USGS 1652 Anderson Dam (Downstream)	1984	16.67	6.19	5.39	28.53	0.3426	Morgan Hill	peer
USGS 5051 Parachute Test Site	1987	15.99	6.54	37.19	77.19	0.4509	Superstition- Hills	peer
USGS 286 Superstition Mtn Camera	1987	7.5	6.54	5.84	36.89	0.7931	Superstition- Hills	peer
Parkfield,CA - Gold Hill 3W; CSMIP, station 36420	2004	3.9	6:00	3.71	18.71	0.532	Parkfield	Cosmos
Parkfield,CA - Cholame 2E; CSMIP, station 36230	2004	14.5	6:00	3.62	22.51	0.469	Parkfield	Cosmos
Parkfield,CA - Cholame 3E; CSMIP, station 36450	2004	14.8	6:00	4.91	25.24	0.602	Parkfield	Cosmos
Coalinga,CA - Slack Canyon; Hidden, ValleyRanch	2004	32.1	6:00	5.72	36.42	0.271	Parkfield	Cosmos
BHRC 99999 Abbar	1990	40.43	7.37	18.96	48.78	0.5051	Manjil	peer
USGS 5047 Rancho De Anza	2005	20.43	5.2	0.51	6.28	0.093	Anza	peer
CDMG 54424 Bishop - Paradise Lodge	1986	17.22	6.19	1.13	4.52	0.0741	Chalfant-Valley	peer
CDMG 54214 Long Valley Dam (L Abut)	1986	23.76	6.19	2.19	7.24	0.0829	Chalfant- Valley	peer
CDMG 54424 Bishop - Paradise Lodge	1986	15.42	6.19	2.5	8.96	0.1472	Chalfant- Valley	peer
CDMG 54T03 Lake Crowley - Shehorn Res.	1986	26.59	6.19	1.14	5.86	0.123	Chalfant- Valley	peer
CDMG 54214 Long Valley Dam (Downst)	1986	23.76	6.19	2.22	5.96	0.0747	Chalfant-Valley	peer
ERD 99999 Mudurnu	1999	41.53	7.14	9.37	11.07	0.0896	Duzce	peer
LAMONT 375 Lamont 375	1999	24.05	7.14	6.09	28.24	0.7367	Duzce	peer
LAMONT 531 Lamont 531	1999	27.74	7.14	8.13	11.93	0.1445	Duzce	peer
LAMONT 1059 Lamont 1059	1999	24.26	7.14	8.26	12.5	0.1305	Duzce	peer
LAMONT 1062 Lamont 1062	1999	29.27	7.14	9.43	13.7	0.2101	Duzce	peer
99999 MZH	1995	98.9	6.9	1.91	5.04	0.0625	Kobe	peer
99999 OKA	1995	100.15	6.9	1.72	3.86	0.0709	Kobe	peer
99999 TOT	1995	123.33	6.9	3.23	10.86	0.0765	Kobe	peer
ERD 99999 Goynuk	1999	77.63	7.51	2.97	10.75	0.1387	Kocaeli	peer
ERD 99999 Izmit	1999	5.31	7.51	14.61	27.02	0.2037	Kocaeli	peer
Maximum	2005	123.3	7.5	37.1	77.8	0.79		
Minimum	1966	3.9	5.2	0.51	2.86	0.05		
Average	1991	36.6	6.6	8.0	19.7	0.24		

In the study of Priestley *et al.* [108] the characterization of ground motion (e.g.,: components and maximum values such as acceleration, velocity and displacement, source mechanism, duration, return period, magnitude) is stated, however in this research components and maximum values, magnitude, source mechanism (reverse and strike-slip fault) and epicenter of the earthquake are considered. All of the earthquake ground motions were downloaded from the strong motion databases of PEER (<http://peer.berkeley.edu/smcat/>) and COSMOS (<http://db.cosmoseq.org/scripts/default.plx>). All the data have been downloaded in November 2013. To select the suitable number of ground motions (104 earthquake), the distribution of ASI

versus PGA of the mentioned ground motions was considered. Figure 4- 4 shows the distribution of PGA versus ASI of the selected 104 ground motions. There is not a uniform distribution for the two intensity measures among the selected ground motions. For the higher intensities, the number of ground motions is lower. However, the number of ground motions is higher at the lower intensity values at which the seismic damage imposed on the bridges is limited. Therefore, considering all the selected 104 ground motions for the time history analyses is not practical.

Imposing all the earthquake motions in the numerical models not only increases the total analysis time noticeably, but also the reliability of fragility curves could be influenced due to the uneven distribution of the intensity measures. Therefore, a sufficient number of earthquake motions were selected among the 104 ground motions data. A new set of data of ground motion was compiled based on each seismic source for the different levels of ASI and PGA is shown in Figures 4- 5 and 4- 6. Mean value curves show that earthquakes from reverse fault mechanisms present a mode for a smaller period (0.24 s) than strike slip faults (0.27 s) and they also have larger amplitude.



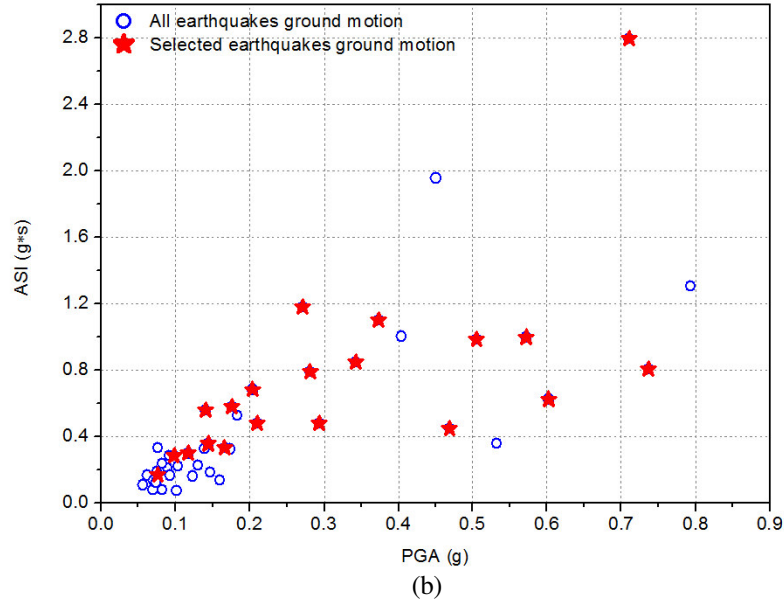


Figure 4- 4: Final selection of ground motions for (a) reverse, and (b) strike slip faults

In this study, a total of 40 ground motion records (20 records from a reverse and 20 records from a strike slip mechanism, respectively) from Iran and other regions having similar faulting mechanisms and seismic potential were selected without scaling, to represent the record-to-record variability. The response spectrum of each ground motion is determined by taking the SRSS of the response spectrum of the two horizontal ground motion components. Tables 4- 4 and 4- 5 report some of the important features of the selected earthquakes and the associated intensity measure parameters of the ground motions.

Table 4- 4: Some important parameters of the selected earthquake ground motions (reverse)

Earthquake	Year	M_w	R (Km)	PGA (g)	ASI (g*s)
Chi-Chi-0.1125g	1999	7.62	101.62	0.1125	0.491401
Chi-Chi-0.1348g	1999	7.62	63.29	0.1348	0.579302
Chi-Chi-0.1748g	1999	7.62	37.83	0.1748	0.814761
Chi-Chi-0.2058g	1999	7.62	47.86	0.2058	0.967536
Chi-Chi-0.2595g	1999	7.62	39.70	0.2595	0.949184
Chi-Chi-0.3643g	1999	7.62	86.39	0.3643	1.118649
Chi-Chi-0.5283g	1999	7.62	95.70	0.5283	1.066492
Chi-Chi-0.0823g	1999	7.62	59.80	0.0823	0.393901
Northridge-0.2148g	1994	6.69	14.92	0.2148	0.760153
Northridge-0.3908g	1994	6.69	18.62	0.3908	0.647099
Northridge-0.4673g	1994	6.69	39.39	0.4673	0.567823
Northridge-0.4898	1994	6.69	40.68	0.4898	1.692820
Northridge-0.5102g	1994	6.69	16.27	0.5102	0.890333
Northridge-0.5908g	1994	6.69	22.45	0.5908	0.976386
Sanfernando-0.2994g	1971	6.61	25.36	0.2994	0.618939
Whittier Narrows-0.3408g	1987	5.99	21.26	0.3408	0.516234
Capemendocino-0.1668g	1992	7.01	53.34	0.1668	0.568378
Capemendocino-0.4244g	1992	7.01	22.64	0.4244	1.278070
Tabas-0.3505g	1978	7.40	20.63	0.3505	0.766511
Tabas-0.8128g	1978	7.40	55.24	0.8128	2.280662

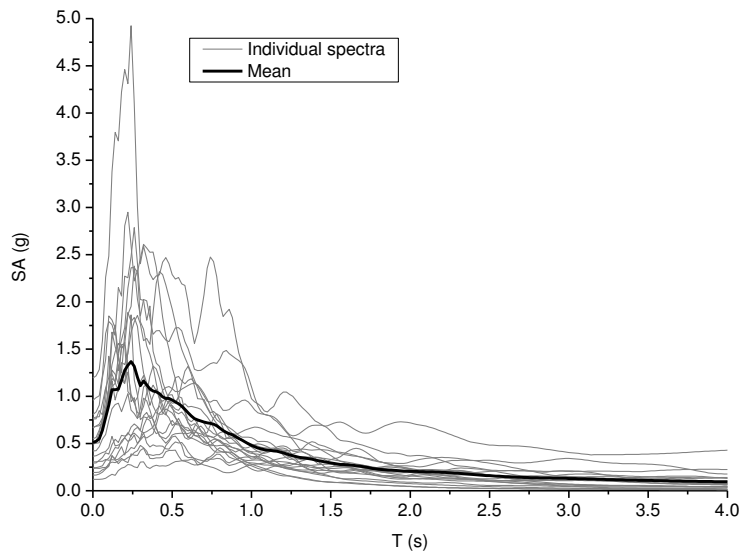


Figure 4- 5: Response spectra (5%) of the selected ground motions for reverse faults

Table 4- 5: Some important parameters of the selected earthquake ground motions (strike-slip)

Earthquake	Year	M_w	R (Km)	PGA (g)	ASI (g*s)
Morgan Hill-0.0983g	1984	6.19	30.05	0.0983	0.284824
Parkfield-0.469g	2004	6.00	14.50	0.4690	0.447411
Parkfield-0.602g	2004	6.00	14.80	0.6020	0.624203
Manjil-0.5051g	1990	7.40	40.43	0.5051	0.986322
Morgan Hill-0.2814g	1984	6.19	36.34	0.2814	0.789886
Morgan Hill-0.3426g	1984	6.19	16.67	0.3426	0.847620
Kobe-0.7105g	1995	6.90	18.27	0.7105	2.794062
Imperial Valley-0.176g	1979	6.53	24.82	0.1760	0.579679
Duzce-0.1445g	1999	7.14	27.74	0.1445	0.356142
Victoria-0.5722g	1980	6.33	33.73	0.5722	0.997996
Parkfield-0.2934g	1966	6.19	40.26	0.2934	0.480003
Landers-0.1407g	1992	7.28	27.33	0.1407	0.560219
Landers-0.3733g	1992	7.28	82.12	0.3733	1.100193
Kobe-0.0765g	1995	6.90	123.33	0.0765	0.166192
Duzce-0.2101g	1999	7.14	29.27	0.2101	0.479420
Duzce-0.7367g	1999	7.14	24.05	0.7367	0.806259
Parkfield-0.271g	2004	6.00	32.10	0.2710	1.179797
Imperial Valley-0.1661g	1979	6.53	48.62	0.1661	0.329791
Duzce-0.1174g	1999	7.14	31.56	0.1174	0.297492
Kojaeli-0.1387g	1999	7.51	77.63	0.1387	0.682200

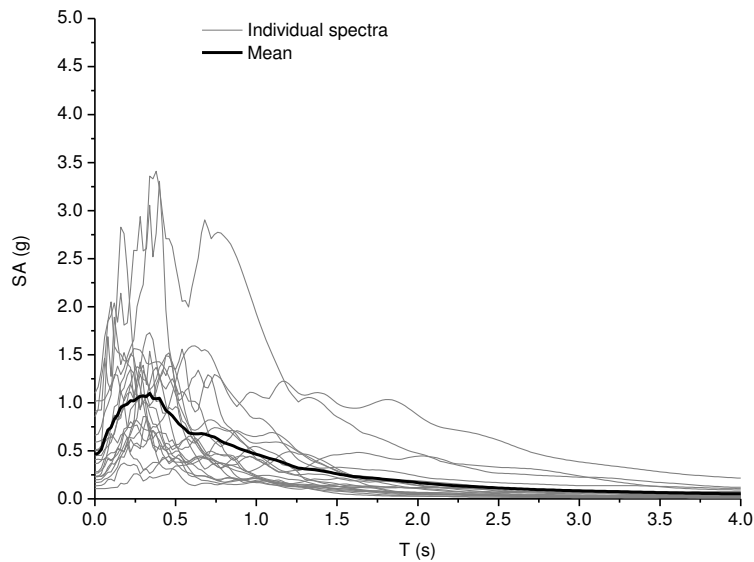


Figure 4- 6: Response spectra (5%) of the selected ground motions for strike slip faults

Chapter 5

5 SEISMIC DAMAGE LIMIT STATES AND UNCERTAINTIES

To generate reliable fragility curves, the definition of bridge damage limit states (LS) is of significant importance. These curves describe the probability of reaching or exceeding each damage state given a level of ground motion, they can be developed empirically or analytically. One of the main sources of uncertainty for estimating fragility curves is associated to the definition of bridge damage states. Previous studies presented several qualitative and quantitative limit state definitions for different bridge damages. Damage in the structure is due to the deformation of the bridge system and its components. Therefore there are two kinds of bridge damage limit state definitions, namely: local and global response parameters that can be defined as engineering demand parameters. Global engineering demand parameters are considered for overall the structural response whereas the local ones are utilized for certain structural components. To obtain reliable fragility curves especial consideration must be given to the selection of the appropriate engineering demand parameters assumed to define the bridge limit states. Since the seismic damage of the bridge is represented by the bridge seismic response, therefore, the selected engineering demand parameters should have good correlation with the seismic damage measure used. Sufficient number of damage limit states should be considered to represent the physical damage on bridges according to the seismic actions. Different codes and studies reported qualitative damage limit state definitions for bridges; however quantitative damage limit state definitions are not widely available for them. It should be noted that one of the main source of uncertainty that is correlated to fragility curves corresponds to the damage state definitions.

5.1 Previous studies

Figure 5- 1 shows previous research work and codes related to the seismic vulnerability assessment of existing bridges. As can be seen in Figure 5- 1, most of the research developed was led in USA, and the lack of investigation in Iran manifests the significant vulnerability

tendency of bridges in this area. The statistical information shows the distribution of some of the important attributes of the limit states, which are determined considering the associated inventory data.

Performance of pre-1990 bridges revealed that these structures are seismically vulnerable. The importance of acceptable seismic behavior for bridges in transportation systems has emphasized the need for seismic safety evaluations of existing bridges. In some countries, there is a lack of detailed studies analyzing the seismic vulnerability of the pre-1990 bridges that allows leading specific tasks to reduce economic losses in the future. Furthermore, fragility curves can incorporate the repair costs and the recovery time for evaluating the seismic performance of a highway system, this methodology is widely applied to assess the seismic vulnerability of bridges located in areas of high seismicity [24]. To clarify the issue in this report previous researches have been studied, and the summary of that is shown in Table 5- 1.

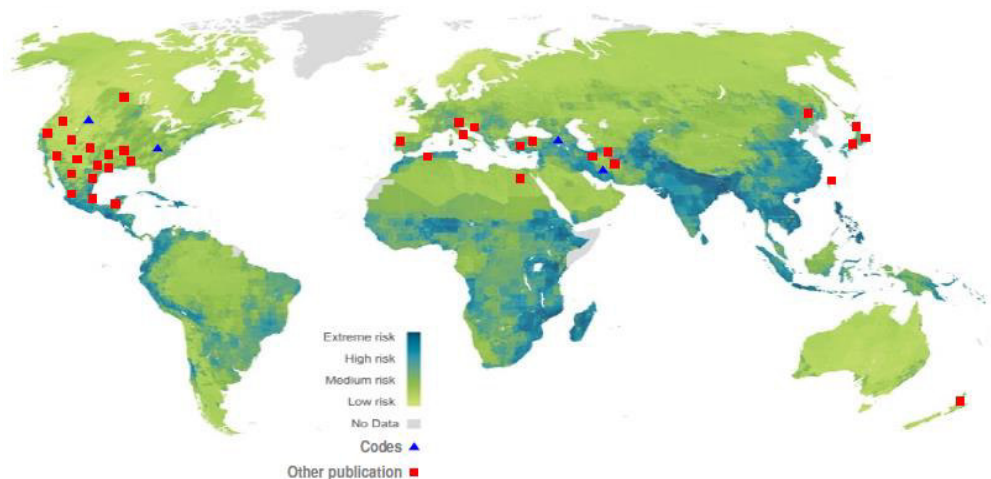


Figure 5- 1: Previous research work and codes related to seismic vulnerability assessment of existing bridges (adapted from <http://www.guardian.co.uk/environment/damian-carrington-blog/2011/oct/26/climate-change-developing-country-impacts-risk#>)

Table 5- 1: Summary of previous researches and codes

Code/ research work Country/ Region	Number of limit states- designation	Qualitative	Quantitative					
			Material		Section	Element	Other	
			Concrete	Steel				
Priestley <i>et al.</i> (1996) USA [108]	3	Serviceability Damage control Survival				$M-\phi$ Figure 5- 2		
Mander (1998) USA [118]	5	No damage Slight Moderate Extensive Complete	<3days <3 weeks <3 months >3 months					0 0.01-0.03 0.02-0.15 0.1-0.4 0.3-1 (Repair cost ratio)
Mander <i>et al.</i> (1999) Central- Southeastern USA [149]	4	Slight Moderate Extensive Complete	Cracking-Spalling Backwall collapse Pier failure Pier collapse				0.01 0.025 0.05 0.075 Table 5- 2	
Kowalsky (2000) USA [150]	2	Serviceability Damage control		0.004 0.015 0.018 0.06 Table 5- 3				
Saxena <i>et al.</i> (2000) USA [151]	5	No damage Slight Moderate Extensive Complete			1 2.01 6.03 11.07 23.65 μ_ϕ			
Hose <i>et al.</i> (2000) USA [152]	5	No damage Slight Moderate Extensive Complete	Visible cracking Cracking Open cracks Width cracks Buckling Table 5- 4	- <1mm 1-2mm >2mm >2mm Table 5- 5				
Kawashima (2000) Japan [153]	3	Minimum Repairable Significant		$0.004 - \epsilon_{cu}$ $0.03-1.5\epsilon_y$ $0.005 - 2\epsilon_{cu}/3$ $0.08 - 2\epsilon_y/3$ ϵ_{cu} ϵ_{sh}	2-4 4-6 8-10 μ_ϕ	1-2 2-4 4-6 μ_d		
Hwang <i>et al.</i> (2001) New Madrid USA [67]	4 5	No damage Cracking Hinging Flexural failure Slight Moderate Extensive Complete	Minor cracking Extensive cracking Hinging in column Flexural of column Table 5- 6		$M1 > M$ $My > M \geq M1$ $M \geq My, \theta < \theta_p$ $M \geq My, \theta > \theta_p$ $M-\phi$ Table 5- 6		$\mu_{cy1} > \mu_d$ $\mu_{cy} > \mu_d > \mu_{cy1}$ $\mu_{c2} > \mu_d > \mu_{cy}$ $\mu_{cmax} > \mu_d > \mu_{c2}$ μ_d Table 5- 7	
Karim and Yamazaki (2003) Japan [154]	5	No damage Slight Moderate Extensive Complete						$0 < DI \leq 0.14$ $0.14 < DI \leq 0.4$ $0.4 < DI \leq 0.6$ $0.6 < DI < 1$ $1 \leq DI$
Hazus (FEMA, 2003) USA [37]	5	No damage Slight Moderate Extensive Complete	No damage Minor cracking Shear cracking Shear failure Column collapse Table 5- 8					
Liao and Loh (2004) Taiwan [155]	4	Slight Moderate Extensive Complete	Minor cracking Moderate crack Shear failure Column collapse Table 5- 9			$\mu_d=2$ $\mu_d=4$ $\mu_d=6$ $\mu_d=9$ μ_d Table 5- 10		

Summary of previous researches and codes (continue)

Elnashai <i>et al.</i> (2004) USA and Greece [56]	5	Undamaged Slight Extensive No collapse Collapse	no damage minor damage significant damage extensive damage collapse Table 5- 11				
Choi <i>et al.</i> (2004) Central- Southeastern USA [69]	4	Slight Moderate Extensive Complete	-			$1 < \mu_d < 2$ $2 < \mu_d < 4$ $4 < \mu_d < 7$ $7 < \mu_d$ μ_d Table 5- 12	
Nateghi <i>et al.</i> (2004) Iran [70]	5	No damage Slight Moderate Extensive Complete	No damage Minor cracking Shear cracking Shear failure Column collapse				$0 < DI \leq 0.14$ $0.14 < DI \leq 0.4$ $0.4 < DI \leq 0.6$ $0.6 < DI < 1$ $1 \leq DI$
Nielson (2005) USA [100]	4	Slight Moderate Extensive Complete		μ_ϕ			
Johnson <i>et al.</i> (2006) USA [156]	4	Slight Moderate Extensive Complete		μ_ϕ			
Kappos <i>et al.</i> (2006) Greece [157]	5	No damage Slight Moderate Extensive Complete	None Small-scale repairs Repair of elements Reconstruction-parts Reconstruction-bridge			$\mu_d = \delta/\delta_y < 0.7$ $\mu_d = \delta/\delta_y > 0.7$ $\mu_d = \delta/\delta_y > 1.5$ $\mu_d = \delta/\delta_y > 3$ $\mu_d = \delta/\delta_y > \mu_u$	
Mander <i>et al.</i> (2007) New Zealand [47]	5	No damage Slight Moderate Extensive Complete	- <3 days <3 weeks <3 months >3 months	$M_{-\phi}$		- 0.62 2.3 4.4 5.64 (drift displacement limit)	
Mander <i>et al.</i> (2007) Japan [47]	5	No damage Slight Moderate Extensive Complete	- <3 days <3 weeks <3 months >3 months	$M_{-\phi}$		- 0.53 1.6 4.6 5.66 (drift displacement limit)	
Mander <i>et al.</i> (2007) Caltrans [47]	5	No damage Slight Moderate Extensive Complete	- <3 days <3 weeks <3 months >3 months			- 0.53 1.9 5.1 6.16 (drift displacement limit)	
Lee <i>et al.</i> (2007) Korea [158]	3	No damage Repairable Significant	minor response occur Inelastic response collapse				$0.5 \leq C/D$ $0.33 \leq C/D < 0.5$ $C/D < 0.33$ C/D (seismic capacity & seismic demand)
Turkish Earthquake Code (2007) [173], [174]	4	Slight Moderate Extensive Complete	-	$M_{-\phi}$ Figure 5- 3			

Summary of previous researches and codes (continue)

Marano <i>et al.</i> (2008) Italy [159]	5	No damage Repairable a) Light b) Moderate Irreparable Life safe Collapse				<0.2 0.4 <1 >1 1.8 >3	
Zhang <i>et al.</i> (2008) USA [160]	4	Slight Moderate Extensive Complete				1< μ_d 2< μ_d 4< μ_d 7< μ_d	γ >100% γ >150% γ >200% γ >250% (shear strain)
Shinozuka <i>et al.</i> (2008) USA [161]	4	no damage minor damage moderate major damage			μ_ϕ based on experimental test as mentioned by Johnson <i>et al.</i>		
Kalantari <i>et al.</i> (2009) Iran [162]	4	Slight Moderate Extensive Complete				1< μ_d <2 2< μ_d <4 4< μ_d <7 7< μ_d	
Azevedo <i>et al.</i> (2010) Portugal [163]	5	No damage Slight Moderate Extensive Complete	No damage Minor cracking Shear cracking Shear failure Column collapse				
Ramanathan <i>et al.</i> (2010) Central-Southeastern USA [164]	4	Slight Moderate Extensive Complete			μ_ϕ	$\mu_{cy1} > \mu_d$ $\mu_{cy} > \mu_d > \mu_{cy1}$ $\mu_{c2} > \mu_d > \mu_{cy}$ $\mu_{cmax} > \mu_d > \mu_{c2}$ μ_d as mentioned in Hwang <i>et al.</i>	
Roy <i>et al.</i> (2010) USA [165]	4	Slight Moderate Extensive Complete			μ_ϕ	$\mu_{cy1} > \mu_d$ $\mu_{cy} > \mu_d > \mu_{cy1}$ $\mu_{c2} > \mu_d > \mu_{cy}$ $\mu_{cmax} > \mu_d > \mu_{c2}$ μ_d as mentioned in Hwang <i>et al.</i>	
Kibboua <i>et al.</i> (2011) Algeria [166]	5	No damage Slight Moderate Extensive Complete					0<DI≤ 0.14 0.14<DI≤0.4 0.4<DI≤0.6 0.6<DI< 1 1≤DI
Iran code (2011) Iran [167]	5	No damage Slight Moderate Extensive Complete	No damage Bridge in elastic zone Extensive cracking Hinging in column Share failure				
Shirazian (2011) Iran [168]	2	Slight Complete	Minor cracking Column collapse			μ_d	
Marano <i>et al.</i> (2011) Italy [169]	3	Slight Moderate Heavy			$M-\phi$		
Donatello <i>et al.</i> (2011) Italy [170]	3	Slight Moderate Sever					
Tavares <i>et al.</i> (2012) Canada [26]	4	Slight Moderate Extensive Complete			μ_ϕ	$\mu_{cy1} > \mu_d$ $\mu_{cy} > \mu_d > \mu_{cy1}$ $\mu_{c2} > \mu_d > \mu_{cy}$ $\mu_{cmax} > \mu_d > \mu_{c2}$ μ_d as mentioned in Hwang <i>et al.</i>	

Summary of previous researches and codes (continue)

Islam (2012) Egypt [171]	5	No damage Slight Moderate Extensive Complete					$0 < DI \leq 0.14$ $0.14 < DI \leq 0.4$ $0.4 < DI \leq 0.6$ $0.6 < DI < 1$ $1 \leq DI$ as mentioned in Karim & Yamazaki
Banerjee <i>et al.</i> (2013) USA [172]	4	no damage minor damage moderate major damage			μ_ϕ based on experimental test as mentioned by Johnson <i>et al.</i>		
Jara <i>et al.</i> (2013) Mexico [23]	4	Slight Moderate Extensive Complete			$M-\phi$		

In the following, some tables and figures are discussed in detail. In the study of Priestley *et al.* [108] qualitative and quantitative limit states were presented for member and structure responses. In the member seismic response cracking, yield, spalling and ultimate limit states are considered as qualitative which is shown schematically with respect to the moment-curvature diagram in Figure 5- 2 (a). Also three structural limit states, namely: serviceability, damage control, and survival are considered as well, which is shown in Figure 5- 2 (b) by presenting the yield point of an idealized force-displacement curve. An average range of displacement ductility ratios are employed to describe both qualitative and quantitative limit states. On the other hand, the quantitative limit states were presented by considering a moment curvature diagram.

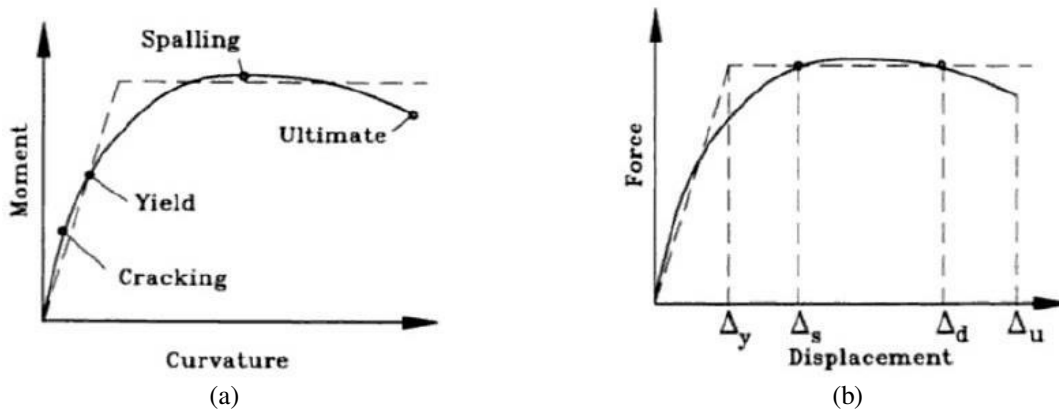


Figure 5- 2: Schematic representation of limit states, (a) member limit state, (b) structure limit state (Priestley *et al.* [108])

Basöz and Mander [77] presented five damage states for highway bridge components, which is in line with the HAZUS limit states definition, listed in Table 5- 2 with their corresponding failure mechanisms. In this study the columns drift was considered to predict several damage

states for the non-seismically and the seismically designed bridges. Note that by increasing the bridge damage state, the displacement limits for girder bridges with weak bearings and strong piers increase as well. For each damage limit state, Banerjee and Shinozuka [62] used the given drift limits as a quantity limit state in terms of the rotational ductility of column.

Table 5- 2: Drift and displacement limits for each damage state (Basöz and Mander) [77]

Damage State	Failure Mechanisms	Range of Repair Cost Ratios		Displacement Limits for Weak Bearings and Strong Pier (m)
		Non-seismic	Seismic	
Slight damage	Cracking, spalling	0.005	0.01	0.05
Moderate damage	Bond, abutment back wall collapse	0.01	0.025	0.1
Extensive damage	Pier concrete failure	0.02	0.05	0.175
Complete damage	Deck unseating, pier collapse	0.05	0.075	0.3

Kowalsky [150] used two damage limit states namely: “serviceability” and “damage control”, that are considered for circular RC bridge columns. In the serviceability limit state, repair is not necessary after the occurrence of an earthquake; however damage control limit state suggests that only repairable damage occurs. Also these damage limit states were considered based on concrete compression and steel tension strain limits which are listed in Table 5- 3.

Table 5- 3: Quantitative damage limit state definitions (Kowalsky) [150]

Limit State	Concrete Strain Limit	Steel Strain Limit
Serviceability	0.004	0.015
Damage Control	0.018	0.06

Hose *et al.* [152] specified five limit states and performance levels. The seismic damage of the bridges was characterized in order to socio-economic descriptions at five selected performance levels. The classification of five damage states as well as socio-economic and repair descriptions are listed in Table 5- 4.

Table 5- 4: Bridge damage assessment (Hose *et al.*) [152]

Level	Damage Classification	Damage Description	Repair Description	Socio-economic Description
I	No	Barely visible cracking	No repair	Fully operational
II	Minor	Cracking	Possible repair	Operational
III	Moderate	Open cracks, onset of spalling	Minimum repair	Life safety
IV	Major	Very wide cracks, extended concrete spalling	Repair	Near collapse
V	Local failure /Collapse	Visible permanent deformation, buckling/rupture of reinforcement	Replacement	Collapse

In this study the bridge damage is explained based on the structure capacity from concrete cracking to strength degradation. To clarify the issue the engineering terms were chosen for the five performance levels rather than the socio-economic definitions. Table 5- 5 presents qualitative and quantitative performance descriptions, namely: crack widths, crack angles, and regions of spalling in terms of five performance levels. It should be noted that several engineering demand parameters were studied for each performance level, for quantitative descriptions using experimental result of various column test and numerical modeling. Steel and concrete strains, plastic rotation, curvature and displacement ductility demands, principal compression and tension stress, residual deformation index, drift ratio, equivalent viscous damping ratio and normalized effective stiffness, are investigated as engineering demand parameters.

Table 5- 5: Bridge performance assessment (Hose *et al.*) [152]

No.	Performance Level	Qualitative Performance Description	Quantitative Performance Description
I	Cracking	Onset of hairline cracks	Cracks barely visible
II	Yielding	Theoretical first yield of longitudinal reinforcement	Crack widths < 1mm
III	Initiation of local mechanism	Initiation of inelastic deformation. Onset of concrete spalling.	Crack widths 1-2mm. Length of spalled region > 1/10 cross-section depth
	Full development of local mechanism	Development of diagonal cracks	Crack widths > 2mm. Diagonal cracks extend over 2/3 cross-section depth. Length of spalled region > 1/2 cross-section depth
IV	Strength degradation	Wide crack widths/spalling over full local mechanism region	
V	Strength degradation	Buckling of main reinforcement. Rupture of transverse reinforcement. Crushing of core concrete	Crack widths > 2mm in concrete core. Measurable dilation > 5% of original member dimension

Hwang *et al.* [67] presented two different approaches for the seismic damage assessment and the seismic fragility analysis of bridges. In the first approach, damage states for the response parameters such as column in shear and flexure, and bearings are defined, as well as component-by-component assessment of seismic damage was performed. For bearings two damage states were defined to consider yield and ultimate shear capacity. Column shear capacity was compared with the column shear demand in order to define whether or not columns face any shear damage. Finally, for the flexural capacity of columns, four damage states were considered. Table 5- 6 shows damage description of each damage state, and its limit state principles. M_i is the column moment at the first yielding of the longitudinal bar, whereas M_y is the yield moment at the idealized moment curvature diagram of the column sections. θ_p is the plastic hinge rotation with ε_c equal to 0.002 and 0.004 for the columns with and without lap splices at the bottom of the columns, respectively.

Table 5- 6: Seismic damage assessment criteria for columns in flexure (Hwang *et al.*) [67]

Criterion	Description of Damage	Column Status
$M_1 > M$	No reinforcing steel yielding, minor cracking in concrete	No Damage,(OK)
$M_y > M \geq M_1$	Tensional reinforcement yielding and extensive cracking in concrete	Cracking,(C)
$M \geq M_y, \theta < \theta_p$	Hinging in column, but no failure of column	Hinging, (H)
$M \geq M_y, \theta > \theta_p$	Flexural failure of column	Flexural failure, (F)

In the second approach, the overall seismic damage was considered to develop fragility functions. In this study the displacement ductility was defined as the damage state for engineering demand parameter, as defined by equation 5.1.

$$\mu_{ci} = \frac{\Delta y_i}{\Delta_{y1}} \quad (5.1)$$

where μ_{ci} is the ductility demand at the i^{th} damage state, Δ_{yi} is the relative displacement of the limit state i at the top of a column, and Δ_{y1} is the relative displacement of a column when the longitudinal reinforcing bars reach the first yield. Table 5- 7 presents the damage states definition according to Hwang *et al.* [67].

Table 5- 7: Bridge damage states by displacement ductility ratios (Hwang *et al.*) [67]

Damage States		Criterion
S	Slight/Minor Damage	$\mu_{cy} > \mu_d > \mu_{cy1}$
M	Moderate Damage	$\mu_{c2} > \mu_d > \mu_{cy}$
E	Extensive Damage	$\mu_{cmax} > \mu_d > \mu_{c2}$
C	Complete Damage	$\mu_d > \mu_{cmax}$

μ_{cy1} is the displacement ductility ratio at the first longitudinal bar yield. μ_{cy} is the yield displacement ductility ratio of the column which will explain in section 5.3. μ_{c2} is the displacement ductility ratio with $\varepsilon_c=0.002$ or $\varepsilon_c=0.004$. μ_{cmax} is the maximum displacement ductility ratio, which is defined as; $\mu_{cmax} = \mu_{c2} + 3.0$.

Five qualitative damage states are defined for highway bridge components in HAZUS (FEMA, 2003) [37], namely ds₁: no damage, ds₂: slight/minor, ds₃: moderate, ds₄: extensive and ds₅: complete damage, as defined in Table 5- 8. As it is mentioned in the table, qualitative descriptions are presented in details; however a quantitative description of these damage states is not defined. For the bridge components and the whole structure system, each damage state has its own functional and operational interpretation. By increasing bridge damage level, more time to recovery time for operational and functional issues is required for the bridge.

Table 5- 8: Definitions of damage states by HAZUS (FEMA) [37]

Damage States	Definitions
None (ds1)	No bridge damage
Slight/Minor (ds2)	Minor cracking and spalling to the abutment, cracks in shear keys at abutments, minor spalling and cracks at hinges, minor spalling at the column (damage requires no more than cosmetic repair) or minor cracking to the deck.
Moderate (ds3)	Any column experiencing moderate (shear cracks) cracking and spalling (column structurally still sound), moderate movement of the abutment (<2"), extensive cracking and spalling of shear keys, any connection having cracked shear keys or bent bolts, keeper bar failure without unseating, rocker bearing failure or moderate settlement of the approach.
Extensive (ds4)	Any column degrading without collapse – shear failure - (column structurally unsafe), significant residual movement at connections, or major settlement approach, vertical offset of the abutment, differential settlement at connections, shear key failure at abutments.
Complete (ds5)	Any column collapsing and connection losing all bearing support, which may lead to imminent deck collapse, tilting of substructure due to foundation failure.

Four damage states were defined in the study of Liao and Loh [155] for highway bridges, which are in line with the ones defined by HAZUS. Table 5- 9 reports the qualitative description of each damage state for bridge components.

Table 5- 9: Damage state description for bridge components (Liao and Loh) [155]

Damage States	Qualitative Descriptions
Slight Damage	Minor cracks and spalling at the column, abutment, girder or deck, cracks at shear key, cracks at expansion joint or approach slab
Moderate Damage	Column experiencing moderate cracks and spalling, abutment failure without collapse, shear key failure or restrainer failure without unseating
Extensive Damage	Any column degrading without collapse or shear failure, significant movement at connections, significant offset of abutment
Complete Damage	Any column collapse or large movement of connections, deck collapse, tilting of substructure due to ground failure

Liao and Loh [155] developed analytical fragility curves utilizing quantified damage limit states based on ductility and displacement, Table 5- 10. In this study, the ductility limits were definite for strong bearings and weak pier due to the design type used for the bridge, weather the bridge was designed accounting for seismic considerations or designed with a conventional design. Although the displacement limits were taken in terms of strong pier and weak bearings, girder seat length was considered to define the complete damage state. As it is presented in the table for moderate and extensive damage states, numerical function were given without any physical meaning for the associated damage state.

Table 5- 10: Ductility and displacement limits for each damage state (Liao and Loh) [155]

Damage State	Ductility limits for weak pier and strong bearings		Displacement limits
	Seismic Design	Conventional Design (non-seismic design)	Weak bearings and strong pier
Slight	$\mu = 2.0$	$\mu = 1.0$	Yield Displacement
Moderate	$\mu = 4.0$	$\mu = \min(1+ (\mu_f-1)/2, 2.0)$	10 cm
Extensive	$\mu = 6.0$	$\mu = \min(\mu_f, 3.0)$	20 cm
Complete	$\mu = 9.0$	$\mu = 4.5$ or pier reach its ultimate capacity	$\min(40\text{cm}, 2N/3)$

μ_f : corresponding ductility at occurrence of flexure to shear failure.
N: seat length of a girder at the support.

Five earthquake damage limit states presented Elnashai *et al.* [56], namely: undamaged, slightly damage, extensive damage, no collapse and collapse that are listed in Table 5- 11, including both qualitative and quantitative descriptions. The first limit state, no damage, a small displacement in the structure is expected; on the other words, this damage state occurs when the first longitudinal reinforcing bar reaches the yield. In the slightly damage limit state, minor structural damage happen after an earthquake such as member flexural strength may have been reached, but concrete spalling in plastic hinges does not occur. Significant structure damage is expected in third damage, extensive damage, no repair should be considered; otherwise the bridge would be

out of service after earthquake. In the mentioned limit state, the concrete core remains without damage, buckling of the longitudinal reinforcement or rupture of transverse reinforcement do not occur as well. Below the four limit state is the extensive damage that happens for the bridge, but the global collapse is not expected. In this case, the repair may be neither possible nor cost-effective. Finally, the last limit state corresponds to the global collapse; it corresponds to the failure of the structure to tolerate any type of gravity loads.

Table 5- 11: Definition of damage states for bridge components (Elnashai *et al.*) [56]

No.	Performance Level	Qualitative Performance Description	Quantitative Performance Description
1	Undamaged	no damage should take place and the expected response is of small displacement amplitude	yielding of the first longitudinal row of reinforcing bars occurs at a level of transverse load equal to 75% of the yield load V_y
2	Slightly	Member flexural strengths may have been reached, and limited ductility developed	maximum usable strain of 0.3%,
3	Extensively	Rupture of transverse reinforcement or buckling of longitudinal reinforcement should not occur and core concrete in plastic hinge regions should not need replacement	a displacement capacity that is the average of LS2 and LS4
4	No collapse	square and wall sections showed that crushing of confined concrete and buckling of longitudinal reinforcement occurs	compression stress drops to less than $0.5 f_{cc}$
5	Collapse	Collapse of the bridge is appear	ultimate strain ϵ_{cu}

In the study of Choi *et al.* [69], column ductility demand, steel fixed and expansion bearing deformations, and elastomeric bearing deformations were defined as damage states of bridges, based on qualitative descriptions of the damage states as provided by HAZUS. Table 5- 12 shows the quantitative definitions for each damage state in reference to the mentioned engineering demand parameters, the information is provided based on experimental test results and recommendations from previous studies. The column curvature ductility is taken to quantified damage states based on the non-seismically designed columns by considering lap-slices at the base. For bearings at the pre-stressed concrete girders, the damage states taken into account correspond to the displacement needed for the unseated and the fracture conditions at bearing. However, the problem at the bearings is due to their size and the width of the support.

Table 5- 12: Definition of damage states for bridge components (Choi *et al.*) [69]

Damage State	Engineering Demand Parameters				
	Column(μ)	Steel Bearings (δ , mm)	Expansion Bearings (δ , mm)	Fixed Dowels (δ , mm)	Expansion Dowels (δ , mm)
Slight	$1.0 < \mu < 2.0$	$1 < \delta < 6$	$\delta < 50$	$8 < \delta < 100$	$\delta < 30$
Moderate	$2.0 < \mu < 4.0$	$6 < \delta < 20$	$50 < \delta < 100$	$100 < \delta < 15$	$30 < \delta < 100$
Extensive	$4.0 < \mu < 7.0$	$20 < \delta < 40$	$100 < \delta < 150$	$150 < \delta < 25$	$100 < \delta < 150$
Complete	$7.0 < \mu$	$40 < \delta$	$150 < \delta < 255$	$255 < \delta$	$150 < \delta < 255$

To develop analytical fragility curves, five damage states are employed in the studies of Karim and Yamazaki [68], and Nateghi and Shahsavari [70], namely: no damage, slight, moderate, extensive and complete damages. In the study of Nielson [100], the qualitative limit states employed are based on the HAZUS. In order to define the quantification of damage states, engineering demand parameters are considered, such as column curvature ductility, steel fixed and rocker bearing deformations, elastomeric fixed and expansion bearings deformation, and abutment displacements.

In the study of Avsar and Yakut [173], three damage states are considered, namely: serviceability (LS1), damage control (LS2) and collapse prevention (LS3), according to the Turkish Earthquake Code [174]. Therefore, under the effect of an earthquake ground motion, the four corresponding damage states are termed as slight, moderate, significant, and collapse states. The schematic representation of the three damage limits and their corresponding damage states are presented with respect to the force-deformation curve in Figure 5- 3. In this study damage states of the bridge component are defined according to the engineering demand parameters. For RC column and cap beam, which are expected to face inelastic deformation, curvature and shear demand are considered, however superstructure displacement is defined for deck unseating.

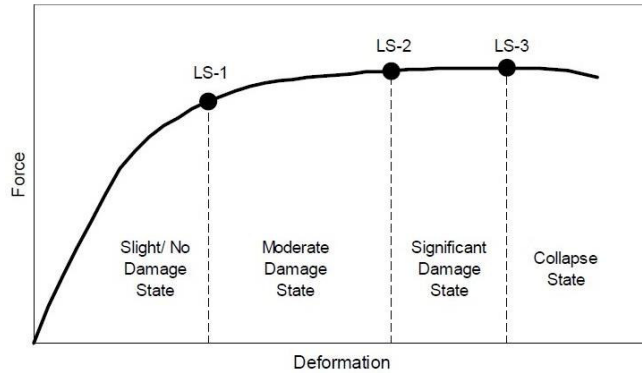


Figure 5- 3: Damage states and damage limits on a force-deformation curve (Avsar and Yakut) [173]

5.2 Damage parameters

Histograms of the previous investigation were obtained, and the results are presented in the following figures. Figure 5- 4 presents a comparison between the number of limit states adopted in different codes and by other researchers. Previous investigation (based on 38 documents) reported that the most used four limit states by researchers and codes that are named: Slight, Moderate, Extensive and Complete. Five damage states are employed by previous researchers: No damage, Slight, Moderate, Extensive and Complete. However, there is not much difference between 4 and 5 LS. The LS which named No damage can be skipped, since it only represents the elastic zone of behavior.

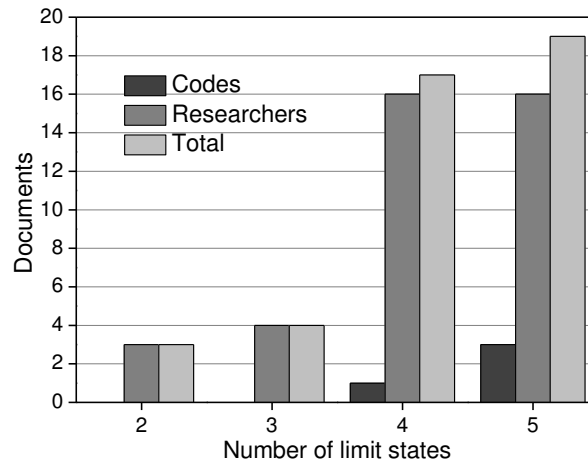


Figure 5- 4: Histogram for the number of limit states used by codes and researchers

Figure 5- 5 provides the comparison of LS in terms of their type: qualitative or quantitative. Qualitative description of five damage states are determined for bridges by HAZUS [53], Figure

5- 5, and by the Iran code [167]. However, Caltrans [44] considers both, qualitative and quantitative measurements. Hwang *et al.* [67] defined four damage states according to the flexural capacity of the columns. Priestley *et al.* [108] considered two structural limit states: serviceability and damage control.

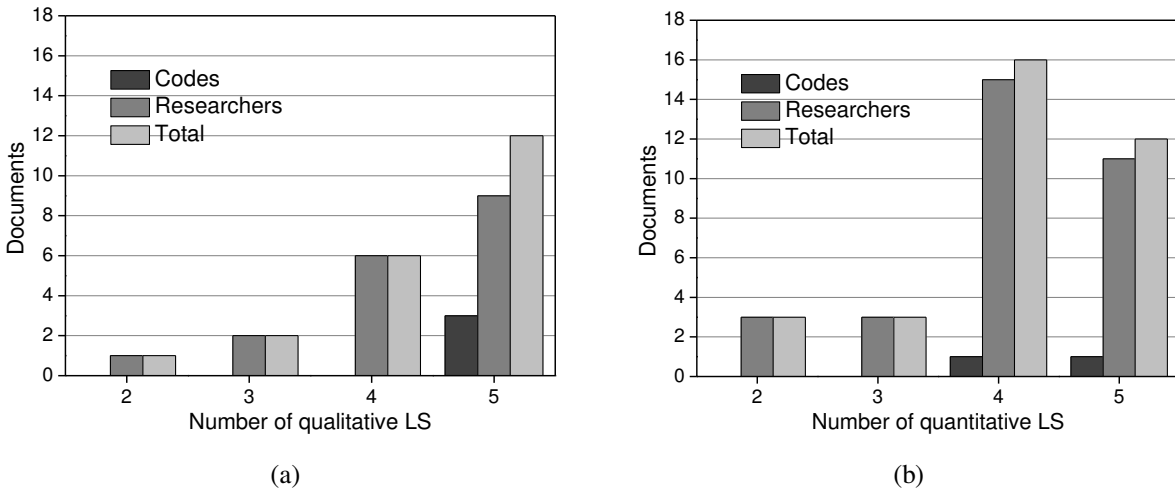


Figure 5- 5: Histogram of limit states for different codes and researchers (a) Qualitative, and (b) quantitative

Different researchers made emphasis on the different properties of the bridge elements by considering the epistemic uncertainties. In previous studies, Figure 5- 6, four different approaches are considered for the seismic damage assessment and the seismic fragility analysis of the bridges. In the first approach, the material properties are considered by researchers to quantify the bridge response. Priestly [108] and Kowalsky [150] proposed a strain limit in their studies. Kawashima [153], in Japan, provided a quantitative strain and ductility limits for the three damage levels. However, Hose [152] considered the crack width in his studies. In the second approach, the bridge seismic damage was evaluated by defining damage states, and by using Moment-Curvature relationships, that is identified through the label "section" in Figure 5- 6. In the third approach, damage limit states were defined to assess the overall seismic damage of the bridges, and the fragility curves were determined, and they are identified with the label "element" in Figure 5- 6. For this purpose, the damage states were defined using engineering demand parameters as the displacement ductility ratio of columns [23, 67]. In the last approach, other limit states were considered for the damage index [154] or for cost analysis [77]. Previous studies proposed different damage indexes. However, the displacement ductility is the most common [175]. In the study of Hwang *et al.* [67] was assumed, the displacement ductility ratio

of the column is used to assess the limit states, namely: slight damage, moderate damage, extensive damage and complete damage.

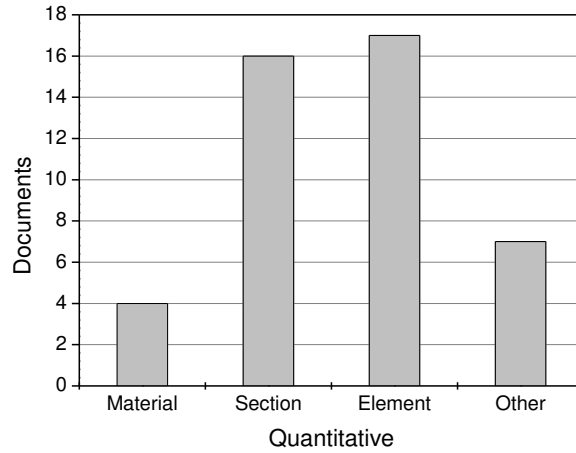


Figure 5- 6: Histogram for the approaches used to assess the bridge damages in previous studies

5.3 Damage states for RC column based on displacement ductility

In this study, the seismic damage is classified in four damage states, as described by Hwang *et al.* [67, 175]. In order to quantify damage states, the relative displacement ductility ratio of a column is used. Zhu *et al.* [176] analyzed a 125-column database and showed that aspect ratios (length/depth) smaller than two conducted to shear failures whereas columns with an aspect ratio greater than four failed in flexure mode. All the (length/depth) ratios in this study are greater than 4, therefore the shear failure mechanism is not considered. The displacement ductility ratio due to figure 3- 7 is defined through Equations:

$$\mu_i = \frac{\Delta_i}{\Delta_1} \quad (5.2)$$

where μ_i = ductility demand at the i^{th} damage state, Δ_i = relative displacement at the top of a column at the corresponding limit state i and Δ_1 = relative displacement of a column when the longitudinal reinforcing bars reach the first yield, calculated as follows:

$$\Delta_1 = \frac{1}{3} \varphi_1 L^2 \quad (5.3)$$

where L = the distance from the plastic hinge to the point of contra-flexure and φ_1 = the curvature correspondent to the relative displacement of a column when the vertical reinforcing bars at the bottom of the column reaches the first yield.

Hence, μ_1 , denotes the first limit state corresponding to a first yield displacement ductility ratio equal to 1. The second damage state, μ_y , represents the yield displacement ductility ratio, calculated as:

$$\mu_2 = \frac{\Delta_2}{\Delta_1} = \frac{\Delta_y}{\Delta_1} = \frac{1}{3} \frac{\varphi_y L^2}{\Delta_1} \quad (5.4)$$

where φ_y = the curvature correspondent to the relative displacement of a column when the vertical reinforcing bars at the bottom of the column reaches the yield (Figure 3- 7). The displacement ductility corresponding to the third damage state (μ_3) is the displacement ductility ratio corresponding to $\varepsilon_c = 0.002$ or $\varepsilon_c = 0.004$ for the columns with or without lap splices, respectively, where ε_c is the compressive strain at the concrete column, hence Δ_3 can be estimated as follow:

$$\mu_3 = \frac{\Delta_3}{\Delta_1} \quad (5.5)$$

$$\Delta_3 = \Delta_2 + \theta_p \left(L - \frac{L_p}{2} \right) \quad (5.6)$$

where θ_p and L_p are the rotation and the plastic hinge length, respectively. The plastic hinge rotation can be calculated by Equation 5.7 and the plastic hinge length can be estimated according to Priestley *et al.* [108]:

$$\theta_p = (\varphi_3 - \varphi_y)L_p \quad (5.7)$$

$$L_p = 0.08L + 0.022f_{ye}d_{bl} \geq 0.044f_{ye}d_{bl} \quad (5.8)$$

Where φ_3 is the curvature of a column when $\varepsilon_c = 0.002$ or $\varepsilon_c = 0.004$ for the columns with or without lap splices, respectively, d_{bl} is the diameter of the longitudinal reinforcing bars. Finally, μ_4 can be calculated as follow [67, 74]:

$$\mu_4 = \mu_3 + 3 \quad (5.9)$$

Four damage limit states (μ_1 , μ_2 , μ_3 , and μ_4) are identified in this research: slight (LS1), moderate (LS2), extensive (LS3), and collapse (LS4). These limit states are similar to those proposed by Hwang *et al.* [67]. In the following sections, the calculations of different limit states are described in detail.

5.4 Uncertainties

Based on previous works and on the available data from past earthquake reports, bridges are classified in terms of the span length (SL) and superstructure type, column height, material properties, connectivity between superstructure and substructure and presence of lap splice in column.

5.4.1 Uncertainties in span length and superstructure type

Depending on the superstructure type, the bridges are classified into different categories [25, 37, 69, 101]. As depicted in Figure 2- 9, in this research, bridges are classified in 3 different groups based on span length and superstructure type: with span length (SL) less than 20 m and slab superstructure type, SL between 20 m and 30 m and I-girder superstructure type and SL with more than 30 m with box girder superstructure. Most of bridges with superstructure length less than 20 m are nominated slab type superstructure. While bridges with SL between 20 m and 30

m have I-girder type superstructure. Around 50% of bridges with span length larger than 30 m have box girder type superstructure. Three major bridge classes were determined based on the primary structural attributes mentioned before. Previous studies show that one of the least vulnerable bridge classes is the slab superstructure type [26]. Hence, among the three major classes, we selected two of them as representatives of most common bridges, excluding the slab superstructure type.

For each of class, in terms of span length and superstructure type, real bridges were selected as case studies that are listed in Table 2-9. A typical configuration for a multi-span simply supported concrete girder bridge (consist of I and box girders) is shown in Figure 5- 7.

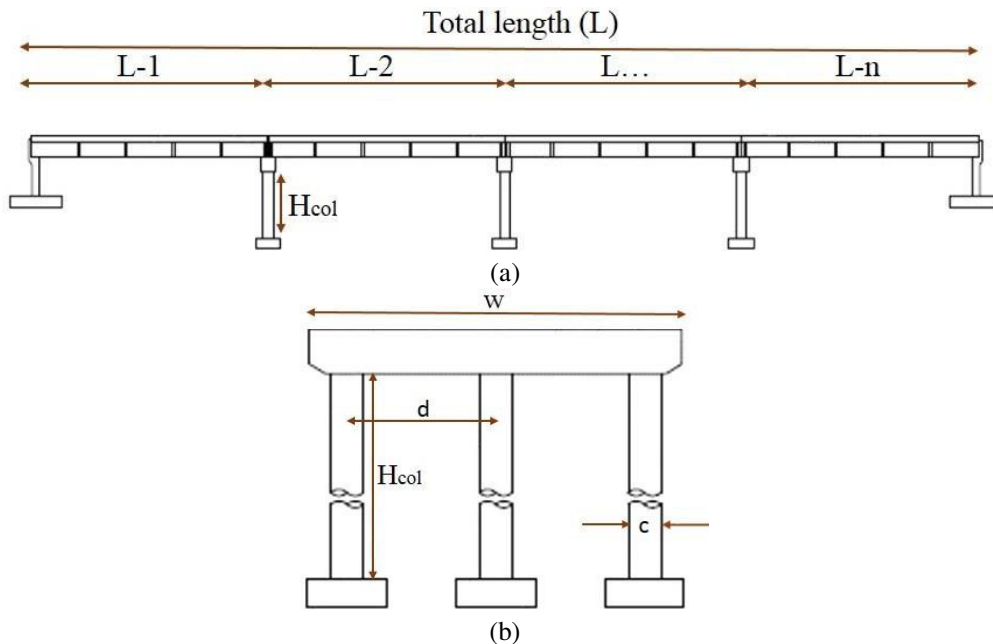


Figure 5- 7: Concrete bridge configuration

Fragility curves are generated for each class of bridges which are represented by 4 bridges samples which are listed in Tables 5- 13 and 5- 14. For nonlinear time history analyses, a total of 40 records due to two different seismic sources (20 earthquake ground motion for reverse fault and 20 for strike slip fault) are employed. Since each bridge is analyzed twice by each ground motion record accounting for two horizontal orthogonal directions to obtain the maximum response, a total of 80 analyses are performed for each bridge, leading to a total number of 640 analyses for the classification conformed by 8 case studies.

Table 5- 13: Structural attributes for the bridge samples for each major bridge class in terms of span length

Bridge classes	Deck type	Max. span length	Longitudinal steel bar (%)	Deck width (m)	Seat length (cm)
20≤SL<30	I girder	20-24	0.91-1.2	12	95
SL≥30	I & Box girder	32-37	0.91-1.56	12-16	95

Table 5- 14: Concrete reinforcing layout for each case study in terms of span length

Bridge classes	Sample ID	Number of spans	No. of column per bent	H _{col} (m)	c (m)	d (m)	Column section	
							Longitudinal bar	Transvers bar
20≤SL<30	1	15.6-24-24-15.6	3	6	1.1	4.5	30Φ22	Φ12@25
	2	6@20	2	10.5	1.3	7	20Φ30	Φ18@20
	3	7@20	2	16	1.4	7	20Φ30	Φ18@20
	4	6@20	2	21	1.4	7	20Φ30	Φ18@20
SL≥30	1	6@32	3	18	1.4	6.4	20Φ30	Φ18@20
	2	6@32	3	9	1.2	6.4	22Φ32	Φ14@5
	3	6@35	3	8	1.2	4.0	26Φ26	Φ12@25
	4	6@37	3	7	1.15	5.0	24Φ25	Φ12@25

5.4.2 Uncertainties in column section and column height

As it can be seen in Figure 2- 8, since the majority of bridges have circular cross-section, therefore fragility curves are developed only for circular column section. Circular sections are considered correspond to multi-span simply supported structures with elastomeric bearings at the abutments and the column bents and integral bridges with elastomeric bearings at the abutments.

In terms of column height, as mention in section 2 bridges are classified in two main groups: short column and high column. Table 2- 6 reveals that the majority of the bridges are simply supported with solid circular columns. Therefore, bridges are classified into 2 major groups in terms of column height as presented in Table 2- 8. In particular geometric characteristics of each bridge model is presented in Tables 5- 15 and 5- 16. In this part, a total of six bridges were selected as case study samples. A total of 40 earthquake ground motions recorded in two seismic sources are employed. Since each bridge is analyzed twice by each ground motion record, into two horizontal orthogonal components, to obtain the maximum response, a total of 80 analyses are performed for each bridge. Therefore, the total number of analyses for these classification criteria is 480.

Table 5- 15: Structural attributes for the bridge samples for each major bridge class in terms of column height

Bridge classes	Column height (m)	Column section (circular)	Longitudinal steel bar (%)	Deck width (m)	Span length (m)
SCC-S	6-10.5	D=1.2-1.3	1.06-1.56	12-16	20-32
HCC-S	16-21	D=1.4	0.91	12-16	20-32

Table 5- 16: Geometric characteristics for each case study in terms of span length

Bridge classes	Sample ID	Number of spans	No. of column per bent	H _{col} (m)	c (m)	d (m)	Column section	
							Longitudinal bar	Transvers bar
SCC-S	1	15.6-24- 24-15.6	3	6	1.1	4.5	30Φ22	Φ12@25
	2	6@32	3	9	1.2	6.4	22Φ32	Φ14@5
	3	6@20	2	10.5	1.3	7.0	20Φ30	Φ18@20
HCC-S	1	7@20	2	16	1.4	7.0	20Φ30	Φ18@20
	2	6@32	3	18	1.4	6.4	20Φ30	Φ18@20
	3	6@20	2	21	1.4	7.0	20Φ30	Φ18@20

5.4.3 Uncertainties in material

The mechanical properties of the structural material play an important role in the seismic performance of bridges. Thus, variation in the mechanical properties of the materials should be considered during the fragility analysis. It is noted that the variations in material strengths have effects on both the strength and stiffness of a bridge [57]. In this study the information collected during the different surveys includes the compressive concrete strength and the yield strength of longitudinal bars.

Based on statistical material properties three compressive strengths of concrete were selected namely: 20, 25 and 30 MPa. Similarly, two yield strengths of the steel were considered, 300 and 400 MPa. The strength parameter combinations conducted to six analytical models. On the other hand, based on real cases, bridges with three column heights, 10.5, 16 and 21 m, were analyzed. The combinations of all parameters generate eighteen bridge samples which is shown in Table 5-17. The analytical models consider piers with two-column bents and three possible heights, namely: 2C-10.5, 2C-16 and 2C-21 for pier heights of 10.5 m, 16 m and 21 m, respectively. The distance between columns in all cases is 7.0 m. The circular column cross sections are 1.3, 1.4 and 1.4 m for 10.5, 16 and 21 m bridge classes, respectively. 20Φ30 bars is used for longitudinal reinforcement and Φ18 spaced at 200 mm, for transverse reinforcement. For this section a total of 40 earthquake ground motions from the two seismic sources due to reverse fault are

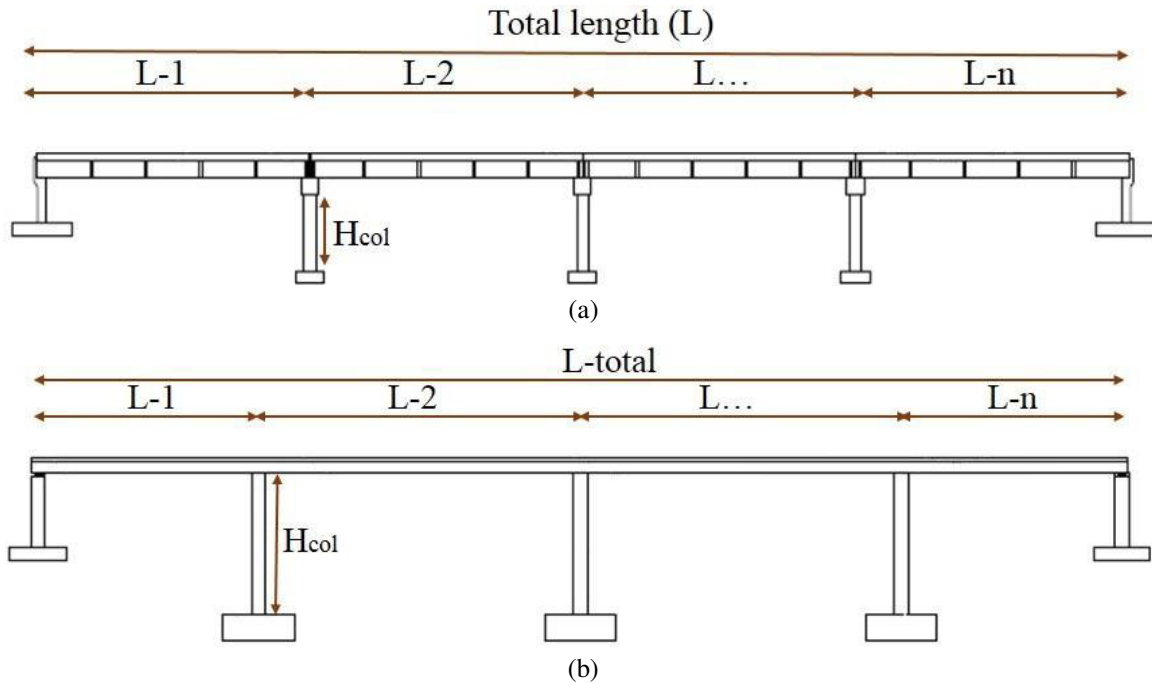
employed. Therefore, the total number of analyses for these classification criteria, which has 18 bridge samples, is 720.

Table 5- 17: Structural attributes for the bridge samples for each major bridge class in terms of material properties

Bridge classes	Column height (m)	f'_c (col) MPa	f_{ye} (bar) MPa	Longitudinal steel bar (%)	Deck width (m)
2C-10.5	10.5	20-30	300-400	0.91-1.06	12
2C-16	16	20-30	300-400	0.91-1.06	12
2C-21	21	20-30	300-400	0.91-1.06	12

5.4.4 Uncertainties in connectivity between superstructure and substructure

Fragility curves are performed for two groups of concrete bridges based on different earthquake databases. Two major bridge classes are analyzed: circular column–continuous or integral (CC-I) and circular column–simply supported (CC-S) bridges as shown in Table 2- 7. In the following a brief explanation is presented for each group of bridge classification. Figure 5- 8 presents the schematic drawings of sample bridges in the longitudinal and transverse directions. Note that different bridge lengths and column heights are also included in the models. Tables 5- 18 and 5- 19 present overall dimension of the bridges and structural attributes for each bridge classification.



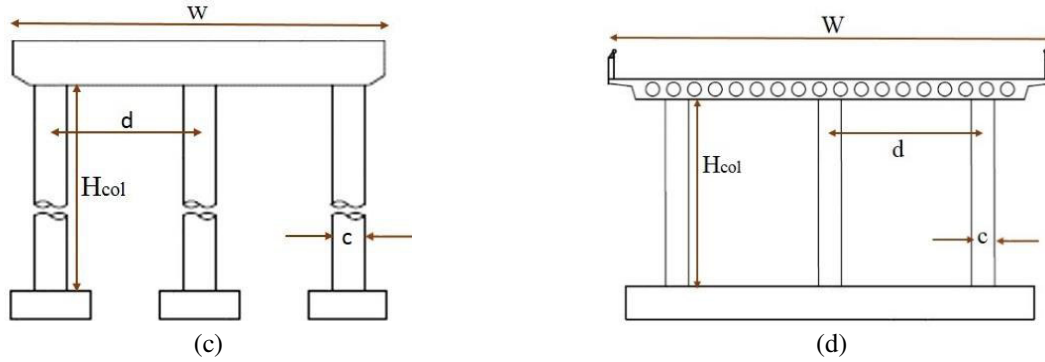


Figure 5- 8: Concrete bridge configuration for two bridge classification: simply support and integral

Table 5- 18: Structural attributes for the bridge samples for each major bridge classes in terms of superstructure connectivity

Bridge classes	Column Height (H_{col}), (m)	Column section	Longitudinal steel ratio (%)	Deck width (W), (m)	Span length (L), (m)	Number of spans
CC-I	4-8	Circular (D=1.0)	1.125	22.5	20	4
CC-S	6-10.5	Circular (D=1.2-1.3)	1.06-1.56	12-16	20-32	4-6

Table 5- 19: Geometric characteristics for each case study in terms of superstructure connectivity

Bridge classes	Sample ID	Number of spans	No. of column per bent	H_{col} (m)	c (m)	d (m)	Column section	
							Longitudinal bar	Transvers bar
CC-S	1	15.6-24-24-15.6	3	6	1.1	4.5	30 Φ 22	Φ 12@25
	2	6@32	3	9	1.2	6.4	22 Φ 32	Φ 14@5
	3	6@20	2	10.5	1.3	7.0	20 Φ 30	Φ 18@20
CC-I	1	4@20	3	4	1.0	8.5	18 Φ 25	Φ 12@20
	2	4@20	3	6	1.0	8.5	18 Φ 25	Φ 12@20
	3	4@20	3	8	1.0	8.5	18 Φ 25	Φ 12@20

5.4.5 Uncertainties in lap splice of the reinforcement

Seismic damage assessment at columns in flexure is proposed by Hwang [67] that uses different limit states. The moderate limit state is completely dependent to the presence of column lap splices. For columns with lap splice, the plastic hinge rotation θ_{p2} is determined at the end of the column when the strain is equal to 0.002 ($\epsilon_c = 0.002$). The column core starts to disintegrate and flexural fail happen when the column plastic hinge rotation is larger than θ_{p2} . However, for column without lap splices, θ_{p4} is the plastic hinge rotation at the bottom of the column with $\epsilon_c = 0.004$. In other words, the column core starts to disintegrate and the column fails in flexure. The inspection was carried out from the bridges, whether or not the lap splices established. In this study, the fragility curves are generated for different classes of bridges based on columns with

and without lap slices. Tables 5- 20, 5- 21 and 5- 22, show the limit states column curvature calculation results for different bridge classifications. In this table φ_1 corresponds to the curvature of the column when vertical bars at the bottom of the column reach the first yield, φ_2 is obtained by extrapolating the line joining the origin and the point corresponding to the first yielding point of a reinforcing bar up to the nominal moment capacity M_n (Figure 3- 7). $\varphi_{3,2}$ and $\varphi_{3,4}$ are the curvature of the column when $\varepsilon_c = 0.002$ or $\varepsilon_c = 0.004$ for the columns with or without lap splices, respectively. μ_1 and μ_2 are the first and second limit states which corresponded to slight and moderate respectively. $\mu_{3,2}$ and $\mu_{3,4}$ are the third damage state when $\varepsilon_c = 0.002$ or $\varepsilon_c = 0.004$. Finally μ_{2max} and μ_{4max} can be calculated as third damage state+3.

It should be noted that in SCC-S classification for 9 m column height $\varphi_{3,2}$ is smaller than φ_2 . The reason could be since in this case study the distance of transversal reinforcement are near to each other and ratio of longitudinal reinforcement is 1.56%, therefore the section seems to be strong due to steel bars. Therefore the compressive strain at the concrete column reach to 0.002 (for $\varphi_{3,2}$), then the vertical reinforcing bars at the bottom of the column reaches the yield (for φ_2).

Table 5- 22 indicates the typical relationship between displacement ductility capacity and column height. It shows that by increasing the column height even the plastic hinge increase but since the rotation of column end decrease therefore the displacement ductility decrease as well, which is explained by Priestley *et al.* [108]. By increasing the axial load the column capacity (EI_e and moment of the section) increases and consequently the ductility and expected damages decrease. However in addition of axial load, other factors like concrete strength, column section, longitudinal and transversal bar ration are also important on ductility [108], therefore as it shows in Figure 5- 9 instead of concerning one factor on ductility, the effect of $p/(f'_c \times A_g)$ has been studied for both bridge classification (HCC-S and SCC-S). As it shows in this figure by increasing this factor, ductility decreasing. Note that for HCC-S classification the ratio $p/(f'_c \times A_g)$ is 0.14, 0.19 and 0.15 for 16, 18 and 21 m column bridges, however the ration of $p/(f'_c \times A_g)$ for SCC-S bridge classification is 0.1, 0.1 and 0.16 for 6, 10.5 and 9 m respectively.

Table 5- 20: Limit states for simply support bridges (HCC-S)

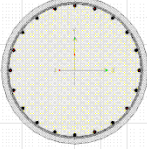
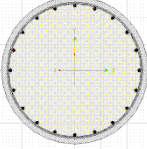
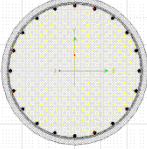
Column shape	Col. height	Direction	L_p (m)	φ_1	φ_2	$\varphi_{3,2}$	$\varphi_{3,4}$	μ_1	μ_2	$\mu_{3,2}$	μ_{2max}	$\mu_{3,4}$	μ_{4max}
	16	Long.	1.5	2.35	3.08	4.50	1.1	1	1.31	1.48	4.48	2.27	5.27
		Trans.	0.9	E-03	E-03	E-03	E-02	1	1.31	1.51	4.51	2.44	5.44
	18	Long.	1.78	3.18	3.99	4.0	1.0	1	1.25	1.26	4.26	1.79	4.79
		Trans.	1.07	E-03	E-03	E-03	E-02	1	1.25	1.26	4.26	1.89	4.89
	21	Long.	1.9	2.37	3.1	5.0	1.2	1	1.31	1.52	4.52	2.21	5.21
		Trans.	1.1	E-03	E-03	E-03	E-02	1	1.31	1.55	4.55	2.35	5.35

Table 5- 21: Limit states for simply support bridges (SCC-S)

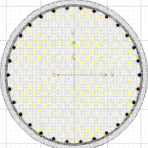
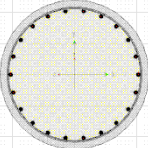
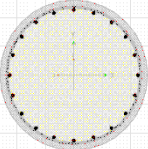
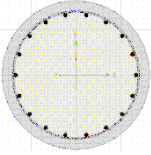
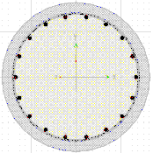
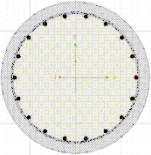
Column shape	Col. height	Direction	L_p (m)	φ_1	φ_2	$\varphi_{3,2}$	$\varphi_{3,4}$	μ_1	μ_2	$\mu_{3,2}$	μ_{2max}	$\mu_{3,4}$	μ_{4max}
	6	Long.	0.70	3.05	3.91	5.50	1.30	1	1.29	1.46	4.46	2.26	5.26
		Trans.	0.40	E-03	E-03	E-03	E-02	1	1.29	1.50	4.50	2.52	5.52
	9	Long.	1.20	4.09	5.42	4.30	1.00	1	1.33	1.23	4.23	1.71	4.71
		Trans.	0.72	E-03	E-03	E-03	E-02	1	1.33	1.20	4.20	1.82	4.82
	10.5	Long.	1.09	2.60	3.41	4.80	1.20	1	1.31	1.47	4.47	2.29	5.29
		Trans.	0.68	E-03	E-03	E-03	E-02	1	1.31	1.51	4.51	2.52	5.52

Table 5- 22: Limit states for integral bridges (CC-I)

Column shape	Col. height	L_p (m)	φ_1	φ_2	$\varphi_{3,2}$	$\varphi_{3,4}$	μ_1	μ_2	$\mu_{3,2}$	μ_{2max}	$\mu_{3,4}$	μ_{4max}
	4	0.43	4.30 E-03	4.60 E-03	4.70 E-03	1.10 E-02	1	1.07	1.08	4.08	1.93	4.93
	6	0.45	4.30 E-03	4.60 E-03	4.70 E-03	1.10 E-02	1	1.07	1.08	4.08	1.70	4.70
	8	0.53	4.30 E-03	4.60 E-03	4.70 E-03	1.10 E-02	1	1.07	1.08	4.08	1.63	4.63

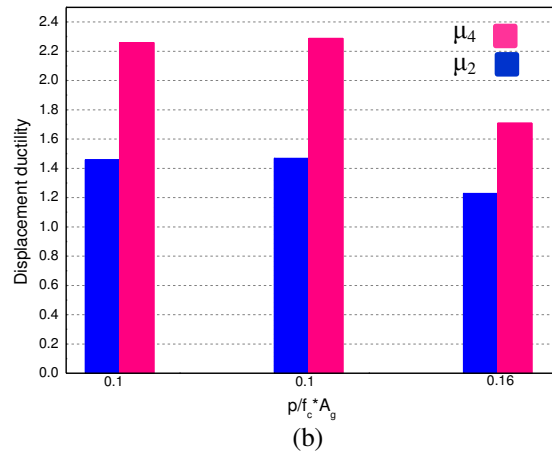
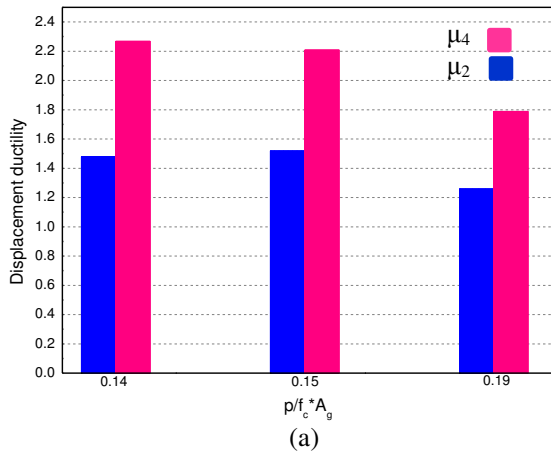


Figure 5- 9: The ratio of $p/(f'_c \times A_g)$ versus ductility for (a) HCC-S, (b) SCC-S bridge classification

Chapter 6

6 DEVELOPMENT OF ANALYTICAL FRAGILITY CURVES

One of the most significant tools in the seismic loss estimation of structures is fragility curves. As described before, fragility curves relate strong motion severity to the probability of reaching or exceeding a certain limit state of behavior [51]. For a specific damage state, the mathematical function of a fragility curve is presented in chapter 1. To perform fragility curves, the seismic response of critical structural components should determine in order to measure expected level of seismic damage through engineering demand parameters. To obtain the damage state of the bridge, the bridge components' seismic demands are compared with the specified damage limits via engineering demand parameters. The damage state for each bridge sample is calculated by repeating this process for all bridge samples under different seismic scenarios. For these purpose, several nonlinear time history analyses are performed to obtain the seismic response of the bridge components. Seismic ground motions with different intensity levels are employed and nonlinear analyses models are considered to obtain the seismic bridge damage by executing an important number of analyses.

6.1 Seismic demand calculation of bridge components

For each bridge sample nonlinear time history analysis, which is believed to be the most reasonable method to estimate the inelastic seismic demand of the structures, are performed to calculate the seismic response of the bridge components. Although nonlinear time history analysis has some deficiency such as convergence problems, extensive amount of run time and post processing efforts, but its capacity to model the inelastic seismic behavior is superior when comparing to the other analyses. According to chapter-3, detailed in analytical models are developed using SAP2000 software [123]. The bridges are subjected to both horizontal components of the ground motions, and nonlinear time history analyses are performed under the selected earthquake data bases. Since an earthquake can hit the bridge in any direction, therefore, in order to obtain the maximum response of the bridge component, each ground motion is employed twice as explained in chapter 4. The dynamic analysis is considered after the

application of gravity loads, for other type of loads are not considered in this study, including wind, truck, snow, etc.

The seismic response of the bridge is determined through the columns' displacement ductility that is employed to measure the damage limit state, according to chapter 5. By considering the absolute maximum of the nonlinear response in longitudinal or transverse direction, maximum response of the bridge components are calculated.

6.2 Methodology used for fragility curves

Fragility curves for class of bridges present the relationship between the probability of reaching or exceeding a certain damage state as a function of ground motion intensities. The main objective of this study is to develop fragility curves for the ordinary highway bridges in Iran designed and constructed according to the pre-1990 code regulations. Furthermore, the effects of span length, material properties, column height, and lap splices for simply supported bridge classification and connectivity between superstructure and substructure were investigated as the major sources of uncertainty in the fragility analysis of bridges. Moreover, the fragility curves developed for this work were derived assuming different focal mechanisms. For this purpose, the following specific methodology is proposed:

1. Classification of common bridges in Iran.
2. Selection of earthquake ground motion records from two seismic sources, based on ground motion intensities.
3. Define the damage limit states for each bridge classification. In this study displacement ductility of column is selected as engineering demand parameter.
4. Creation of numerical 3D bridge classes and seismic analysis accounting for uncertainty in bridge properties. Bridge uncertainties for the selected case studies include column heights, lap splice, span lengths and connectivity between superstructure and substructure. Additionally, the influence of material properties, namely the compressive strength of concrete and the yield strength of steel is described.

5. Determine the performance level of each bridge by comparing demands from nonlinear time history analysis with the damage limits expressed in terms of displacement ductility.
6. Evaluate the performance level of each case study for the given ground motion record and calculate the exceedance probabilities of each damage limit state for each ground motion.
7. Plot the selected intensity measure against the probability of exceedance for each damage state in order to obtain the fragility curves.
8. Generate the fragility curves for major bridge classes and damage limit states by fitting the jaggedly varying fragility points through lognormal distribution function, which depends on a median value and a dispersion parameter (Figure 6- 1). In this graph the x-axis is the seismic intensity measure of the ground motion and y-axis is the probability of reaching or exceeding certain damage limit state.

A through discussion of the underlying concepts and step by step procedure used to obtain fragility curves is given in the following sections.

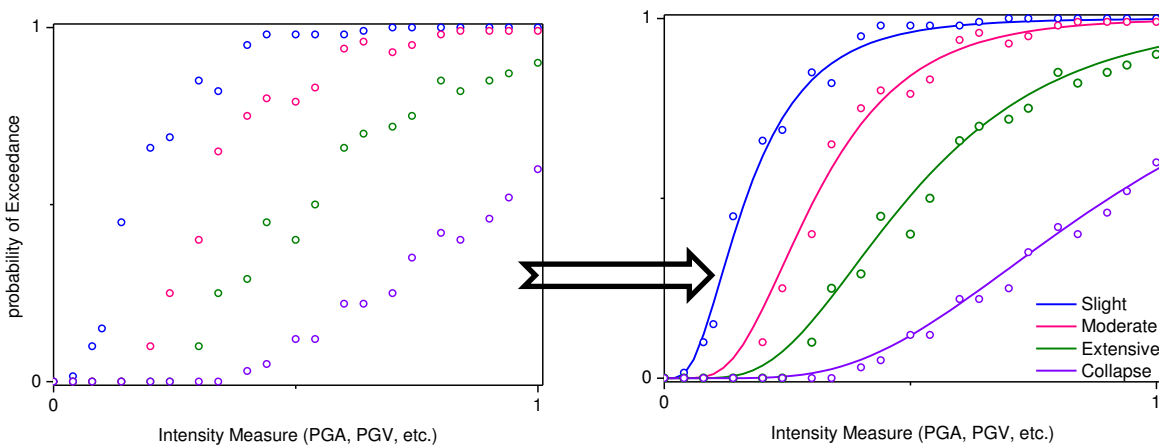


Figure 6- 1: Schematic representation of a fragility curve

6.3 Development of fragility curves

Each bridge was subjected to two orthogonal horizontal components of the ground motions. The maximum absolute ductility demand determines the damage limit state of the bridge column for each seismic record. The number of bridges that reach or exceed a specified damage limit state is

obtained by subjecting the models under the seismic records with a certain intensity measure (PGA and ASI). The intensity measures consider the SRSS of the two horizontal components of the ground motions. The ratio of the number of sample bridges that reach or exceed the specified damage limit state to the total number of sample bridges provides the probability of exceeding the corresponding limit state for a specific intensity. Then, the same process is performed for each ground motion of the two seismic sources and four limit states. As mentioned before, the earthquake ground motions are presented with a proper seismic intensity measure. The distribution of the probability of exceedance as a function of the selected intensity measure is shown schematically in Figure 6- 1. Then, a mathematical expression is used to characterize the jaggedly varying points to achieve smooth fragility curves for a specific damage limit state and bridge class, which is the best fit for the points of the probability of exceedance. A cumulative lognormal probability distribution is utilized to present the probability of exceeding a certain damage limit state in recent studies. Consequently, the fragility curves are generated for each bridge class based on each limit state and intensity measure. Several researches, as well as this study, adopt the lognormal distribution to obtain fragility curves [37, 56, 62, 68, 177]. Each fragility function depends on a median value and an associated dispersion factor (lognormal standard deviation) of ground motion, which is represented by seismic intensity measures. To select the parameters of the lognormal probability density function, the least squares method is applied. The coefficient of determination (R^2) determines how well the fitted curve relates to the data of the fragility functions. This indicator, which varies between 0 and 1, shows how closely the estimated points and the smooth curve obtained by the lognormal distribution. The closer the R^2 value is to 1, the more reliable are the estimated fragility curves. Finally, fragility functions of each bridge class are developed for the intensity measures of PGA employing the procedure described before.

6.4 Fragility curves for major bridge classes

Based on previous research work and on the available data from past earthquake reports, bridges are classified in terms of span length (SL) and superstructure type, column height, material properties due to concrete compressive strength and steel yield stress, connectivity between superstructure and substructure, presence of lap splices in columns for simply support and

integral bridges. At the end fragility function are performed due to intensity measure based on PGA and ASI. By utilizing the above-mentioned procedure, fragility functions were performed for each bridge class. To develop the fragility curves, the median and standard deviation of the lognormal distribution functions were calculated with the least-squares technique for each damage limit state and bridge class. In addition, the coefficient of determination (R^2) was used for each individual fragility curve to obtain the correlation between the exceedance probability points and the developed fragility curves. Details of how the fragility functions are obtained for each uncertainty are described in the following sections.

6.4.1 Span length

Figure 6- 2 shows the fragility curves of the bridge classes in terms of span length and superstructure type subjected to reverse and strike-slip fault movements. The four curves correspond to the limit states: LS1 (slight), LS2 (moderate), LS3 (extensive), and LS4 (collapse), from left to right. The classification developed by the ATC-13 [54] and the FHWA [99] groups the bridges based on the total length and superstructure type, respectively. HAZUS (FEMA, 2003) [37] considers a bridge classification in terms of the number of spans. Nielson *et al.* [100] consider 11 bridge classifications based on construction type, construction material, and the number of spans. Choi *et al.* [69] classify the bridges into four categories in terms of the superstructure type. The comparison of the fragility curves in that study shows that the most vulnerable bridge types are the multi-span simply supported and multi-span continuous steel-girder bridges. Ramanathan *et al.* [178] study due to the influence of evolution of seismic design principles and details on the seismic performance of multi-span concrete box-girder bridge class. In this study, the bridges are classified into groups based on the span length and superstructure type, namely the I-girder superstructure type with SL between 20 and 30 m, and the box girder superstructure type with SL larger than 30 m.

As an example of the influence of the superstructure type and the seismic source on the probability of reaching the limit states, Figure 6- 2 (a) shows that, for $PGA = 0.4g$, the probabilities of reaching or exceeding LS1, LS2, and LS3 of the I girder superstructure type subjected to the reverse fault records are 95, 85, and 42%, respectively. In contrast, Figure 6- 2 (c) indicates that the probabilities of reaching or exceeding LS1, LS2, LS3, and LS4 for the box-

girder superstructure type are 90, 82, 66, and 11%, respectively. The comparison between these two types of superstructures, presented in Figure 6- 2 (a) and (c), shows similar probabilities of exceedance the limit states LS1 and LS2, and that bridges with span lengths larger than 30 m are more vulnerable than the structures with span lengths in the range of 20–30 m in extensive and collapse damage states. Figure 6- 2 (b) and (d) show similar differences between two superstructure types subjected to accelerograms of the strike-slip fault. Figure 6- 2 also displays the importance of the seismic source; the bridges subjected to reverse fault records were clearly more vulnerable than those subjected to the strike-slip fault signals. Table 6- 1 presents the fragility curve parameters for different damage limit states in terms of the span length. In general, the results of this study indicate that, to some extent, bridges are more susceptible to reverse fault ground motions, but a deep and comprehensive study is required to draw an accurate conclusion.

Table 6- 1: Fragility curve parameters for different damage limit states in terms of span length

20≤SL<30												
	<u>Slight (LS1)</u>			<u>Moderate (LS2)</u>			<u>Extensive (LS3)</u>			<u>Collapse (LS4)</u>		
	Median	Disp.	R ²	Median	Disp.	R ²	Median	Disp.	R ²	Median	Disp.	R ²
reverse	-2.13	0.73	0.68	-1.69	0.73	0.60	-0.89	0.52	0.41	-0.25	0.16	0.43
strike slip	-1.38	0.77	0.61	-1.12	0.69	0.44	-0.65	0.43	0.80	-0.11	0.21	0.42
SL≥30												
	<u>Slight (LS1)</u>			<u>Moderate (LS2)</u>			<u>Extensive (LS3)</u>			<u>Collapse (LS4)</u>		
	Median	Disp.	R ²	Median	Disp.	R ²	Median	Disp.	R ²	Median	Disp.	R ²
reverse	-1.75	0.67	0.54	-1.53	0.70	0.61	-1.22	0.75	0.50	-0.27	0.55	0.44
strike slip	-1.32	0.78	0.40	-1.12	0.73	0.59	-0.62	0.47	0.61	-0.13	0.64	0.45

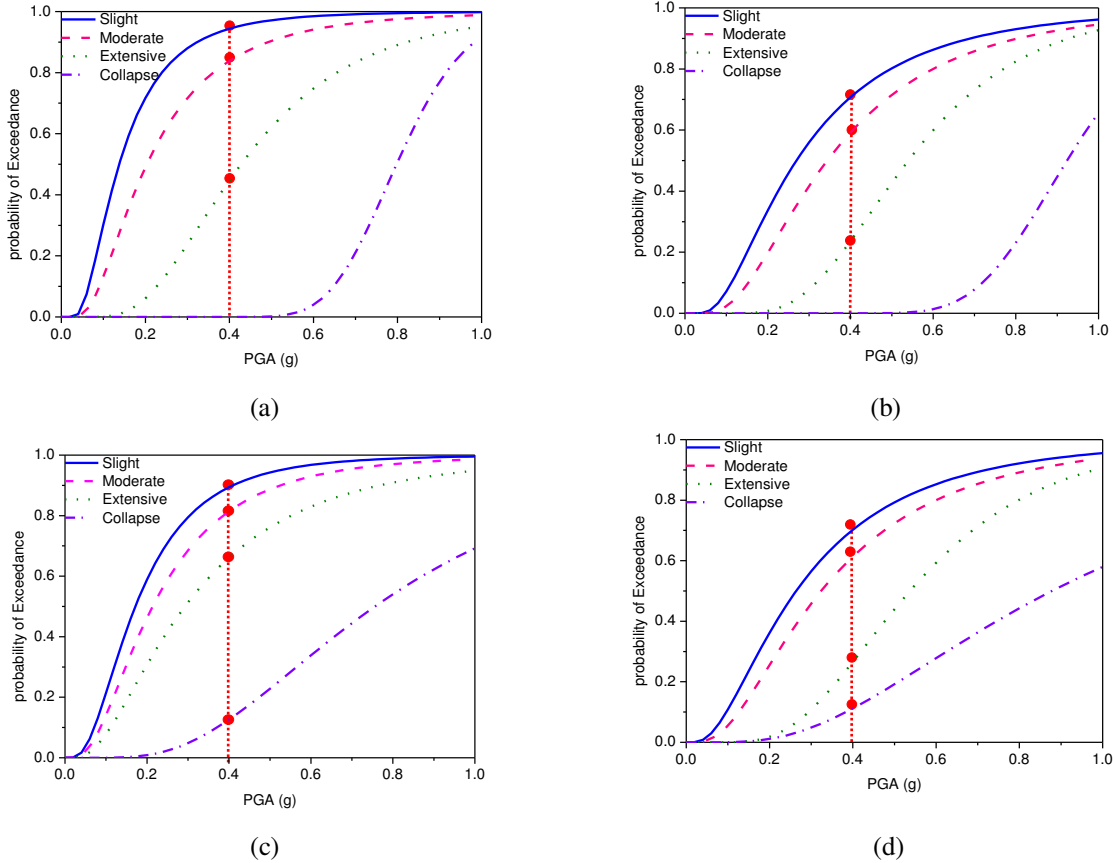


Figure 6- 2: Fragility curves for different damage limit states (PGA) in terms of span length (SL) (a) Reverse & $20 \leq SL < 30$, (b) Strike slip & $SL 20 \leq SL < 30$, (c) Reverse & $SL \geq 30$, and (d) Strike slip & $SL \geq 30$

6.4.2 Column height

Figure 6- 3 and Figure 6- 4 show fragility curves of the bridge classes in terms of column height subjected to reverse and strike-slip fault records using PGA as an intensity measure. These curves are grouped in Figure 6- 5 for the four damage limit states to compare the effect of different seismic sources on the fragility curves. The HCC-S bridges were found to be more vulnerable to seismic effects than SCC-S models. One possible reason for this behavior could be the insufficient longitudinal steel ratio (Table 5- 15). Jara *et al.* [179] found that the longitudinal bar ratio has a significant effect on the moment strength and ductility capacity of the column. By increasing the longitudinal reinforcement ratio, the column capacity increases and consequently the ductility and expected damages decrease. The fragility curves showed that both bridge classes are more vulnerable to the reverse fault records. Figure 4- 5 shows that the maximum amplitude of the mean S_a response spectrum of a reverse fault is greater than the mean S_a value of a strike-slip fault. Therefore the bridges subjected to the reverse fault records displayed larger

demands than the bridges subjected to the reverse fault accelerograms. In addition, the fragility curves show that the failure probability of the Iranian bridges for PGA of less than 0.4g is low. This outcome is consistent with the bridge responses observed during past earthquakes that occurred in Manjil and Bam in Iran [180-182].

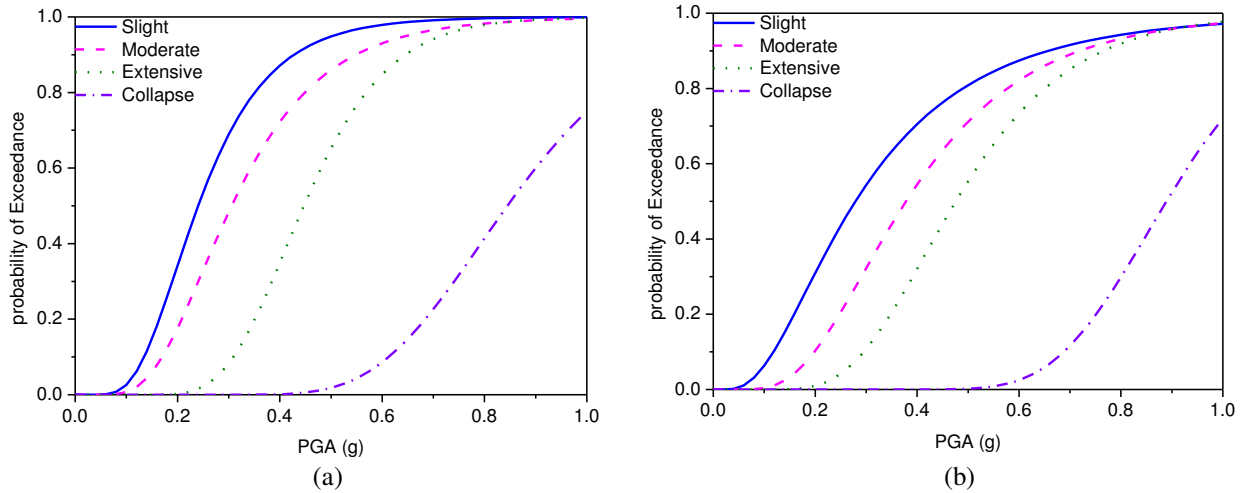


Figure 6- 3: Fragility curves for different damage limit states (PGA) in terms of column height (SCC-S) without lap splice, (a) Revers, and (b) Strike slip

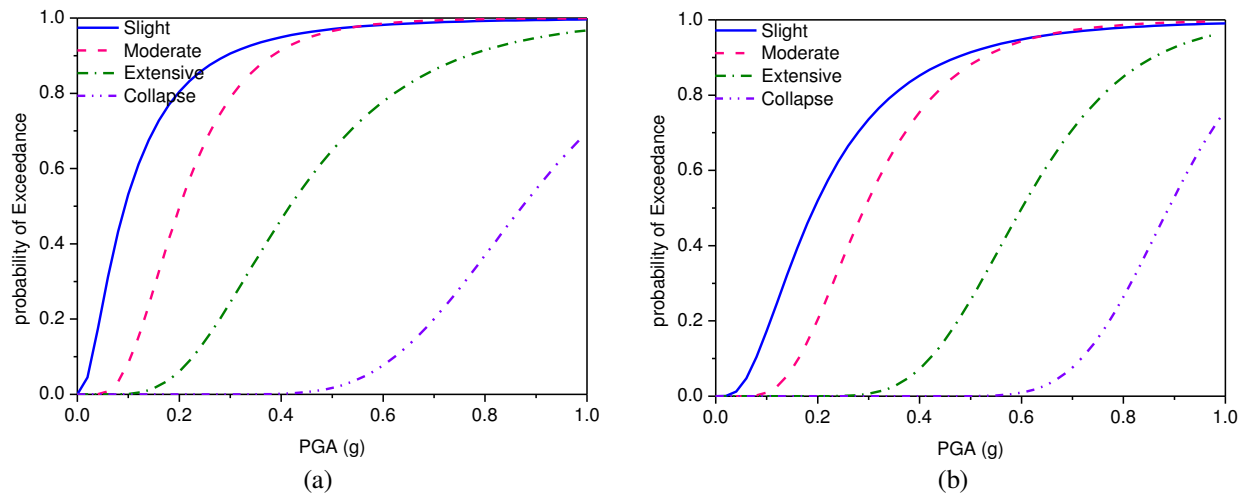


Figure 6- 4: Fragility curves for different damage limit states (PGA) in terms of column height (HCC-S) without lap splice, (a) Revers, and (b) Strike slip

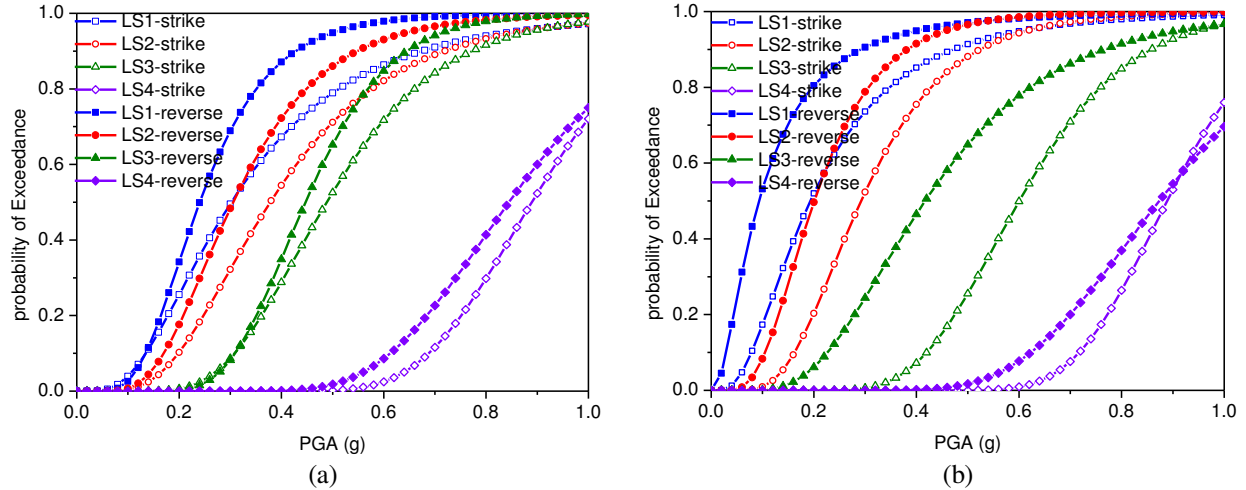


Figure 6- 5: Fragility curves subjected to reverse and strike slip fault for different damage limit states (PGA) in terms of column height without lap splice, (a) SCC-S, and (b) HCC-S

6.4.3 Material

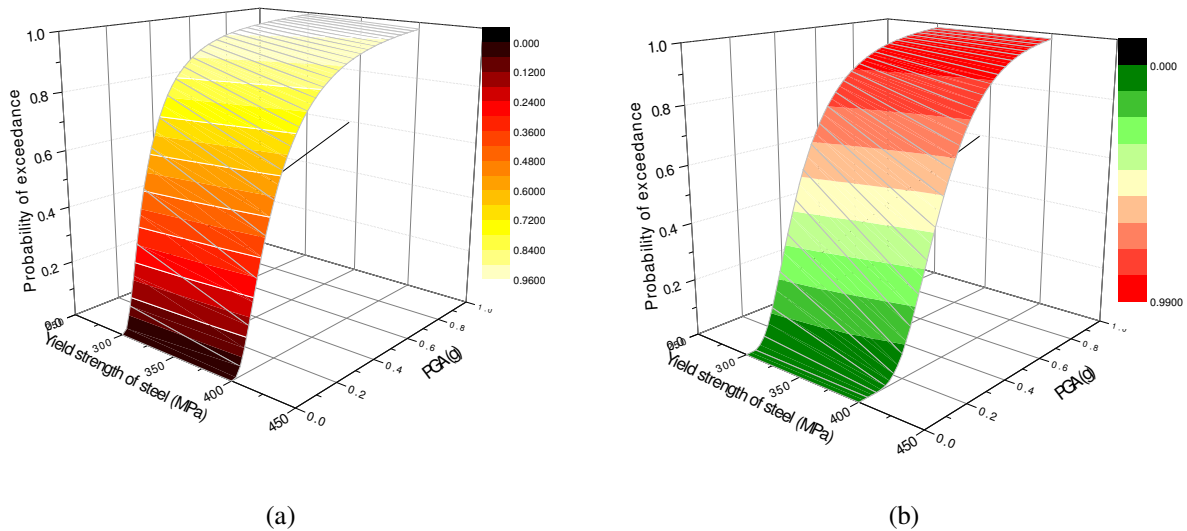
Figure 6- 6 and Figure 6- 7 show the fragility curves for two-column bridges with column heights varying between 10.5 and 21 m. The compressive concrete strength is in the range of 20–30 MPa and the yield stress of steel is between 300 and 400 MPa. The bridge response is significantly less sensitive to the concrete compressive strength compared to the steel yield strength. This outcome is consistent with the bridge responses observed by previous researchers [28]. Table 6- 2 presents the fragility curve parameters for the material properties in terms of compressive concrete strength and steel yield stress.

Table 6- 2: Fragility curve parameters for the material properties in terms of compressive concrete strength and steel yield stress

compressive concrete strength												
compressive concrete strength (MPa)	<u>Slight (LS1)</u>			<u>Moderate (LS2)</u>			<u>Extensive (LS3)</u>			<u>Collapse (LS4)</u>		
	Median	Disp.	R ²	Median	Disp.	R ²	Median	Disp.	R ²	Median	Disp.	R ²
20 (MPa)	-1.74	0.71	0.53	-1.2	0.54	0.51	-0.49	0.46	0.51	-0.15	0.25	0.86
25 (MPa)	-1.60	0.71	0.45	-1.13	0.63	0.53	-0.46	0.43	0.53	-0.11	0.24	0.85
30 (MPa)	-1.46	0.55	0.46	-0.96	0.54	0.55	-0.50	0.41	0.64	-0.08	0.22	0.48

steel yield stress												
steel yield stress (MPa)	<u>Slight (LS1)</u>			<u>Moderate (LS2)</u>			<u>Extensive (LS3)</u>			<u>Collapse (LS4)</u>		
	Median	Disp.	R ²	Median	Disp.	R ²	Median	Disp.	R ²	Median	Disp.	R ²
300 (MPa)	-2.08	0.83	0.53	-1.38	0.63	0.59	-0.77	0.37	0.77	-0.29	0.25	0.91
400 (MPa)	-1.66	0.82	0.43	-0.96	0.46	0.64	-0.48	0.33	0.56	-0.16	0.16	0.92

Figure 6- 6: Fragility curves based on different f'_c , (a) LS-1, (b) LS-2, (c) LS-3, and (d): LS-3



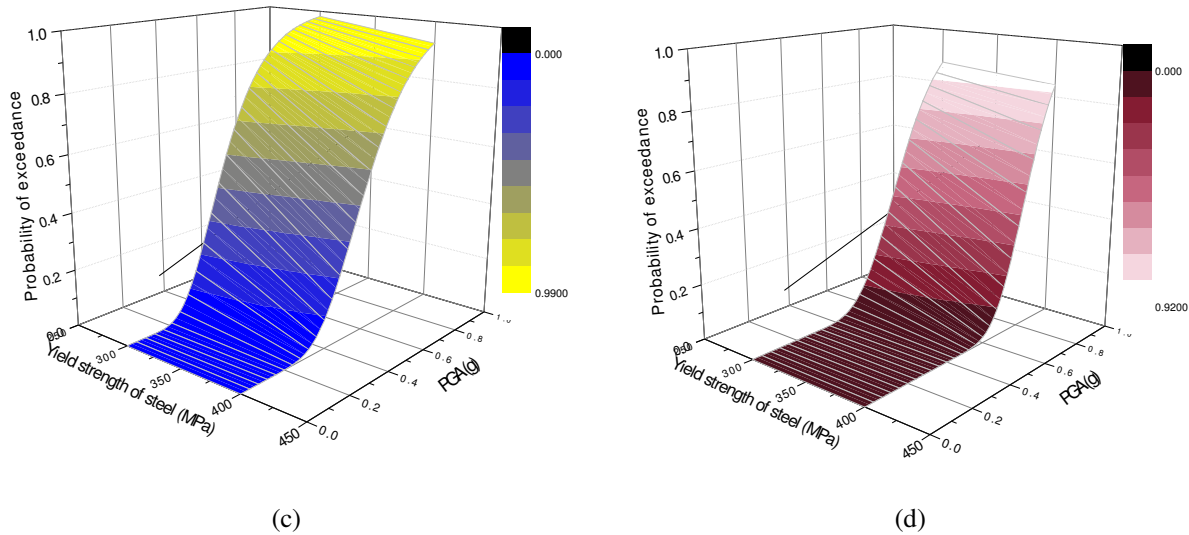


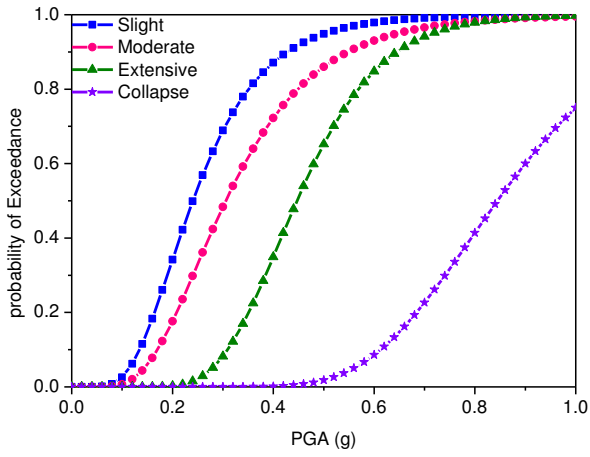
Figure 6- 7: Fragility curves based on different f_y , (a) LS-1, (b) LS-2, (c) LS-3, and (d): LS-3

6.4.4 Connectivity between superstructure and substructure

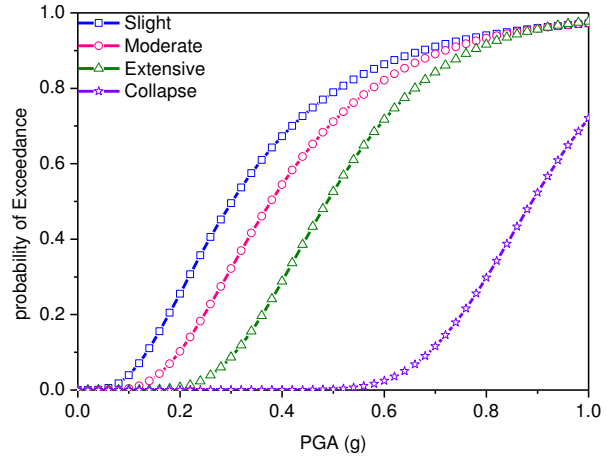
Figure 6- 8 shows the fragility curves for the two bridge classes subjected to reverse and strike-slip fault records using PGA and ASI as intensity measures. CC-S bridges are less vulnerable than the CC-I bridge models. This outcome is consistent with the bridge responses observed by previous researchers [25, 28, 72]. The probability of exceeding extensive damage in a integral bridge is 55% for reverse fault records with $PGA = 0.4g$, whereas it is 40% in a simply supported bridge. One reason for this is that bearings reduce the transfer of inertial forces to the substructure [106].

The fundamental periods range from 0.36 to 0.73 s in the CC-I bridge models and from 0.99 to 1.38 in the CC-S bridge models which is presented in Figure 6- 9. The fundamental periods of CC-S bridges locate the structures in a zone with smaller acceleration demands than those demands of the CC-I bridges. This is one of the reason that shows CC-I bridges are more vulnerable than CC-S ones.

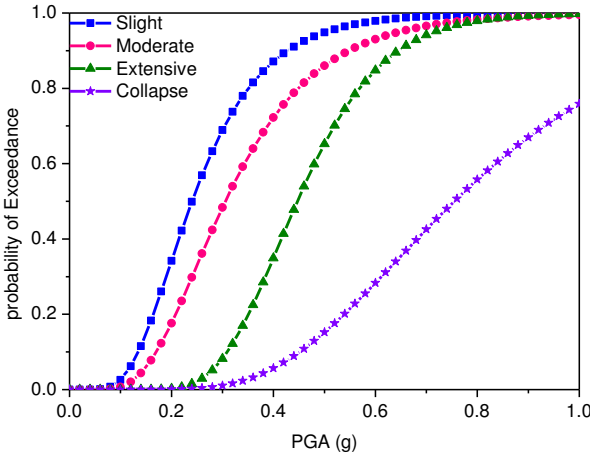
CC-S, Reverse fault, PGA



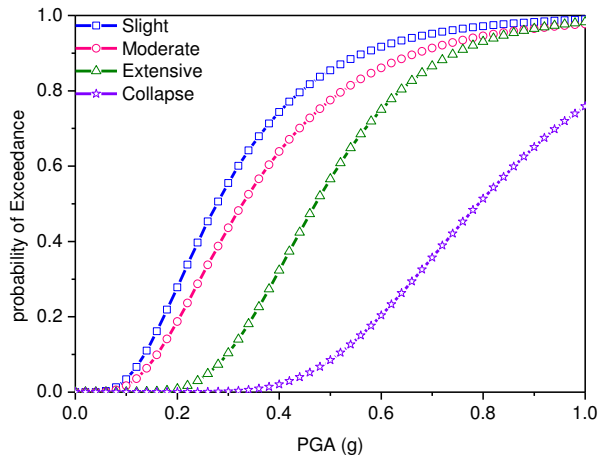
CC-S, Strike-slip fault, PGA



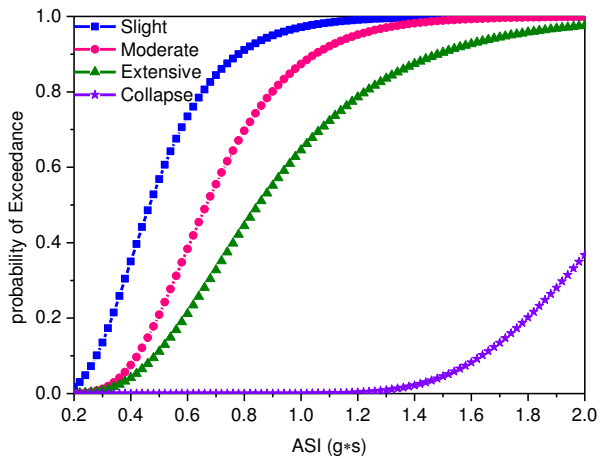
CC-I, Reverse fault, PGA



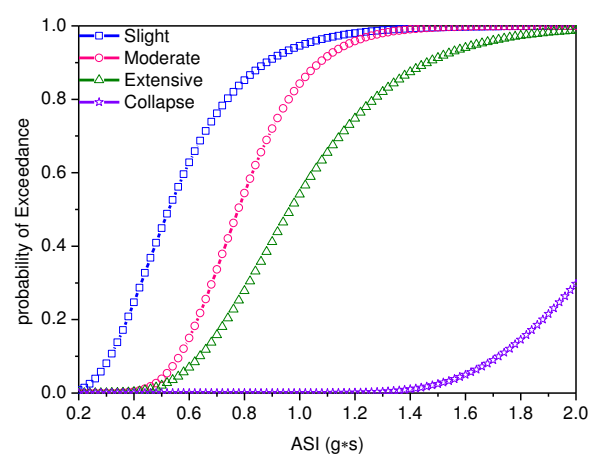
CC-I, Strike-slip fault, PGA



CC-S, Reverse fault, ASI



CC-S, Strike-slip fault, ASI



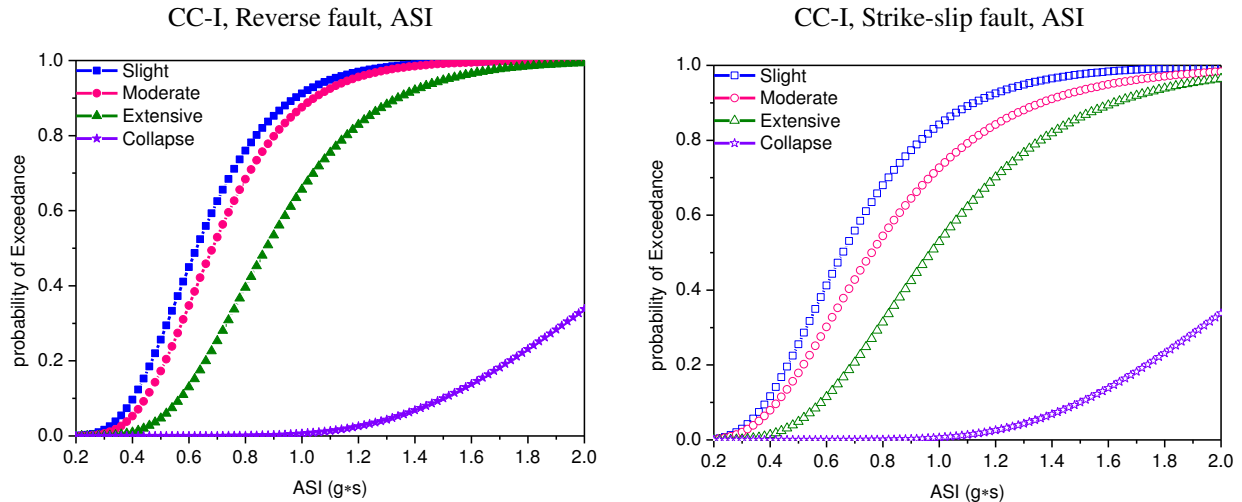


Figure 6- 8: Fragility curves for different damage limit states in terms of PGA and ASI subjected to reverse and strike-slip faults

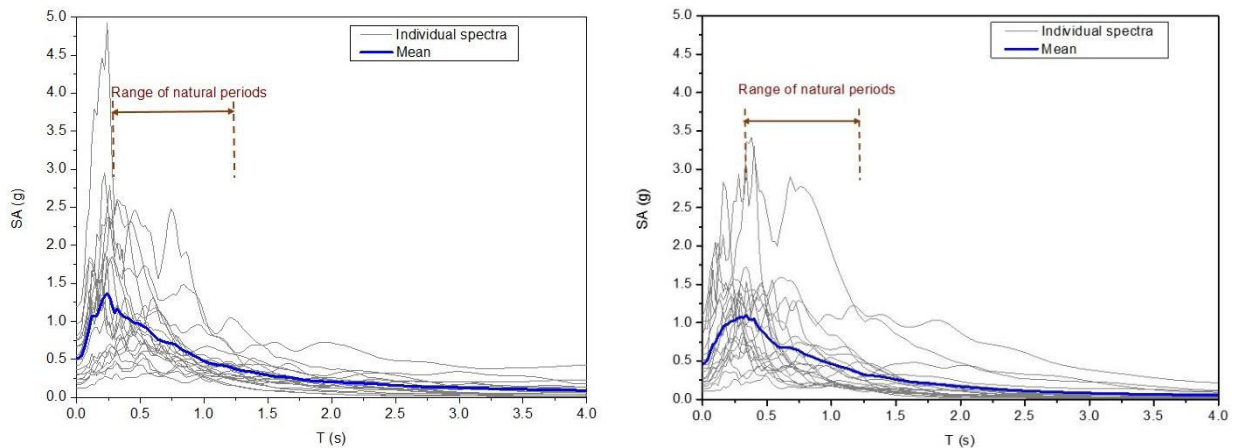


Figure 6- 9: Response spectra of the selected ground motions (5%damping) for (a) reverse and (b) strike-slip faults

The fragility curves show that both bridge classes are more vulnerable to the reverse fault records. The probability of exceeding slight damage for a $PGA = 0.5g$ in the CC-S bridges is 79% for strike-slip faults and 95% for reverse faults (Figure 6- 10 (a)). The same behaviour is observed in other damage limit states, such as the moderate and extensive ones, with increases of 71% to 86%, and 52% to 65%, respectively for both seismic sources. Figure 6- 10 (b) shows that the probability of exceeding slight damage for $PGA = 0.5g$ in the CC-I bridges increases from 85% to 95% for strike-slip and reverse faults, respectively. The same trend is observed for the moderate and extensive limit states, with increases of 78% to 90% and from 55% to 75%. It is

also notable that the probability of reaching the slight damage state in both bridge models subjected to reverse fault records is 95%; conversely, the probabilities of reaching this damage state in the CC-S and the CC-I bridges are 79 and 85%, respectively. Similar results were found for the moderate damage state. In general, the bridges subjected to the reverse fault records displayed larger demands than the bridges subjected to the strike-slip fault ones.

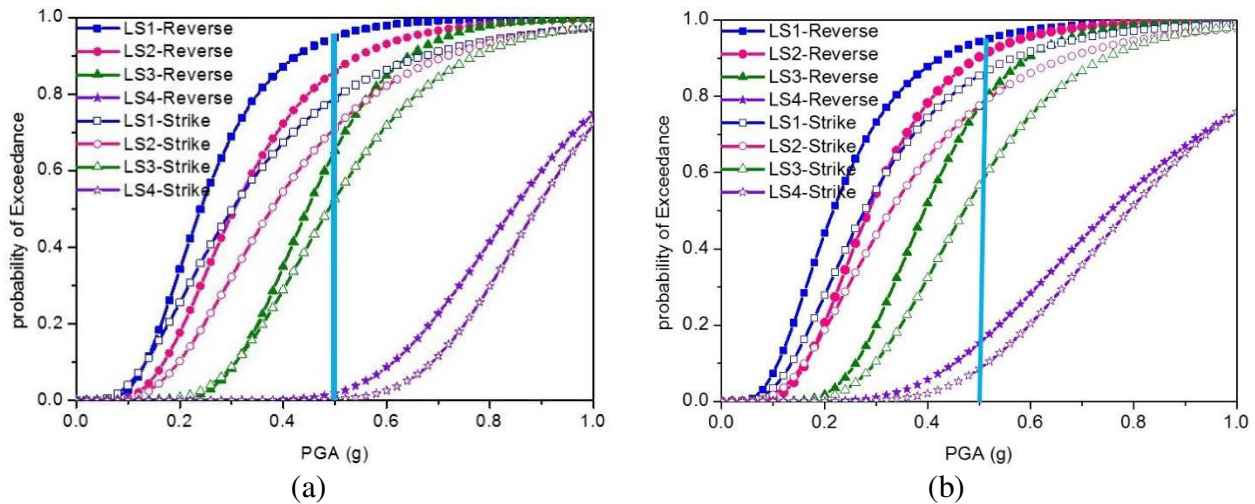


Figure 6- 10: Fragility curves subjected to reverse and strike-slip fault for different damage limit states in terms of PGA for (a) CC-S and (b) CC-I bridge classification

6.4.5 Present of lap splice

Figure 6- 11 shows the fragility curves as a function of PGA for bridge columns with and without a lap splice column (HCC-S) subjected to both groups of ground motions. A lap splice has a considerable effect on the fragility curve, making the columns with lap splices more vulnerable to seismic effects than those without them. Therefore, lap splices in longitudinal reinforcements should not be used in critical locations of ductile elements [44, 183, 184]. However, in old bridges is common to have lap splices near the base of the columns, as mentioned before, the extensive and consequently collapse limit states are completely linked to the presence of column lap splices. Figure 6- 12 displays the fragility curves for the records of the two seismic sources; the graphs present only the LS3 (extensive damage) and LS4 (collapse) limit states because the difference between LS1 and LS2 is negligible. As indicated in Figure 6- 12, for a $PGA = 0.4g$, the probabilities of reaching or exceeding extensive damages (LS3) with and without lap splices are 48 and 80%, respectively, for a reverse fault, whereas these probabilities are 8 and 58%, respectively for a strike-slip source. In other words, the fragility

curves indicate that the selected typical the pre-1990 bridges are sensitive to the fault mechanism and the bridges are more vulnerable to the action of accelerograms generated in reverse faults. The fragility curves also show that the failure probability (LS4) for the mentioned PGA is low.

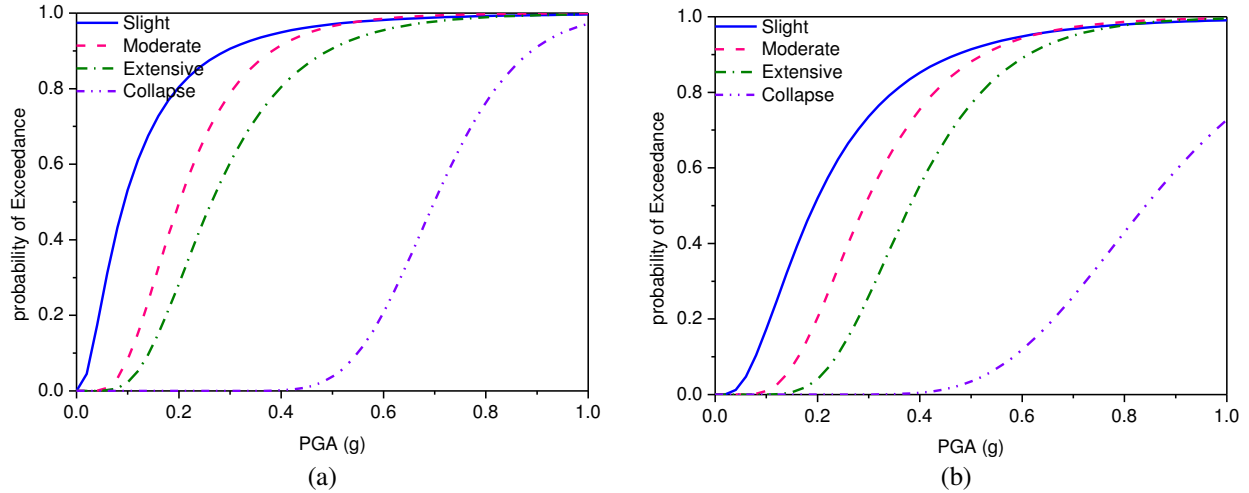
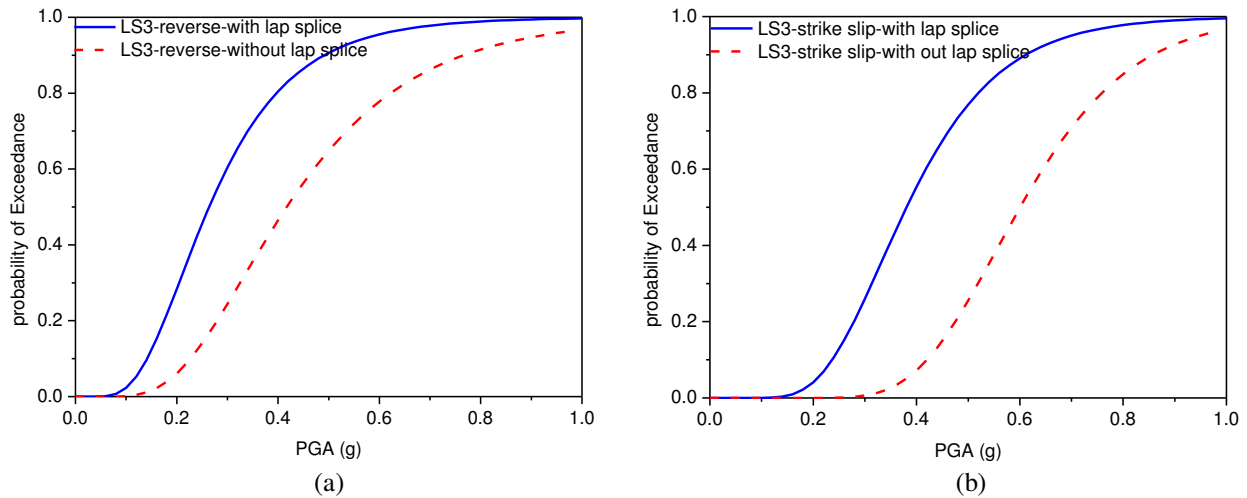


Figure 6- 11: Fragility curves for different damage limit states (PGA) in terms of column height (HCC-S) with lap splice, (a) Revers, and (b) Strike slip



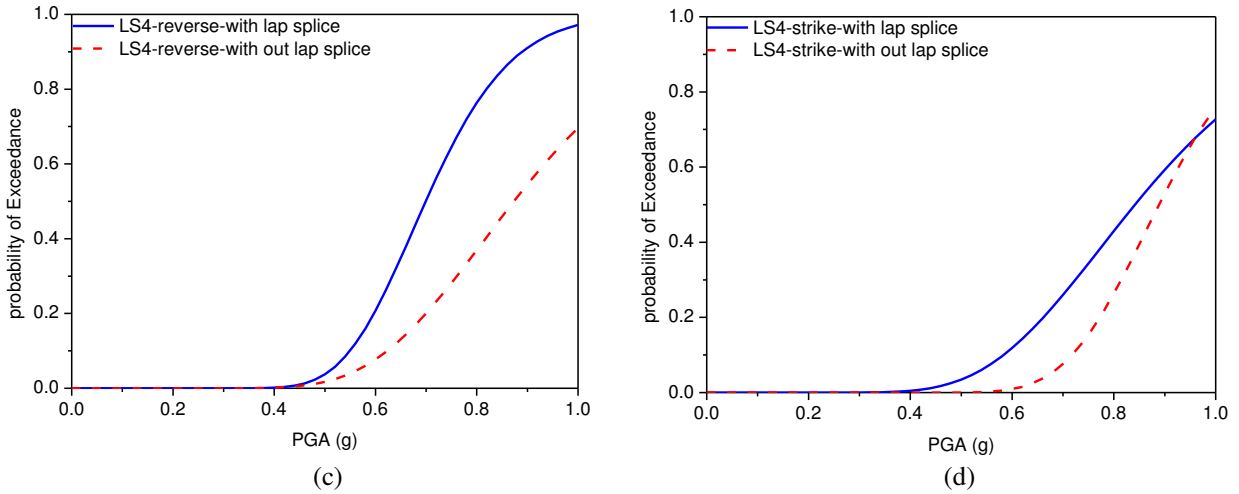


Figure 6- 12: Fragility curves for different damage limit states (PGA) in function of the presence or not of lap splice in columns for HCC-S, (a) LS3-reverse fault, (b) LS3-strike slip fault, (c) LS4-reverse fault, and (d) LS4-strike slip fault

Hwang *et al.* [67] proposed different damage limit states for columns to obtain the fragility curves for critical bridge components.

Table 5- 22 presents the relation among four curvature demands ($\varphi_1, \varphi_2, \varphi_{3,2}, \varphi_{3,4}$) and displacement ductility. However, the curvature for an extensive limit state depends on the presence of column lap splices. $\theta_{3,2}$ is the plastic hinge rotation of a column with lap splices for a strain equal to 0.002 ($\varepsilon_c = 0.002$). If the plastic hinge rotation is larger than this value ($\theta_{3,2}$), the column core starts to disintegrate and bending failure happens. $\theta_{3,4}$ is the plastic hinge rotation related to $\varepsilon_c = 0.004$ for columns without lap splices. The fragility curves for two classes of bridges based on columns with and without lap splices were calculated. Figure 6- 13 presents the fragility curves for the CC-S and CC-I bridges in columns with and without lap splices subjected to both groups of ground motions. Figure 6- 13 displays extensive (LS3) and collapse (LS4) limit states because these damage limit states are relevant when lap splices exist. Figure 6- 13 shows that the seismic records of reverse faults make the bridges more vulnerable than the structures subjected to seismic records of strike-slips. It should be noted that the probability of reaching a specific limit state in CC-I bridges is higher than that probability in CC-S bridges. At low values of PGA, the differences between the graphs are large, but as PGA increases the differences are lower. Figure 6- 13 (a & b) shows that small differences are found among fragility curves of the two seismic sources for limit state LS3 and PGA greater than 0.65g. Smaller PGA's make more notable the presence of lap splices. In integral bridges (graphs c & d), the trend is similar in the threshold of PGA=0.7g. Old bridges with lap splices exhibited high seismic vulnerability. These structures must be carefully evaluated as candidates to be retrofitted to reduce the failure probability in future seismic events. The analyses of existing bridges showed that more damage implies more influence of the lap splices. The presence of lap splices increases, from 62% to 79%, the probability of reaching or exceeding LS3 limit state for reverse fault records and PGA = 0.5g for CC-S. However, the change is more important for LS4; in this case, the models with lap splices increase the probability of reaching or exceeding the limit state from 2% to 28%. In contrast, Figure 6- 13 (b) indicates that the probabilities of reaching or exceeding LS3 are 70 and 58%, and for LS4 are 16 and 1% respectively.

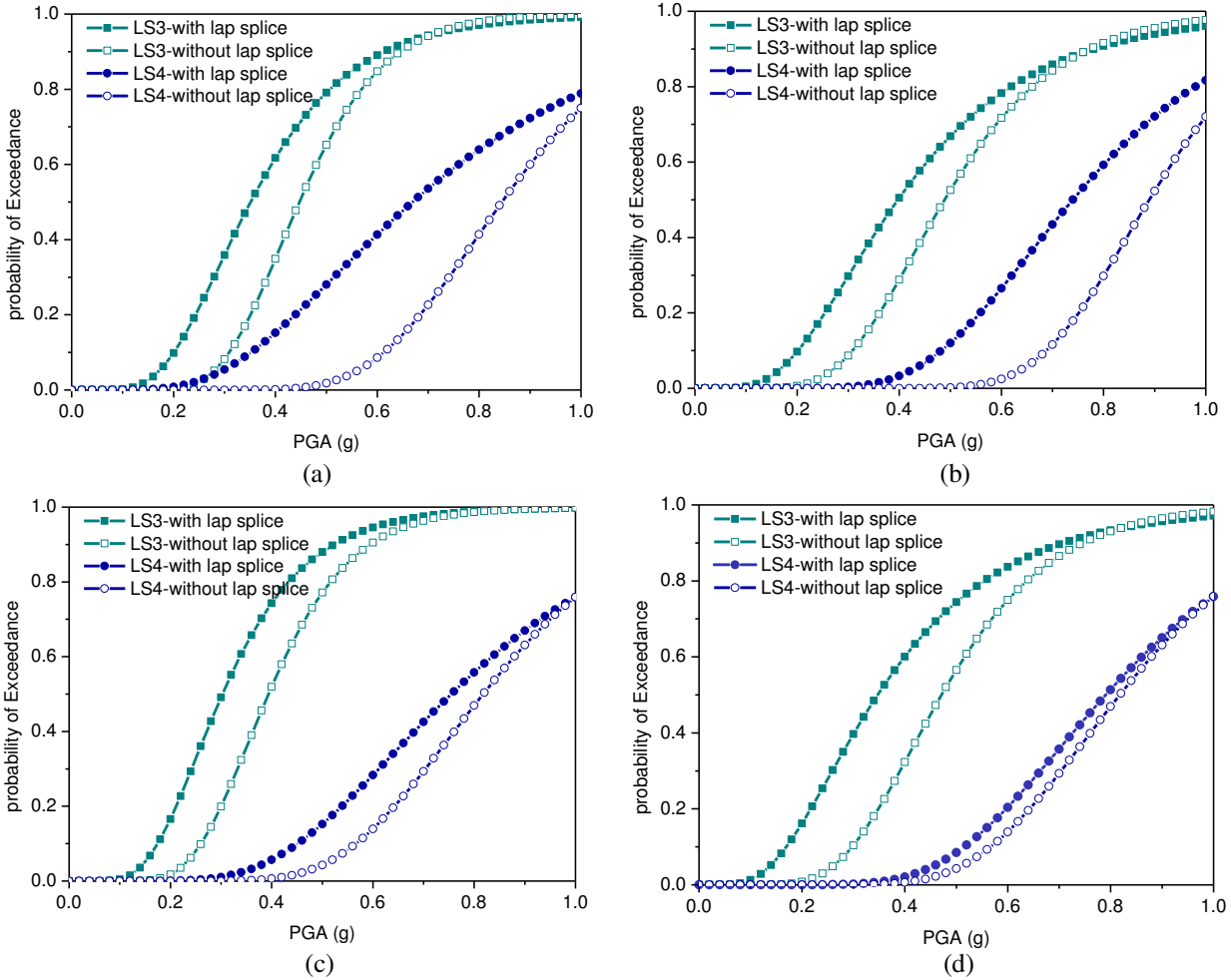


Figure 6- 13: Fragility curves for different damage limit states (PGA) as a function of the presence or not of lap splice in columns for two groups of classification, (a) CC-S-LS3&LS4-reverse fault, (b) CC-S-LS3&LS4-strike-slip fault, (c) CC-I-LS3&LS4-reverse fault, and (d): CC-I-LS3&LS4-strike-slip fault

6.4.6 Fragility curves due to intensity measure

Table 6- 3 presents the parameters of the lognormal probability distribution used to obtain the fragility curves of the HCC-S bridge class for each damage limit state. By employing the least-squares technique, the median and standard deviation of the lognormal probability distribution function were calculated. The correlation between the exceedance probability points and the fragility curves is calculated with the coefficient of determination (R^2). Table 6- 3 shows the PGA had the lowest coefficient of determination whereas ASI presented the highest one. This indicates that the use of ASI as intensity measure leads to fragility curves with a better correlation than those developed by using PGA. Therefore, the fragility curves generated based on ASI was found to be more realistic when estimating the damage limit state of the bridges.

Table 6- 3: Fragility curve parameters of the HCC-S

HCC-S subjected to reverse fault												
Intensity measure	<u>Slight (LS1)</u>			<u>Moderate (LS2)</u>			<u>Extensive (LS3)</u>			<u>Collapse (LS4)</u>		
	Median	Disp.	R ²	Median	Disp.	R ²	Median	Disp.	R ²	Median	Disp.	R ²
PGA (g)	-2.36	0.88	0.44	-1.6	0.50	0.76	-0.87	0.47	0.69	-0.13	0.26	0.50
ASI (g*s)	-1.79	0.41	0.84	-1.47	0.43	0.81	-0.86	0.19	0.83	-0.10	0.16	0.85
HCC-S subjected to strike slip fault												
Intensity measure	<u>Slight (LS1)</u>			<u>Moderate (LS2)</u>			<u>Extensive (LS3)</u>			<u>Collapse (LS4)</u>		
	Median	Disp.	R ²	Median	Disp.	R ²	Median	Disp.	R ²	Median	Disp.	R ²
PGA (g)	-1.63	0.69	0.52	-1.22	0.45	0.41	-0.51	0.28	0.43	-0.12	0.16	0.71
ASI (g*s)	-1.65	0.64	0.96	-1.23	0.49	0.87	-0.51	0.23	0.905	-0.091	0.16	0.96

Table 6- 4 shows the parameters of the lognormal density function used to obtain the fragility curves. Table 6- 4 shows the ASI intensity measure has a higher coefficient of determination than PGA. For example, CC-I bridges subjected to reverse fault records have R² coefficients of 0.96 and 0.92 when using the ASI intensity measure for the slight and moderate limit states, respectively. However, these values are 0.43 and 0.51 when using PGA as the intensity measure. Fragility curves computed with the ASI intensity measure have a better correlation with exceedance probability points than the fragility curves developed by using PGA. To clarify this issue Figure 6- 14 shows the jaggedly varying points and smooth fragility curve for CC-I bridge classification due to slight limit state based on PGA and ASI intensity measures respectively.

Table 6- 4: Fragility curve parameters of the CC-S and CC-I bridge classes

CC-S in terms of PGA(g)												
Faults	Slight (LS1)			Moderate (LS2)			Extensive (LS3)			Collapse (LS4)		
	Median	Disp.	R ²	Median	Disp.	R ²	Median	Disp.	R ²	Median	Disp.	R ²
Reverse	-1.41	0.44	0.66	-1.18	0.45	0.69	-0.80	0.28	0.72	-0.16	0.25	0.68
Strike-slip	-1.19	0.62	0.53	-0.97	0.50	0.53	-0.71	0.35	0.69	-0.16	0.20	0.71

CC-S in terms of ASI (g*s)												
Faults	Slight (LS1)			Moderate (LS2)			Extensive (LS3)			Collapse (LS4)		
	Median	Disp.	R ²	Median	Disp.	R ²	Median	Disp.	R ²	Median	Disp.	R ²
Reverse	-0.76	0.40	0.83	-0.40	0.35	0.76	-0.16	0.43	0.76	0.76	0.21	0.66
Strike-slip	-0.64	0.40	0.72	-0.25	0.25	0.66	-0.03	0.32	0.51	0.8	0.2	0.62

CC-I in terms of PGA(g)												
Faults	Slight (LS1)			Moderate (LS2)			Extensive (LS3)			Collapse (LS4)		
	Median	Disp.	R ²	Median	Disp.	R ²	Median	Disp.	R ²	Median	Disp.	R ²
Reverse	-1.52	0.52	0.43	-1.25	0.43	0.51	-0.92	0.32	0.86	-0.28	0.40	0.83
Strike-slip	-1.27	0.55	0.59	-1.11	0.55	0.59	-0.75	0.35	0.68	-0.23	0.33	0.85

CC-I in terms of ASI (g*s)												
Faults	Slight (LS1)			Moderate (LS2)			Extensive (LS3)			Collapse (LS4)		
	Median	Disp.	R ²	Median	Disp.	R ²	Median	Disp.	R ²	Median	Disp.	R ²
Reverse	-0.46	0.34	0.96	-0.37	0.33	0.92	-0.13	0.33	0.86	0.82	0.30	0.66
6Strike-slip	-0.41	0.41	0.64	-0.27	0.45	0.73	-0.03	0.40	0.37	0.84	0.33	0.66

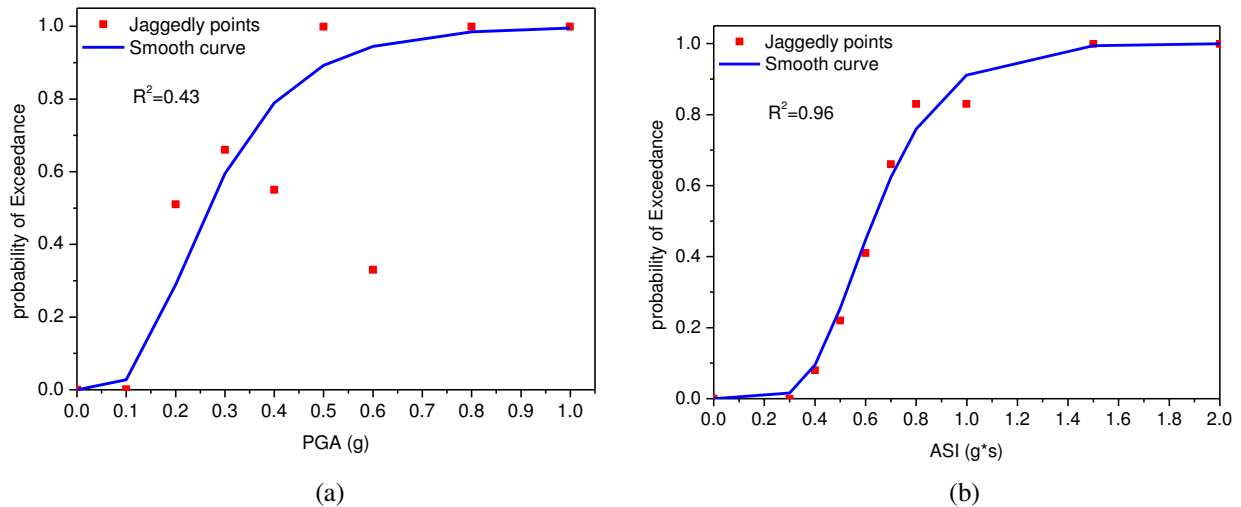


Figure 6- 14: Comparison between jaggedly varying points and smooth fragility curve for CC-I bridge classification due to slight limit state based on (a): PGA and (b):ASI intensity measures

Chapter 7

7 STOCHASTIC COLLOCATION BASED ANALYSIS OF CONCRETE BRIDGES WITH UNCERTAIN PARAMETERS

Recently, different approaches have been developed by researchers to assess the seismic vulnerability of bridges in the deterministic and probabilistic domain by using linear and nonlinear analyses [25-28]. Most of the recent works on seismic vulnerability analyses considered the seismic action as a random variable. However, for reliable results, bridge structure parameters such as bridge geometry, material properties, and boundary conditions, which cause the randomness of the structure's seismic response, should be included in the framework of a stochastic process. On the other hand, most deterministic studies yield a nominal design and the impact of structure uncertainties is ignored. By considering a stochastic method, the impact of uncertainties is included in the analysis and, accordingly, the results are more reliable and trustworthy.

Several researchers demonstrated different methods of evaluating the dynamic response of structures, and MC was considered as one of the most effective methods for determining stochastic response statistics [185-189]. Nevertheless, all of these works on the stochastic response of concrete bridges assumed that the bearing and abutment stiffness are deterministic variables.

The objective of this chapter is to assess the stochastic response of a concrete bridge with uncertain parameters of vertical and shear stiffness for bearings, and longitudinal and transverse stiffness for abutments. First, the uncertainty in the input parameters and the response of the system are presented based on gPC expansion. Then the non-intrusive method as a set of collocation points is selected to calculate the unknown coefficients of the gPC function. Subsequently the results are compared with a sampling method such as the MC simulation, and a non-sampling method such as the collocation method. Although there are only a few number of

collocation points, the results are in a good agreement with the MC simulation, sampling method.

7.1 Polynomial chaos discretization of random parameters

The polynomial chaos expansion was first proposed by Wiener [86] as homogeneous chaos expansion. Later, Cameron and Martin [190] presented a method based on spectral expansion that converges in the least-squares method for any random variables with finite variance. Recently, several researches applied the idea of polynomial chaos expansion extensively [89, 90, 93, 191, 192]. By utilizing the gPC function, uncertainties can be approximated by the sum of polynomials with random variables, and the unknown coefficient parameters can be determined. In this way, Hermite polynomials should be used for Gaussian variables. However, Laguerre polynomials apply for Gamma distributions, whereas Jacobi polynomials are the best function for Beta distributions [94]. Using this approach, the random variable U , which is defined on a probability space, is defined as [191]:

$$U = \sum_{i=0}^N u_i \psi_i(\xi) \quad (7.1)$$

The unknown deterministic coefficients u_i are determined as:

$$u_i = \frac{1}{\psi_i^2} \int_{\Omega} U \psi_i(\xi) p(\xi) d\xi \quad (7.2)$$

where p is the joint PDF of the random vector ξ . Therefore, the expected value and the variance of U are defined as:

$$\mathbb{E}[U] = \sum_{i=1}^{\infty} u_i \mathbb{E}[\psi_0, \psi_i] = u_0 \quad (7.3)$$

$$\sigma_u^2 = \sum_{i=1}^{\infty} \sum_{j=1}^{\infty} u_i u_j \langle \psi_i, \psi_j \rangle = \sum_{i=1}^{\infty} u_i^2 h_i^2 \quad (7.4)$$

Higher statistical moments can be calculated by deriving similar functions [191]. The spectral discretization methods are the key advantage for the efficient stochastic reduced basis representations of uncertainty. In these methods, to reduce the order of a complex system, the deterministic Galerkin projection and collocation methods are applied. Hence, the input random variables are employed as a truncated expansion. Therefore, the smallest number of terms in the function is required because the eigenvalue of the covariance function declines quickly. Also, the system response is considered as gPC expansions by employing the orthogonal basis due to the random variables. Based on the finite element model outputs, the unknown coefficients of the gPC expansions are determined. However, the key advantage of spectral discretization is the combination of the mentioned method with the special discretization, e.g., FEM of the system.

7.2 Spectral stochastic modelling for seismic analyses

A multi-span simply supported bridge with concrete girders located in a highly seismic zone in Iran is considered as a typical structure in this study. The FEM model of the concrete bridge is derived in the matrix form as:

$$\mathbf{M}\ddot{\mathbf{u}} + \mathbf{C}(\mathbf{u})\dot{\mathbf{u}} + \mathbf{K}(\mathbf{u})\mathbf{u} = -\mathbf{M}\ddot{\mathbf{u}}_g \quad (7.5)$$

in which \mathbf{M} , \mathbf{C} , and \mathbf{K} are the mass, damping, and stiffness matrices, respectively, $\ddot{\mathbf{u}}$ is the acceleration vector, \mathbf{u} is the nodal displacement, $\dot{\mathbf{u}}$ is the velocity vector, and $\ddot{\mathbf{u}}_g$ is the vector of support motion. The bridge structures can have geometric or material non-linear behaviour. Hence the geometric nonlinearity is considered by P-delta or large displacement effects associated with the application of external loads on the displaced configuration of a structure. Material nonlinearity refers to the inelastic structural response from the displacements beyond the yield strength and could be characterized by a force–deformation relationship. In nonlinear

dynamic analysis, mass and stiffness proportional damping is commonly assumed and is referred to as Rayleigh damping. The damping matrix proportional to the mass and stiffness matrices is:

$$\mathbf{C}(\mathbf{u}) = \alpha\mathbf{M} + \beta\mathbf{K}(\mathbf{u}) \quad (7.6)$$

where α and β are the mass and stiffness proportional damping coefficients. Since the stiffness matrix is characterized by material and geometric nonlinearity, the damping matrix is nonlinear as well. For the present research, the vertical and shear stiffness, for bearings and the longitudinal and transverse stiffness for abutments, are considered as uncertain parameters. Therefore, the overall stiffness and the damping matrix of the concrete bridge become uncertain. Assuming this, Equation (7.5) becomes:

$$\mathbf{M}\ddot{\mathbf{u}}(t, \xi) + \mathbf{C}(\mathbf{u}, \xi)\dot{\mathbf{u}}(t, \xi) + \mathbf{K}(\mathbf{u}, \xi)\mathbf{u}(t, \xi) = -\mathbf{M}\ddot{\mathbf{u}}_g \quad (7.7)$$

where $\mathbf{u}(t, \xi)$ is the unknown displacement vector, and the random vector ξ is the vector of random variables representing the randomness at uncertain input parameters. In general, the random variable vector ξ correlates with various random spaces, and the created random vector ξ is related to the new random space Ω , which is made up of each individual random space due to each random variable [191]. Here, all random variables belong to various random Hilbert spaces. The uncertain stiffness for bearings and abutments can be represented by truncated generalized polynomial chaos (gPC) expansions as follows:

$$\mathbf{K}(\xi) = \sum_{i_1=0}^{N_1} k_{i_1} \psi_{i_1}(\xi) \quad (7.8)$$

in which k_{i_1} and $\psi_{i_1}(\xi)$ are the deterministic unknown coefficients matrix and the stochastic basis function, respectively. The response of the structure is modelled as a random field and can be represented by the gPC expansion as:

$$\mathbf{U}(t, \boldsymbol{\xi}) = \sum_{i_2=0}^{N_2} u_{i_2}(t) \psi_{i_2}(\boldsymbol{\xi}) \quad (7.9)$$

where $u_{i_2}(t)$ and $\psi_{i_2}(\boldsymbol{\xi})$ are the deterministic unknown coefficient and the stochastic basis function of the structure response, respectively. By substituting these expansions into Equation (7.7), an approximated stochastic equation of the system can be obtained. The stochastic approximation error is defined by Equation (7.10) and represents the approximation error related to the random space discretization and the spatial discretization error in the FEM. To minimize the error, any optimization process could be implemented due to the random space discretization.

$$\begin{aligned} \epsilon(t, \boldsymbol{\xi}) = & \mathbf{M} \sum_{i_2=0}^{N_2} \ddot{u}_{i_2}(t) \psi_{i_2}(\boldsymbol{\xi}) + (\alpha \mathbf{M} + \beta \sum_{i_1=0}^{N_1} k_{i_1} \psi_{i_1}(\boldsymbol{\xi})) \sum_{i_2=0}^{N_2} \dot{u}_{i_2}(t) \psi_{i_2}(\boldsymbol{\xi}) \\ & + \sum_{i_1=0}^{N_1} k_{i_1} \psi_{i_1}(\boldsymbol{\xi}) \sum_{i_2=0}^{N_2} u_{i_2}(t) \psi_{i_2}(\boldsymbol{\xi}) + \mathbf{M} \ddot{\mathbf{u}}_g \end{aligned} \quad (7.10)$$

To optimize the problem and minimize this error, available facilities and information are required. One possibility is to minimize the error between the statistical moment obtained from the theoretical or experimental results and the gPC expansion of the response. Another method is to use the deterministic response of the system as the specific roots of the orthogonal polynomial, and to minimize the least squares errors between this response and the response obtained by the gPC expansion. Commonly, there are two different methods that can be utilized to solve the stochastic finite element model: intrusive and non-intrusive methods. In the intrusive method, access to the data of the FEM or the corresponding equations seems to be necessary. However, in the non-intrusive method, the FEM and governing equations are considered as black-box. The selection of each method depends on the available information. In the case of a linear system with available equations, the first method could be used by applying the Galerkin projection, whereas the nonlinear equation could be solved by the application of the non-intrusive method.

In this study, the following specific methodology for numerical simulation is proposed by considering the non-intrusive method.

7.3 Numerical Study

A multi-span simply supported bridge with concrete girders located in a highly seismic zone in Iran is considered as a typical structure for this study. The bridge has four spans with a total length of 79.2 m, and it is supported on three multi-column bents with three columns per bent. The span lengths are 15.6, 24, 24, and 15.6 m with a bridge width of 11.95 m. The cap beam is a rectangular element of 1.9 by 2.0 m, and the circular columns have a diameter of 1.1 m. The column height of the piers is 6 m. Each column includes 30 vertical bars with a diameter of 22 mm and spiral hoops with a diameter of 12 mm spaced at 250 mm. The gap between deck and abutment is 50 mm, and the gap between decks at each span is 100 mm. The concrete girders are supported on elastomeric-type bearings. The geometric characteristics of the bridge in the longitudinal and transverse directions are indicated in Figure 7- 1. Table 7- 1 displays the statistical analysis of the material properties. Material properties for the confined and unconfined concrete strength parameters are estimated using the approach described by Mander *et al.* [118]. The bilinear steel material model with kinematic hardening is utilized to model the relationship for the steel reinforcement. Three-dimensional time history analysis is conducted using the structural component model. The performance of individual components and their connectivity are relevant variables for the seismic behaviour of highway bridges.

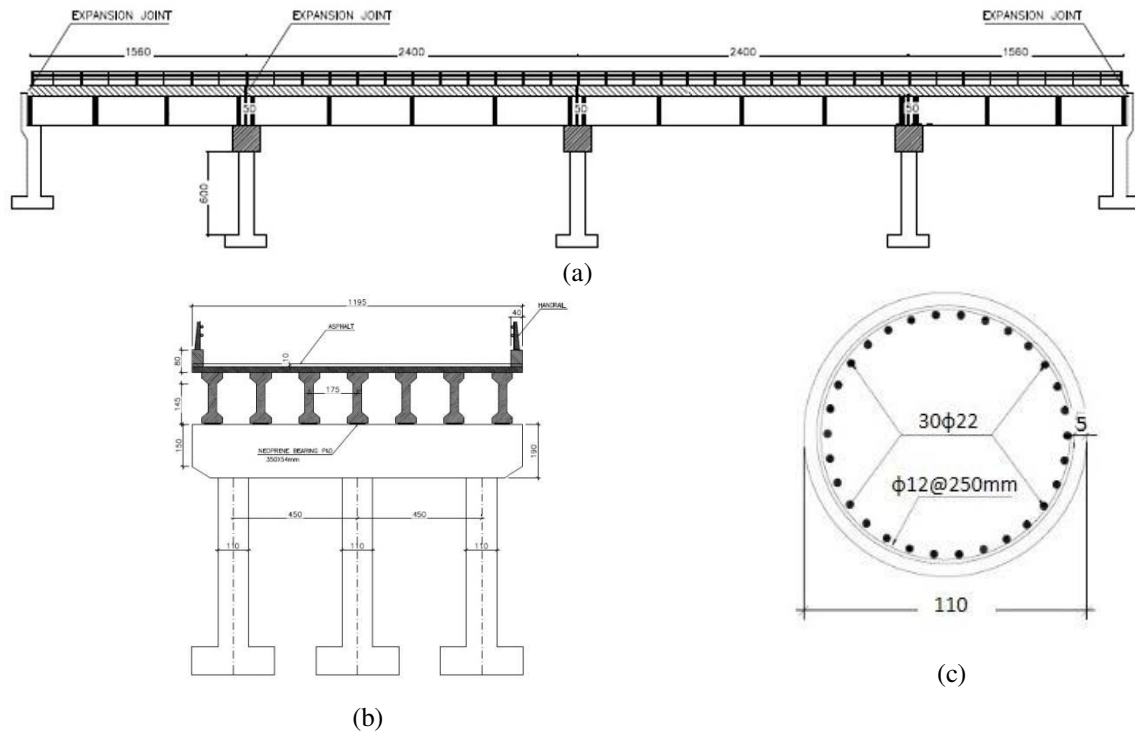


Figure 7- 1: The geometric characteristics of the bridge

Table 7- 1: Material properties of concrete bridge

f'_c (col)	f'_c (cap beam)	f'_c (girder)	f_{ye} (bar)	f_{su} (bar)
MPa	MPa	MPa	MPa	MPa
24	24	28	400	600

The superstructure is composed of cast-in-place reinforced concrete and box concrete slab girders. The bent system and abutments constitute the substructure of the bridge. Elastomeric bearings are located between the substructure and superstructure as an isolation unit. To model the vertical and lateral bearing stiffness, spring elements are selected as proposed by Priestley *et al.* [108] that is described in chapter-3. Frame elements with six degrees of freedom at each node are used to model the columns, bent caps, and girders; the deck and diaphragms are modelled with shell elements. To denote the mass distribution through the element length, the superstructure is divided into a sufficient number of small element segments. Bents, columns, and cap beams are modelled with frame elements with six degrees of freedom at each node. The effects of abutments and backfill soil are modelled as elastic springs by taking into account the Caltrans recommendations [44].

7.3.1 Representation of uncertain parameters

The selection of the uncertain input parameters is the first step in considering the parameter uncertainty in the stochastic formulation. Each parameter defines a standard random variable ζ_i to be considered in the gPC expansion. Previous researchers adopted lognormal or uniform distribution to describe the bearing stiffness and uniform distributions for the abutment stiffness [25, 26, 177]. In this study, it is assumed that the mass matrix is deterministic, and the stiffness parameters in bearings and abutments are random variables. The system random vector ζ_i represents the random variables as:

$$\xi_i = \{\xi_1, \xi_2\}^T \quad (7.11)$$

where ξ_1 and ξ_2 are the random variable vectors that belong to various random Hilbert spaces. Lognormal distributions, LN (6.54, 0.0167) and LN (0.89, 0.27), describe respectively, the vertical and shear bearing stiffnesses K_v and K_s . The uniform distributions, U (8.1, 12.2) and U (18.35, 27.83), define respectively, the longitudinal and transverse abutment stiffnesses K_{al} and K_{at} . These probability functions have mean values of $K_v = 695$, $K_s = 2.53$, $K_{al} = 10.14$, and $K_{at} = 22.94$ (kN/mm). In this study, all the model parameters are considered to be independent and are defined by an individual random variable ζ_i .

7.3.2 Unknown coefficients for uncertain parameters

The bearing stiffness can be presented by an N^{th} order Hermite polynomial whereas the abutment stiffness by a Legendre polynomial.

$$K_v(\xi_1) = \sum_{i=0}^2 K_{v_i} H_i(\xi_1) \quad K_s(\xi_1) = \sum_{i=0}^2 K_{s_i} H_i(\xi_1) \quad (7.12)$$

$$K_{al}(\xi_2) = \sum_{i=0}^1 K_{al_i} L_i(\xi_2) \quad K_{at}(\xi_2) = \sum_{i=0}^1 K_{at_i} L_i(\xi_2) \quad (7.13)$$

where $H_0(\xi_1) = 1, H_1(\xi_1) = \xi_1, H_2(\xi_1) = \xi_1^2 - 1$ and $L_0(\xi_2) = 1, L_1(\xi_2) = \xi_2$

The deterministic gPC coefficients K_{vi}, K_{si}, K_{ali} and K_{ati} are calculated based on Galerkin projection for each uncertain parameter. For example, the function used to calculate the deterministic coefficients in $K_v(\zeta_l)$, by considering the log-normal PDF representing the random variable ξ_1 and using the stochastic Galerkin projection [37], is:

$$K_{v_i} = \frac{1}{\langle H_i^2 \rangle} \int_{-\infty}^{+\infty} e^{(\mu + \sigma \xi_1)} H_l(\xi_1) f(\xi_1) d\xi_1, \quad l = 0, 1, 2 \quad (7.14)$$

where the inner product in the Hilbert space is defined by $\langle H_i^2 \rangle$, $H_l(\xi_1)$ is the test function that multiplies both sides of the first expansion, and $f(\xi_1)$ is the PDF of the random variable ξ_1 . K_{si}, K_{ali} and K_{ati} can be calculated with a similar projection. Table 7- 2 displays the results of the gPC-coefficients up to order 3.

Table 7- 2 shows that the coefficients for K_{vi} and K_{si} decay quickly when increasing i . Due to the optional Legendre orthogonal basis, the coefficients for K_{ali} and K_{ati} converge rapidly. Since the influence of higher order coefficients is small, only three first expansions are considered for the truncated Hermite-gPC, while two first expansions are selected for the Legendre-gPC. Figure 7- 2 presents the constructed PDFs with a good accuracy in relation to the theoretical PDF obtained from equations (7.12) and (7.13).

Table 7- 2: The gPC-coefficients of the uncertain parameters

	$i=0$	$i=1$	$i=2$	$i=3$
K_{vi}	695	11.8	0.1	0.0006
K_{si}	2.53	0.7	0.093	0.0085
K_{ali}	10.15	2.05	0.0	0.0
K_{ati}	23	4.74	0.0	0.0

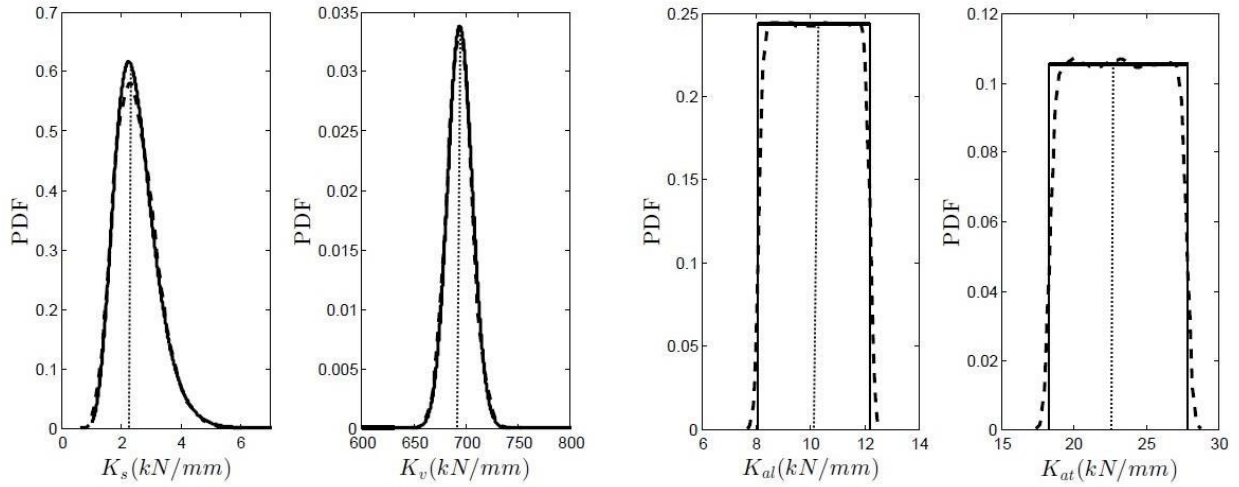


Figure 7- 2: Reconstruction of the PDF of the uncertain parameters K_{si} , K_{vi} , K_{ali} and K_{ati} with the gPC (dashed) compared with the theoretical PDF (bold lines). The dotted vertical lines indicate the mean values

Zero and the roots of the polynomial that is one order higher could be used to approximate the input of the system. Therefore, the roots of the third order of the Hermite polynomial which are 0, -1.73 and 1.73 are employed for ζ_1 . However, for ζ_2 the roots of the second order of the Legendre polynomial which are 0, -0.577 and 0.577 are considered as well. By applying gPC-coefficients (7.12) and (7.13) becomes:

$$K_v(\xi_1) = 695 + 11.8(\xi_1) + 0.1(\xi_1^2 - 1) \quad K_s(\xi_1) = 2.53 + 0.7(\xi_1) + 0.093(\xi_1^2 - 1) \quad (7.15)$$

$$K_{al}(\xi_2) = 10.15 + 2.05(\xi_2) \quad K_{at}(\xi_2) = 23 + 4.74(\xi_2) \quad (7.16)$$

By considering the roots of Hermit and Legendre polynomial in equations (7.15) and (7.16), nine sets of analyses can be obtained which is shown as follows (Table 7- 3):

Table 7- 3: Bearing and abutments stiffness as input parameter for 9 sets of analyses

		K_v	K_s	K_{al}	K_{at}
1 st run	$\zeta_1 = 0, \zeta_2 = 0$	695	2.53	10.15	23:00
2 nd run	$\zeta_1 = 0, \zeta_2 = -0.577$	695	2.53	8.97	20.26
3 rd run	$\zeta_1 = 0, \zeta_2 = 0.577$	695	2.53	11.33	25.73
4 th run	$\zeta_1 = -1.73, \zeta_2 = 0$	674.7	1.50	10.15	23:00
5 th run	$\zeta_1 = -1.73, \zeta_2 = -0.577$	674.7	1.50	8.97	20.26
6 th run	$\zeta_1 = -1.73, \zeta_2 = 0.577$	674.7	1.50	11.33	25.73
7 th run	$\zeta_1 = 1.73, \zeta_2 = 0$	715.6	3.92	10.15	23:00
8 th run	$\zeta_1 = 1.73, \zeta_2 = -0.577$	715.6	3.92	8.97	20.26
9 th run	$\zeta_1 = 1.73, \zeta_2 = 0.577$	715.6	3.92	11.33	25.73

7.3.3 Approximate polynomial model of the response

The output response of the system based on time variation is presented in Equation (7.9). In the polynomial, the number of expansions grows rapidly due to the dimension and the order of expansion. The second order of gPC-expansion is selected to investigate the effects of the parameter uncertainty on the system response. Hence Equation (7.9) can be presented as:

$$\mathbf{U}(t, \xi_1, \xi_2) = \sum_{i_2=0}^{N_2} u_{i_2}(t) \boldsymbol{\psi}_{i_2}(\xi_1, \xi_2) \quad (7.17)$$

in which $u_{i_2}(t)$ is the deterministic coefficient of the gPC expansion at each time step,

$$\boldsymbol{\psi}(\xi_1, \xi_2) = \mathbf{H}(\xi_1) \otimes \mathbf{L}(\xi_2), \text{ and}$$

$$\psi_0(\xi_1, \xi_2) = H_0(\xi_1)L_0(\xi_2) = 1$$

$$\psi_1(\xi_1, \xi_2) = H_1(\xi_1)L_0(\xi_2), H_0(\xi_1)L_1(\xi_2) = \{\xi_1, \xi_2\}$$

$$\psi_2(\xi_1, \xi_2) = H_2(\xi_1)L_0(\xi_2), H_1(\xi_1)L_1(\xi_2), H_0(\xi_1)L_2(\xi_2) = \{\xi_1\xi_2, \xi_1^2 - 1\}$$

$$\mathbf{U}(t, \xi_1, \xi_2) = u_0(t) + u_1(t)\xi_1 + u_2(t)\xi_2 + u_3(t)(\xi_1^2 - 1) + u_4(t)(\xi_1\xi_2)$$

7.3.4 Determination of collocation points for the response

The collocation point is performed with respect to the orthogonal basis $\psi(\xi_1, \xi_2)$ to calculate the unknown coefficients. The bridge response is obtained for the input parameters selected for specific values of the uncertain random variable ξ . Zero and the roots of the polynomial that is one order higher could be used to approximate the response of the system. In this study, the roots of the third order of the Hermite polynomial are employed for (ξ_1) . However, for (ξ_2) the roots of the second order of the Legendre polynomial are considered as well. After determining the unknown coefficients, as presented in Figure 7- 3, it can be seen that the first coefficient (u_0), which represents the mean response, has more influence. Moreover, the effect of higher order coefficients is very small, showing the effectiveness of the gPC expansion with respect to the convergence of the response. After a set of input random variables has been generated, then these points are the input data used to develop a deterministic model of the concrete bridge. The dynamic analysis using a 3-D model of a concrete bridge is performed for each set of input parameters, and the response of the system is achieved. Equation (7.17) is uninitialized to determine the unknown coefficients $u_{i2}(t)$ at each time step. The least squares method can be applied to calculate the simulation equations when the number of unknown coefficients is inferior to the number of collocation points.

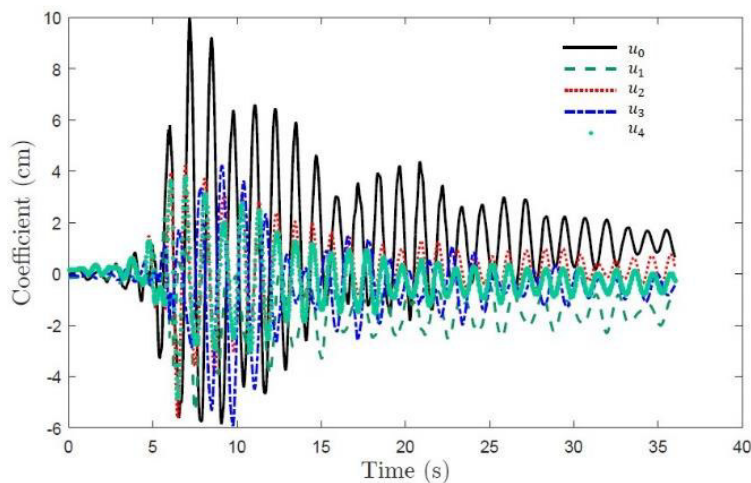


Figure 7- 3: Time history of the gPC expansion coefficients

7.4 Spectral stochastic modelling of seismic analyses

As mentioned earlier, the polynomial coefficients are calculated and are substituted into equation (7.17). Therefore, the bridge response can be calculated considering the uncertain input random variable at each time step. Figure 7- 4 presents the maximum displacement demand of the bridge at different time instants, obtained with gPC expansion for nine sets of input variables and 430 Monte Carlo simulations. For comparison, Figure 7- 4 also shows the maximum displacement for a deterministic analysis with the mean value.

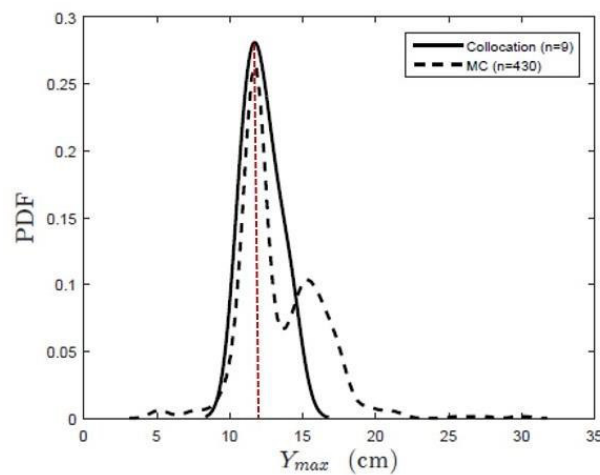


Figure 7- 4: Comparison of probability distributions of the maximum displacement quantities obtained using gPC expansion and the MC simulation

Structural safety is specified more precisely in the probabilistic approach with reliability analysis. It should be considered that the peak values of response quantities from the deterministic analysis are inadequate to accurately define the probability of failure. Note that the probability distributions of the response quantity in terms of the maximum displacement are obtained. The response of the concrete bridge is determined by utilizing equation (7.5) for 430 MC simulations by considering input parameters. Time-history analyses with a 3-D model are performed to determine the peak response in order to plot the probability distribution. The probability distribution of the peak response could be predicted with gPC expansion by considering nine collocation points with sufficient accuracy compared to the MC simulation. Moreover, in gPC expansion there is a simple relationship between the uncertain input parameters with the form of polynomial expansion and the selected response quantity. Therefore,

the use of gPC expansion to work with the uncertainty of input parameters of analyses of the bridge takes less computation time than the MC simulation.

Further, it is evident that the peak response displacement in the deterministic analysis is near to the zone of maximum amplitude in the probability density function. The mean value, μ , and variance, σ^2 , of the response are obtained as follows:

$$\mu = u_0, \quad \sigma^2 = \sum_{i=0}^N u_{i2}(t)^2 h_i^2 \quad (7.18)$$

In gPC expansion, the convergence of the uncertain parameter must be distinguished from the convergence of its statistical moments. Therefore, the accuracy of the expansion based on the mean and the variance is also discussed in this research. Note that the convergence for higher moments is ignored because in most cases the convergence of the approximation fails for higher moments [191]. Figure 7- 5 (a) shows the mean value in gPC expansion has remarkable agreement with that obtained by the MC simulation. It should be noted that the mean value obtained by the MC simulation is equal to the first coefficient response of the stochastic basis function of the bridge. However, the standard deviation does not show good agreement with the results of 430 MC simulations, as shown in Figure 7- 5 (b). The figures show that the error function of the mean value has a faster rate of convergence than the standard deviation function. Clearly, one possibility to solve the error in this plot is to increase the order of gPC expansion.

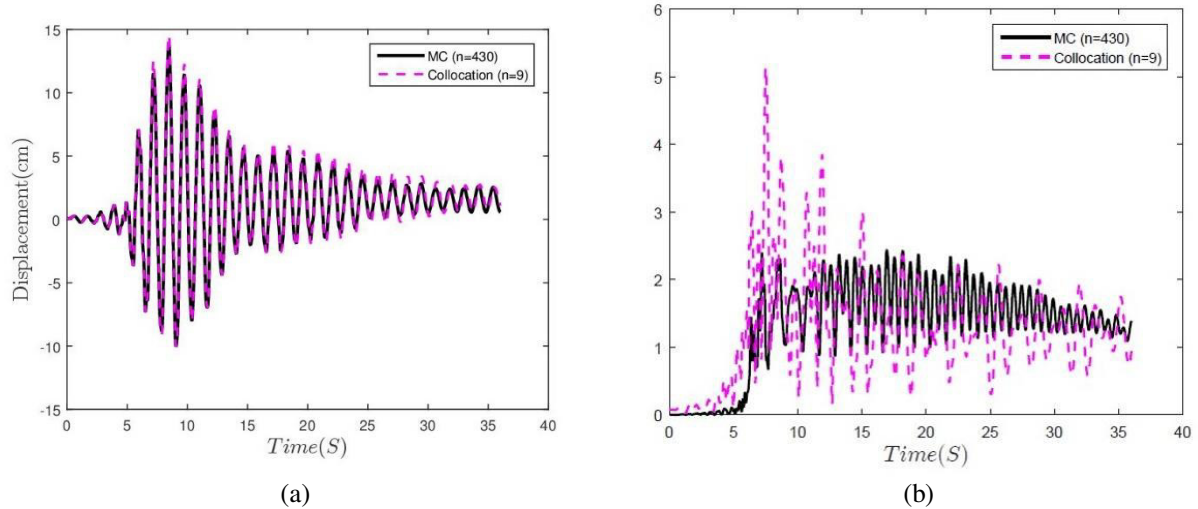


Figure 7- 5: Comparison (a) mean value, and (b) standard deviation value of the displacement quantities obtained using gPC expansion and the MC simulation

A general stochastic FEM has been proposed to assess the response of a typical RC bridge considering stiffness uncertainties in bearings and abutments. The non-sampling based stochastic methods have been used to discretize the random parameters and system responses. Particularly, the gPC expansions were used to approximate the system parameters and responses, respectively. The use of a non-intrusive method determines the system responses at sample collocation points generated from an orthogonal random basis that were used in the gPC expansions. The numerical simulation uses a step-by-step procedure to determine the structural response. A simply supported concrete bridge located in a highly seismic zone is presented as a case study. Time history analyses of a 3-D model are performed to obtain the maximum displacement demands. The mean value and the standard deviation of the response quantity are computed from the gPC expansion and the MC simulation. The efficiency of the method is evident when comparing the gPC expansion and the MC simulation. From the numerical study, it can be concluded that the use of the gPC expansion in dynamic analysis of RC bridges with uncertainties is an efficient methodology and that compared with the MC simulation, the computational time taken is significantly lower when using gPC expansion.

Chapter 8

8 CONCLUSIONS AND FUTURE WORKS

8.1 Summary

This dissertation focuses on the development of analytical fragility curves for the pre-1990 highway bridges in Iran. In this study, 56 representative highway bridges of the most common bridges in Iran constructed in 1980s are selected and classified in terms of span number, skewness, column number per bent and maximum column height. Since the single span bridges are less vulnerable when compared to the multiple-span bridges, single span bridges are neglected and not considered in this research. The parameters considered for grouping the bridge structures are the column height, lap splices for simply support and integral bridges, span length, steel reinforcement yield strength, and concrete compressive strength. Nonlinear time history analyses using 3-D models were conducted for each set of bridge samples subjected to earthquake ground motions with different intensities. The selected family of seismic records originated in strike-slip and reverse fault seismic sources. In this study, two horizontal orthogonal components are considered in the nonlinear time history analyses. On the other hand the intensity measure of each ground motion is determined by calculating the SRSS of the intensity measures of the two horizontal components of the ground motion. Each bridge was subjected to two orthogonal horizontal components of the ground motions. The maximum absolute ductility demand determines the damage limit state of the bridge column for each seismic record. A total of 40 earthquake ground motions from the two seismic sources are employed. Since each bridge is analyzed twice by each ground motion record, into two horizontal orthogonal components, to obtain the maximum response, a total of 80 analyses for each bridge are performed.

We also analyze the influence of the earthquake mechanism on the seismic vulnerability of the bridges, using as a performance parameter the displacement ductility demand of the piers. To calculate the maximum seismic response of the bridge components obtained from the nonlinear analyses, the engineering demand parameters are also considered. Based on this parameter, damage states were established to determine fragility curves that evaluate the probability of

reaching or exceeding the structural capacity as a function of a seismic intensity under each ground motion record, which is represented by the intensity measures of PGA and ASI. A cumulative lognormal probability distribution is utilized to present the probability of exceeding a certain damage limit state in recent studies. Consequently, the fragility curves are generated for each bridge class based on each limit state and intensity measure. For each curve the coefficients of determination are computed due to the investigated intensity measures.

As mentioned before nonlinear time history analysis has some drawbacks such as converge problems, require extensive amount of run time and post processing efforts. Hence, a large number of simulations are required to achieve reasonable results, which is extremely expensive and time consuming, becoming insufferable when complex systems such as bridges are investigated. Therefore, the sampling stochastic methods, such as the MC simulation techniques, are very expensive from a computational point of view, particularly for huge structure models. Therefore instead of the sampling method, non-sampling stochastic method based on polynomial chaos (gPC) expansion is utilized. The uncertain parameters include the vertical and shear stiffness of bearings, and the lateral stiffness of abutments in the longitudinal and transverse directions presented by the truncated gPC expansions. In addition, the system response is presented by gPC expansions with unknown deterministic coefficients. The Galerkin method is employed to calculate a set of deterministic equations. The unknown gPC coefficients of the system response are determined by a non-intrusive solution as a set of collocation points and the results are compared with the Monte Carlo simulations.

8.2 Conclusions

On the basis of the results obtained, the following conclusions can be drawn:

- The main objective of this work is the development of fragility curves for highway bridge classes common in the highway transportation system in Iran. These curves are useful tools to be utilized to assess the seismic vulnerability of the bridges. Also fragility curves can be employed for pre-earthquake preparedness plans and post-earthquake emergency response plans as well as use in seismic risk associated with existing ordinary highway bridges in Iran.

- The results show that the PGA had the lowest coefficient of determination whereas ASI presented the highest one. This indicates that the use of ASI as the intensity measure leads to fragility curves with a better correlation than those developed by using PGA.
- The results show that column height, span length, and lap splices had a significant effect on the seismic vulnerability of the bridges, whereas material properties, particularly concrete compressive strength, did not have a notable impact on the seismic vulnerability of the structures.
- Pre-1990 bridges in all classes due to selected ground motions subjected to reverse fault records were more vulnerable than the ones subjected to the strike-slip fault. Note that the maximum amplitude of the mean S_a response spectrum of reverse fault records is greater than the mean S_a value of strike-slip fault accelerograms. Therefore, bridges subjected to the reverse fault records displayed larger demands than the bridges subjected to reverse fault accelerograms. The fragility curves showed that all bridge classes are more vulnerable to reverse fault records due to selected records.
- The reduction in the longitudinal reinforcement of the HCC-S bridge classification with several column heights increased the expected damage probability.
- The bridges with lap splices clearly exhibited higher seismic vulnerability when compared to the bridge models without lap splices.
- In terms of the span length, the probabilities of reaching the LS1 and LS2 limit states were similar for the two types of superstructures analyzed. However, the bridges with span lengths larger than 30 m and box-girder type superstructures were more vulnerable for the LS3 and LS4 limit states. On the contrary, the bridges presented similar behaviors when subjected to the strike-slip fault records.
- The developed fragility curves can be the basis of loss estimation models as well as the framework of retrofit prioritization strategies for bridges. The study shows that the bridges subjected to earthquakes originated on reverse faults are more vulnerable than the structures excited by strike-slip earthquakes. If the seismic hazard assessment of a region

shows that a family of vulnerable bridges is located in a site where the seismic hazard is mainly governed by one of the seismic sources, the interventions should prioritize the structures affected by the reverse fault movements. However, if the bridges are located in the seismic zones with important contributions of both types of seismic sources, the interventions must be hierarchized by considering the bridges' vulnerability, among other variables. Moreover, high column bridges with lap splices, and bridges with span lengths of more than 30 m should be carefully analyzed as candidates to be retrofitted.

- The results show that the CC-S bridges perform consistently better than the CC-I structures. RC columns of the integral bridges are more vulnerable to seismic damage than simply supported bridges. This is understandable considering that monolithic bridges transfer more demands from deck to columns when the bridge is seismically loaded. Another reason is related to the frequency content of the seismic records and the fundamental period of the CC-I bridges, which ranges from 0.36 to 0.73 s, whereas the periods of the CC-S bridges vary between 0.99 and 1.38 s. It should be mentioned that integral bridges performed consistently better in terms of durability since the lack of joints means that chloride-laden water cannot seep from the surface into the substructure to attack the girders and bearings. Furthermore, maintenance involving the bearings themselves is avoided. Elastomeric glands are susceptible of filling up by trash, clods, and small stones and may fail to function. Furthermore, steel bearings can be exposed to corrosion and elastomers can be split or ruptured due to a sudden and unpredictable movement. Hence integral bridge construction provides better durability performance, and lower operating costs of bridge design.
- The results show that even though a small number of samplings (nine sets) are used in the stochastic method based on gPC expansion, the probability distribution of maximum displacement has a remarkable similarity to that of 430 MC simulations. The peak response displacement in deterministic analysis is also near to the zone of the maximum amplitude of the probability density function. The mean value obtained with gPC expansion has a remarkable agreement with MC simulation and the error function in the mean value converges faster than that of the standard deviation.

8.3 Recommendations for future studies

In the light of the studies accompanied in this dissertation, the following suggestion can be proposed towards future research on the subject:

- To investigate the effect of bridge local site on the seismic response, soil structure interaction could be considered by using reliable modeling.
- To enhance the reliability of the bridge classification, wide nation highway bridges needs to be considered in the inventory data. Basic information such as location and its coordinates, local site, the construction year.
- For calibration purposes, new bridge damage data and new earthquakes could be considered for reliable analytical fragility curves.
- To perform the fragility curves for other type of columns such as wall type or inverted T cap beams could be investigated.
- Bridge irregularities such as curved bridges, or differences in column section or column heights which leads to strength and stiffness variation for multi column bridges.
- To develop fragility curves for other performance parameters such as shear in column, superstructure displacement, effect of pounding between the deck and abutment back wall bearing, could be considered. Also for different limit states curvature ductility or damage index could be considered.
- Other intensity measure such as PGV, PGD, PGA/PGV ratio could be considered to develop the fragility curves.
- For non-sampling stochastic method based on polynomial chaos (gPC) expansion, other type of uncertainties such as ground motion earthquake databases could be considered, fragility curves developed and the result could be compared with fragility curves due to real ground motion and generated earthquake databases.

- As shows in the results the PGA had the lowest coefficient of determination whereas ASI presented the highest one. This indicates that the use of ASI as the intensity measure leads to fragility curves with a better correlation than those developed by using PGA. For future study this comparison can be applied to other bridge classification in terms of column height (SCC-S), different span length, and material properties.

References

1. Basoz, N., Kiremidjian, A.S., *Evaluation of bridge damage data from the Loma Prieta and Northridge CA earthquakes (Report No. MCEER-98-0004)*. 1997: Buffalo, NY: MCEER, University at Buffalo, The State University of New York.
2. Mackie, K., Stojadinovic, B., *Fragility Basis for California Highway Overpass Bridge Seismic Decision Making*. 2005, University of California, Berkeley, CA: PEER Report 2005/02, Pacific Earthquake Engineering Research Center.
3. Liao, D., Yen, P.W. . *A linkage tool for analyzing earthquake traffic impact in micro level based on seismic risk assessment and traffic simulation*. in *International Conference and Exhibition on Computing for Geospatial Research and Application*. 2010. Washington, DC.
4. Padgett, J.E., Dennemann, K., Ghosh, J. , *Risk-based seismic life-cycle costbenefit (LCC-B) analysis for bridge retrofit assessment*. *Structural Safety*, 2010. **32**(3): p. 165-173.
5. Zhou, Y., Banerjee, S., Shinozuka, M. , *Socio-economic effect of seismic retrofit of bridges for highway transportation networks: A pilot study*. *Structure and Infrastructure Engineering*, 2010. **6**(1-2): p. 145-157.
6. Luna, R., Hoffman, D., Lawrence, W.T. , *Estimation of earthquake loss due to bridge damage in the St. Louis Metropolitan Area. I: Direct losses*. *Natural Hazards Review*, 2008. **9**(1): p. 1-11.
7. Bruneau, M., Chang, S. E., Eguchi, R. T., Lee, G. C., O'Rourke, T. D., Reinhorn, A. M., Shinozuka, M., Tierney, K., Wallace, W. A., Winterfeldt, D., *A Framework to Quantitatively Assess and Enhance the Seismic Resilience of Communities*. *Earthquake Spectra*, 2003. **19**(4): p. 733-752.
8. Memari, A.M., Harris, H. G., Hamid, A. A., *seismic evaluation of reinforced concrete piers in low to moderate seismic regions*. *Electronic Journal of Structural Engineering*, 2011. **11**: p. 57-68.
9. Housner, G.W., Thiel, C. C., *The continuing challenge: report on the performance of state bridges in the Northridge earthquake*. *Earthquake Spectra*, 1995. **11**(4): p. 607-636.
10. Tavakoli, B., Ghafory, M., *Seismic hazard assessment of Iran*. *ANNALI DI GEOFISICA*, 1999. **42**(6).
11. Eshghi, S., Razzaghi, M. S, *The behavior of special structures during the Bam earthquake of 26 December 2003*. *JSEE: Special Issue on Bam Earthquake*, 2004: p. 197-207.
12. Mahdi, T., Mahdi, A., *Reconstruction and Retrofitting of Buildings after Recent Earthquakes In Iran*. *Procedia Engineering*, 2013. **54**: p. 127 – 139.
13. Buratti, N., Tavano, M., *Dynamic buckling and seismic fragility of anchored steel tanks by the added mass method*. *Earthquake Engng Struct. Dyn.*, 2014. **43**: p. 1-21.
14. Census, N.P.a.H., *The President's Office Deputy of Strategic Planning and Control*. 2011.
15. Amante, C., Eakins, B. W., *ETOPO1 1 ARC-MINUTE GLOBAL RELIEF MODEL: PROCEDURES, DATA SOURCES AND ANALYSIS* 2009, NATIONAL OCEANIC AND ATMOSPHERIC ADMINISTRATION, National Environmental Satellite, Data, and Information Service, National Geophysical Data Center Marine Geology and Geophysics Division
16. Geological Survey of Iran [GSI], *dataset of Iranian active and quaternary faults*. 2005.
17. Ibrion, M., Parsizadeh, F., PakdamanNaeni, M., Mokhtari, M., Nadim, F., *Handling of dead people after two large earthquake disasters in Iran: Tabas 1978 and Bam 2003 – Survivors'*

- perspectives, beliefs, funerary rituals, resilience and risk*. International Journal of Disaster Risk Reduction, 2015. **11**: p. 60–77.
18. Haeri, S.M., Zolfaghary, M.R., *On the earthquake induced liquefaction in Astaneh, Iran*, in *Earthquake Engineering, Tenth World Conference 1992*, Balkema, Rotterdam.
 19. Rossetto, T., Elnashai, A.S., *Derivation of vulnerability functions for European type RC structures based on observational data*. Engineering Structures, 2003. **25**: p. 1241–1263.
 20. Baker, J.W., *Vector-valued ground motion intensity measures for probabilistic seismic demand analysis*. 2005, in Department of Civil and Environmental Engineering, University of Stanford: Stanford, CA: U.S.
 21. Varum, H., Sousa, R., Delgado, W., Fernandes, C., Costa, A., Jara, J. M. Álvarez, J.J., *Comparative structural response of two steel bridges constructed 100 years apart*. Structure and Infrastructure Engineering, 2011. **7**(11): p. 843-855.
 22. Nicknam, A., Mosleh, A., Hamidi, H., *Seismic Performance Evaluation of Urban Bridge using Static Nonlinear Procedure, Case Study: Hafez Bridge*. Procedia Engineering, 2011. **14**: p. 2350-2357.
 23. Jara, J.M., Galvan ,A., Jara, M. Olmos, B., *Procedure for determining the seismic vulnerability of an irregular isolated bridge*. Structure and Infrastructure Engineering, 2013. **9**(6): p. 516-528.
 24. Jara, J.M., Jara, M., Olmos, B., Villanueva, D., Varum, H. *Expected seismic performance of irregular isolated bridges*. in *Bridge Maintenance, Safety, Management, Resilience and Sustainability, Proceedings of the Sixth International IABMAS Conference*. 2012. Italy.
 25. Nielson, B.G., DesRoches, R., *Analytical seismic fragility curves for typical bridges in the Central and Southeastern United States*. Earthquake Spectra, 2007. **23**(3): p. 615–633.
 26. Tavares, D.H., Padgett, J.E., Paultre, P., *Fragility curves of typical as-built highway bridges in eastern Canada*. Engineering Structures, 2012. **40**: p. 107–118.
 27. Billah, A.H.M.M., Alam, M.S., Bhuiyan, A.R., *Fragility analysis of retrofitted multi-column bridge bent subjected to near fault and far field ground motion*. ASCE Journal of Bridge Engineering, 2013. **18**(10): p. 992–1004.
 28. Pan, Y., Agrawal, A.K., Ghosn, M., Alampalli, S., *Seismic fragility of multi-span simply supported steel highway bridges in New York State. I: Bridge modeling, parametric analysis, and retrofit design*. ASCE Journal of Bridge Engineering, 2010. **15**(5): p. 448–461.
 29. Basoz, N., Kiremidjian, A., King, S.A., Law, K.H., *Statistical analysis of bridge damage data from the 1994 Northridge, Ca, Earthquake*. Earthquake Spectra, 1999. **15**(1): p. 25–54.
 30. Yamazaki, F., Hamada, T., Motoyama, H., Yamauchi, H., *Earthquake damage assessment of expressway bridges in Japan*. 2000, Technical Council on Lifeline Earthquake Engineering (TCLEE). p. 361–370.
 31. Kawashima, K., *Damage of bridges resulting from fault rupture in the 1999 Kocaeli and Duzce, Turkey Earthquakes and the 1999 Chi-Chi, Taiwan Earthquake*. Structural Engineering/Earthquake Engineering, JSCE, 2002. **19**(2): p. 179s–197s.
 32. Hsu, Y.T., Fu, C.C., *Seismic effect on highway bridges in Chi Chi earthquake*. Journal of Performance of Constructed Facilities, 2004. **18**(1): p. 47-53.
 33. Eshghi, S., Ahari, M.N., *Performance of transportation systems in the 2003 Bam, Iran, Earthquake*. Earthquake Spectra, 2005. **21**(S1): p. 455-468.

34. Whitman, R.V., Biggs, J.M., Brennan, J.E., Cornell, A.C., Neufville, R.L., Vanmarcke, E.H., *Seismic design decision analysis*. ASCE Journal of Structural Division, 1975. **101**: p. 1067–1084.
35. ATC, *Seismic vulnerability and impact of disruption of life lines in the Coterminous United States. (Report No. ATC-25)*. 1991: Redwood City, CA: Applied Technology Council.
36. HAZUS, *MH 2.0, Technical Manual*. 1997, Washington, DC: Federal Emergency Management Agency.
37. FEMA, *HAZUS-MH MRI: Technical Manual*. 2003: Federal Emergency Management Agency, Washington DC.
38. Rodrigues, H., Arêde, A., Varum, H., Costa, A. , *Damage evolution in reinforced concrete columns subjected to biaxial loading*. Earthquake Engng Struct. Dyn, 2013. **42**: p. 239-259.
39. Chaulagain, H., Rodrigues, H., Jara, J., Spacone, E., Varum, H. , *Seismic response of current RC buildings in Nepal: A comparative analysis of different design/construction*. Engineering Structures, 2013. **49**: p. 284–294.
40. Varum, H., Pinto, A., Costa, A., Vila Real, P. , *Simplified models for assessment and optimal redesign of irregular planar frames*. Engineering Structures, 2012. **42**: p. 245–257.
41. Mosleh, A., Varum, H., Rodrigues, H., Costa, A. *Response assessment of an existing building designed for earthquake loading*. in *EURODYN 2014*. 2014. Porto, Portugal: Proceedings of the 9th International Conference on Structural Dynamics.
42. Mollaioli, F., Lucchini, A., Cheng, Y., Monti, G. , *Intensity measures for the seismic response prediction of base-isolated buildings*. Bulletin of Earthquake Engineering, 2013. **11**(5): p. 1841-1866.
43. Bojórquez, E., Iervolino, I., Reyes-Salazar, A., Ruiz, S.E. , *Comparing vector-valued intensity measures for fragility analysis of steel frames in case of narrow-band ground motions*. Engineering Structures, 2012. **45**: p. 472-480.
44. Caltrans, *Seismic Design Criteria Version 1.7*. 2013, California Department of Transportation, Sacramento, CA.
45. Kawashima, K., Sakai, J., Takemura, H., *Evaluation of seismic performance of Japanese bridge piers designed with the previous codes*. 1998: Proceedings of the 2nd Japan–UK Workshop on Implications of Recent Earthquakes on Seismic Risk, Technical Report TIT/EERG 98-6. p. 303–316.
46. Kim, S.H., Shinozuka, M., *Development of fragility curves of bridges retrofitted by column jacketing*. Probabilistic Engineering Mechanics, 2004. **19**: p. 105-112.
47. Mander, J., Dhakal, R., Mashiko, N., Solberg, K., *Incremental dynamic analysis applied to seismic financial risk assessment of bridges*. Engineering Structures, 2007. **29**: p. 2662–2672.
48. Zhang, J., Huo, Y. , *Evaluating effectiveness and optimum design of isolation devices for highway bridges using the fragility function method*. Engineering Structures, 2009. **31**: p. 1648-1660.
49. Huang, Q., Gardoni, P., Hurlbaeus, S. , *Probabilistic Seismic Demand Models and Fragility Estimates for Reinforced Concrete Highway Bridges with One Single-Column Bent*. Journal of Engineering Mechanics, 2010. **136**(11): p. 1340-1353.
50. Ellingwood, B.R., Rosowsky, D. V., Li, Y., Kim, J. H, *Fragility assessment of light-frame wood construction subjected to wind and earthquake hazards*. J. Struct. Eng., 2004: p. 1921–1930.
51. Razzaghi, M.S., Eshghi, S., *Probabilistic seismic safety assessment of precode cylindrical oil tanks. J Performance of Constructed Facilities*. (ASCE), 2014.

52. Jeon, J., Shafieezadeh, A., Lee, D., Choi, E., DesRoches, R., *Damage assessment of older highway bridges subjected to three-dimensional ground motions: Characterization of shear–axial force interaction on seismic fragilities*. Engineering Structures, 2015. **87**: p. 47-57.
53. NIBS. Earthquake Loss Methodology, HAZUS 99, Technical manual. Vol. 2. 1999, Washington DC, USA.
54. Applied Technology Council (ATC), *Earthquake Damage Evaluation Data for California, Report No. ATC-13*. 1985, Redwood City, California.
55. Der Kiureghian, A., *Bayesian methods for seismic fragility assessment of lifeline components*. In: Taylor C, VanMarcke E, editors. Acceptable risk processes: lifelines and natural hazards, ASCE council on disaster reduction and technical council on lifeline earthquake engineering monograph, 2002. **21**: p. 61-77.
56. Elnashai, A., Borzi, B., Vlachos, S., *Deformation-based vulnerability functions for RC bridges*. Structural Engineering and Mechanics, 2004. **17**: p. 215–244.
57. Shinozuka, M., Feng, M.Q., Kim, H.K., Kim, S.H., *Nonlinear static procedure for fragility curve development*. ASCE Journal of Engineering Mechanics, 2000b. **126**: p. 1287–1296.
58. Shinozuka, M., Feng, M.Q., Kim, H., Uzawa, T., Ueda, T., *Statistical analysis of fragility curves, (Report No. MCEER-03-0002)*. 2001: MCEER, University at Buffalo. Buffalo, NY: The State University of New York.
59. Yazgan, U., *Empirical seismic fragility assessment with explicit modeling of spatial ground motion variability*. Engineering Structures, 2015. **100**(1): p. 479–489.
60. Yamazaki, F., Onishi, J., Tayama, S., *Earthquake Damage Assessment of Expressway Structure in Japan*. Asian-Pacific Symposium on Structural Reliability and its Applications, 1999: p. 1-10.
61. Hwang, H., Jernigan, J.B., Lin, Y.W., *Evaluation of seismic damage to Memphis bridges and highway systems*. ASCE Journal of Bridge Engineering, 2000. **5**: p. 322–330.
62. Banerjee, S., Shinozuka, M., *Nonlinear static procedure for seismic vulnerability assessment of bridges*. Computer-Aided Civil and Infrastructure, 2007. **22**: p. 293-305.
63. Dutta, A., Mander, J. B., *Seismic fragility analysis of highway bridges*. 1998, Proc. Of INCEDE MCEER Ctr-Ctr Workshop on Earthquake Engineering Frontiers in Transportation Systems: Tokyo, Japan.
64. Loh, C.H., Liao, W. I., Chai, J. F., *Effect of near-fault earthquake on bridges: lessons learned from Chi-Chi earthquake*. Earthquake Engineering and Engineering Vibration, 2002. **1**(1): p. 86-93.
65. Monti, G., Nistico, N., *Simple probability-based assessment of bridges under scenario earthquakes*. Journal of Bridge Engineering, 2002. **7**: p. 104-114.
66. Siqueiraa, G., Sandab, A., Paultreb, P., Padgett, J., *Fragility curves for isolated bridges in eastern Canada using experimental results*. Engineering Structures, 2014. **74**(1): p. 311-324.
67. Hwang, H., Liu, J., Chiu, Y., *Seismic fragility analysis of highway bridges*. 2001, Center for Earthquake Research and Information The University of Memphis, MAEC RR-4 Project.
68. Karim, K.R., Yamazaki, F., *A simplified method of constructing fragility curves for highway bridges*. Earthquake Engineering and Structural Dynamics, 2003. **32**: p. 1603–1626.
69. Choi, E., DesRoches, R., Nielson, B., *Seismic fragility of typical bridges in moderate seismic zones*. Engineering Structures, 2004. **26**(2): p. 187-199.

70. Nateghi, F., Shahsavari, V.L., *Development of Fragility and Reliability Curves for Seismic Evaluation of a Major Prestressed Concrete Bridge*, in *13th World Conference on Earthquake Engineering*. 2004: Vancouver, B.C. Canada.
71. Mosleh, A., Razzaghi, M., Jara, J., Varum, H., *Seismic Fragility Analysis of Typical Pre-1990 Bridges due to Near and Far-Field Ground Motions*. *International Journal of Advanced Structural Engineering and Mechanics*, 2016(DOI:10.1007/s40091-016-0108-y).
72. Choine, M., Connor, A., Padgett, J., *Comparison between the Seismic Performance of Integral and Jointed Concrete Bridges*. *Journal of Earthquake Engineering*, 2015. **19**: p. 172-191.
73. Yang, C., Werner, S., DesRoches, R., *Seismic fragility analysis of skewed bridges in the central southeastern United States*. *Engineering Structures*, 2015. **83**(15): p. 116–128.
74. FHWA, *Seismic Retrofitting Manual for Highway Bridges 1995*, Publication No.FHWA-RD-94-052, Office of Engineering and Highway Operations R&D, Federal Highway Administration,McLean, VA.
75. AASHTO, *Guide Specifications for LRFD Seismic Bridge Design*. 1996, Washington D.C.: American Association of State Highway and Transportation Officials 16th Ed. with 2001 Interims.
76. ATC, *Seismic evaluation and retrofit of concrete buildings (Report No. ATC-40)*. 1996: Redwood City, CA: Applied Technology Council.
77. Mander, J.B., *Fragility curve development for assessing the seismic vulnerability of highway bridges*. 1999: University at Buffalo, State University of New York.
78. Saha, S.K., Sepahvand, K., Matsagar, V.A., Jain, A.K., Marburg, S., *Stochastic analysis of base-isolated liquid storage tanks with uncertain isolator parameters under random excitation*. *Engineering Structures*, 2013. **57**: p. 465-474.
79. Jacob, C., Sepahvand, K., Matsagar, V.A., Marburg, S., *Stochastic seismic response of base-isolated buildings*. *International Journal of Applied Mechanics*, 2013. **5**(1): p. 1-21.
80. Carrera, J.C., *Earthquake Engineering and Engineering Seismology*, in *Istituto Universitario di Studi Superiori*. 2008, Università degli Studi di Pavia.
81. Feng, Q.H., Yuan, W.C., Chang, C.C., *Compound stochastic seismic vulnerability analysis and seismic risk evaluation for super large cable-stayed bridge*. *Earthquake Resistant Structures Design Assessment and Rehabilitation*, 2012.
82. Abu-Dabous, S., Alkass, S. , *A stochastic method for condition rating of concrete bridges*, in *Construction Research Congress*. 2010. p. 558-567.
83. Gladysz, M., niady, P., *Spectral density of the bridge beam response with uncertain parameters under a random train of moving forces*. *Archives of Civil and Mechanical Engineering*, 2009. **9**(3): p. 31-47.
84. Sgambi, L., Garavaglia, E., Basso, N., Bontempi, F. , *Monte carlo simulation for seismic analysis of a long span suspension bridge*. *Engineering Structures*, 2014. **78**: p. 100-111.
85. Sepahvand, K., Marburg, S., Hardtke, H.K. , *Numerical solution of one-dimensional wave equation with stochastic parameters using generalized polynomial chaos expansion*. *Journal of Computational Acoustics*, 2007. **15**: p. 579-593.
86. Wiener, N., *The homogeneous chaos*. *American Journal of Mathematics*, 1938. **60**: p. 897-936.
87. Ghanem, R.G., Spanos, P.D. , *Stochastic finite elements: A spectral approach*. 1991, New York, USA: Springer-Verlag.

88. Ghanem, R., Spanos, P.D. , *Polynomial chaos in stochastic finite elements*. Journal of Applied Mechanics, 1990. **57**(1): p. 197-202.
89. Kersaudy, P., Mostarshedi, S., Sudret, B., Picon, O., Wiart, J. , *Stochastic analysis of scattered field by building facades using polynomial chaos*. IEEE Transactions on Antennas and Propagation, 2014. **62**(16).
90. Sudret, B., Mai, C.V. , *Computing derivative-based global sensitivity measures using polynomial chaos expansions*. Reliability Engineering and System Safety, 2015. **134**: p. 241-250.
91. Schueller, G.I.A., *A state-of-the-art report on computational stochastic mechanics*. Probabilistic Engineering Mechanics, 1997. **12**(4): p. 197-321.
92. Sepahvand, K., Scheffer, M., Marburg, S. , *Uncertainty quantification in natural frequencies and radiated acoustic power of composite plates: Analytical and experimental investigation*. Applied Acoustics, 2015. **87**: p. 23-29.
93. Sepahvand, K., Marburg, S., Hardtke, H.K. , *Stochastic free vibration of orthotropic plates using generalized polynomial chaos expansion*. Journal of Sound and Vibration, 2012. **331**(1): p. 167-179.
94. Xiu, D., Karniadakis, G., *The wieneraskey polynomial chaos for stochastic differential equations*. SIAM J Sci Comput, 2002. **24**(2): p. 619-644.
95. Xiu, D., Karniadakis, G., *Modeling uncertainty in flow simulations via generalized polynomial chaos*. Journal Comput Phys, 2003. **187**(1): p. 167-2003.
96. 2800, S.N., *Iranian Code for Seismic Resistant Design of Buildings, Second Edition*. 1999, Iran: Building and Housing Research Centre.
97. *Iranian Code of Practice for Seismic Resistant Design of Buildings, Standard No. 2800, Third Edition*. 2007, Iran: Building and Housing Research Centre.
98. *Publication No. 389.: The Code of Practice for the Analysis and Design of Concrete Bridges, Appendix to Iranian Concrete Code of Practice for Analysis and Design of Building Structures*. 2009, Iran: Office of Deputy for Strategic Supervision Bureau of Technical Execution System.
99. (FHWA), *Federal Highway Administration Recording and Coding Guide for the Structure Inventory and Appraisal of the Nation's Bridges*, Rep. No. FHWA-ED-89-044, Ofc. Of Engrg., Bridge Division. 1988, Washington, D.C.
100. Nielson, B.G., *Analytical Fragility Curves for Highway Bridges in Moderate Seismic Zones*, in *Georgia Institute of Technology*. 2005: Atlanta, Georgia.
101. Avsar, O., Yakut, A., Caner, A., *Analytical Fragility Curves for Ordinary Highway Bridges in Turkey*. Earthquake Spectra, 2011. **27**(4): p. 971-996.
102. The Highways Agency, *Design Manual for Roads and Bridges*, ed. T.H. Agency. Vol. 1, Section 3. 2001, The Highways Agency, The Stationery Office, Norwich.
103. Denton, S., Tsionis, G., *The evolution of Eurocodes for bridge design 2012*, European Commission, Joint Research Centre, Institute for the Protection and Security of the Citizen, Luxembourg.
104. Mistry, V.C., *Integral Abutment and Jointless Bridges* in *THE 2005 – FHWA CONFERENCE Integral Abutment and Jointless Bridges (IAJB)*. 2005: Baltimore, Maryland.
105. Paraschos, A., Amde, A. M., *A survey on the status of use, problems and costs associated with integral abutment bridges*. 2011, Available: <http://www.betterroads.com/integral-abutmentbridges>.

106. Frosch, R.J., Kreger, M.E., Talbott, A.M., *Earthquake resistance of integral abutment bridges*. 2009, Conducted in Cooperation with the Indiana Department of Transportation and the Federal Highway Administration
107. Shinozuka, M., Feng, M.Q., Lee, J., Naganuma, T., *Statistical analysis of fragility curves*. Journal of Engineering Mechanics, 2000. **126**(12): p. 1224-1231.
108. Priestley, M.J.N., Seible, F., Calvi, G. M., *Seismic design and retrofitting of bridges*. 1996, New York: John Wiley & Sons.
109. ATC, *Improved Seismic Design Criteria for California Bridges: Provisional Recommendations*. 1996: Redwood City, California.
110. DesRoches, R., Choi, E., Leon, R.T., Dyke, S.J., Aschheim, M., *Seismic Response of Multiple Span Steel Bridges in Central and Southeastern United States I: As Built*. ASCE Journal of Bridge Engineering, 2004. **9**: p. 464-473.
111. Choi, E., *Seismic Analysis and Retrofit of Mid-America Bridges*. 2002: PhD Thesis, Georgia Institute of Technology.
112. Cheng, F.Y., Lou, K.Y., Sheng, L.H., *Collapse Studies of Freeway Bridges During the Northridge Earthquake*, in *6th US National Conference on Earthquake Engineering*. 1998: Seattle, WA. EERI.
113. Wissawapaisal, C., Aschheim, M., *Modeling the Transverse Response of Short Bridges Subjected to Earthquakes*. 2000: Mid-America Earthquake Center, CD Release 00-05.
114. Aviram, A., Mackie, K.R., Stojadinovic, B., *Guidelines for Nonlinear Analysis of Bridge Structures in California*. 2008, College of Engineering University of California, Berkeley: PEER Report 2008/03 Pacific Earthquake Engineering Research Center.
115. Wilson, E.L., *Three Dimensional Static and Dynamic Analysis of Structures*, in *Computers and Structures*. 2002: Berkeley, Calif.
116. Bazant, Z.P., Bhat, P.D., *Endochronic theory of inelasticity and failure of concrete*. J. Engrg. Mech. Div, 1976. **102**: p. 701-722.
117. Kent, D.C., Park, R., *Flexural Members with Confined Concrete*. Journal of the Structural Division, 1971. **97**: p. 1969-1990.
118. Mander, J.B., Priestley, M. J. N., and Park, R., *Observed stress strain behavior of confined concrete*. J. Struct. Eng., 1988. **114**(8): p. 1827-1849.
119. sheikh, S., Uzumeri, M., *Strength and ductility of confined concrete columns*. Proceeding, ASCE, 1980. **106**: p. 1079-1102.
120. Imbsen, R., A., *Peoposed AASHTO Guide Specifications for LRFD Seismic Bridge Design*. 2007, Imbsen Consulting, Sacramento, CA.
121. Avsar, O., *FRAGILITY BASED SEISMIC VULNERABILITY ASSESSMENT OF ORDINARY HIGHWAY BRIDGES IN TURKEY*, in *Civil Engineering Department*. 2009, MIDDLE EAST TECHNICAL UNIVERSITY.
122. Avsar, O., Caner, A., Yakut, A., *Effect of Cap Beam to Column Inertia Ratio on Transverse Seismic Response of Multi Column Bridge Bents*, in *14th World Conference on Earthquake Engineering*. 2008: Beijing, China.
123. Computers and Structures Inc. CSI. SAP2000 V-14, *Integrated finite element analysis and design of structures basic analysis reference manual*. 2009: Berkeley (CA, USA).

124. Priestley, M.J.N., Park, R., *Strength and ductility of concrete bridge columns under seismic loading*. ACI Structural Journal, 1987. **84**(1): p. 61–76.
125. Caltrans, *Bridge Design Specifications-Seismic Design Criteria, Ver. 1.3*. 2004, California Department of Transportation, Sacramento, California.
126. Ventura, C.E., Finn, W.D.L., Felber, A.J. , *Ambient Vibration Study of the Painter Street Overpass, in 7th Canadian Conference on Earthquake Engineering*. 1995: Montreal. p. 787-794.
127. Wilson, J.C., Tan, B.S., *Bridge Abutments: Formulation of Simple Model for Earthquake Response Analysis*. Journal of Engineering Mechanics, ASCE, 1990. **116**(8): p. 1828-1837.
128. Goel, R.K., Chopra, A.K. , *Evaluation of Bridge Abutment Capacity and Stiffness during Earthquakes*. Earthquake Spectra, 1997. **13**(1): p. 1-23.
129. Lam, I., and Martin, G.R., *Seismic design of highway bridge foundations*. U.S. Dept. of Transportation Federal Highway Administration, Research, Development, and Technology., 1986.
130. Shamsabadi, A., *Three-Dimensional Nonlinear Seismic Soil-Abutment-Foundation Structure Interaction Analysis of Skewed Bridges, in Department of Civil and Environmental Engineering*. 2007, University of Southern California: Los Angeles, CA.
131. Maroney, B.H., *Large Scale Abutment Tests to Determine Stiffness and Ultimate Strength Under Seismic Loading*. 1995, University of California: Davis, CA.
132. Stewart, P.S., Taciroglu, E., Wallace, J.W., Ahlberg, E.R., Lemnitzer, A., Rha, C., and Tehrani, P.K. , *Full Scale Cyclic Testing of Foundation Support Systems for Highway Bridges, Part II: Abutment Backwalls*. 2007, Department of Civil and Environmental Engineering, University of California: Los Angeles, CA.
133. Shamsabadi, A., Rollins, K.M., and Kapuskar, M., *Nonlinear Soil-Abutment-Bridge Structure Interaction for Seismic Performance-based Design*. J. Geotech. & Geoenviron. Eng., ASCE, 2007. **133**(6): p. 707-720.
134. Kwon, O.S., Elnashai, A.S., *The Effect of Material and Ground Motion Uncertainty on the Seismic Vulnerability Curves of RC Structure*. Engineering Structures, 2006. **28**: p. 289–303.
135. Padgett, J.E., Nielson, B. G. and DesRoches, R. , *Selection of optimal intensity measures in probabilistic seismic demand models of highway bridge portfolios*. EARTHQUAKE ENGINEERING AND STRUCTURAL DYNAMICS, 2008. **37**: p. 711–725.
136. Bradley, B.A., Burks, L.S., Baker, J.W., *Ground motion selection for simulation-based seismic hazard and structural reliability assessment*. Earthq Eng Struct Dyn., 2015. **44**(13): p. 2321-2340.
137. Zelaschi, C., Monteiro, R., Pinho, R. , *Improved fragility functions for RC bridge populations, in 5th ECCOMAS Thematic Conference on Computational Methods in Structural Dynamics and Earthquake Engineering (COMPdyn 2015)*. 2015: Crete Island, Greece.
138. Dhakal, R.P., Mander, J.B. and Mashiko, N., *Identification of Critical Ground Motions for Seismic Performance Assessment of Structures*. Earthquake Engineering and Structural Dynamics, 2006. **35**: p. 989-1008.
139. Kramer, S.L., *Geotechnical Earthquake Engineering*. 1996: Prentice-Hall, Englewood Cliffs, N.J.
140. Von Thun, J.L., Rochim, L.H., Scott, G.A. and Wilson, J.A., *Earthquake Ground Motions for Design and Analysis of Dams, Earthquake Engineering and Soil Dynamics II Recent Advances in Ground-Motion Evaluation*. Geotechnical Special Publication, 1998. **20**: p. 463-481.

141. Yakut, A., Yilmaz, H., *Correlation of Deformation Demands with Ground Motion Intensity*. ASCE Journal of Structural Engineering, 2008. **134**(12): p. 1818-1828.
142. Baker, J., Cornell, C.A., *Which Spectral Acceleration Are You Using?* Earthquake Spectra, 2006. **22**(2): p. 293–312.
143. Berberian, M., *Natural Hazard and the First Earthquake Catalogue of Iran, Historical Hazards in Iran Prior to 1900*, ed. IIEES. Vol. 1. 1994. 603.
144. Padgett, J.E., DesRoches, R., *Sensitivity of Seismic Response and Fragility to Parameter Uncertainty*. ASCE Journal of Structural Engineering, 2007. **133**(12): p. 1710-1718.
145. Priestley, M.J.N., Calvi, G.M., Kowalsky, M.J. , *Displacement-Based Seismic Design of Structures*. 2007, IUSS Press, Pavia, Italy.
146. Bommer, J.J., Acevedo, A.B., *The Use of Real Earthquake Accelerograms as Input to Dynamic Analysis*. Journal of Earthquake Engineering, 2004. **8**(1): p. 43-92.
147. Naeim, F., Lew, M., *On the use of Design Spectrum Compatible Time Histories*. Earthquake Spectra, 1995. **11**(1): p. 111-127.
148. FEMA 368, *NEHRP Recommended Provisions for Seismic Regulations for New Buildings & Other Structures*, 2000, Washington, DC.
149. Mander, J.B., Basoz, N., *Seismic Fragility Curve Theory for Highway Bridges*, in *5th US Conference on Lifeline Earthquake Engineering*. 1999: Seattle, WA, USA.
150. Kowalsky, M.J., 2000, *Deformation Limit States for Circular Reinforced Concrete Bridge Columns*. ASCE Journal of Structural Engineering, 2000. **126**(8): p. 869-878.
151. Saxena, V., Deodatis, G. and Shinozuka, G., Feng, M. , *Development of Fragility Curves for Multi-Span Reinforced Concrete Bridges*. 2000, Princeton University, Princeton.
152. Hose, Y., Silva, P., Seible, F., *Development of a Performance Evaluation Database for Concrete Bridge Components and Systems under Simulated Seismic Loads*. Earthquake Spectra, 2000. **16**(2): p. 413–442.
153. Kawashima, K., *Seismic design and retrofit of bridges*, in *Proceedings of 12wcee*. 2000: Newzealand.
154. Karim, K.R., Yamazaki, F. , *Effect of earthquake ground motions on fragility curves of highway bridge piers based on numerical simulation*. Earthquake Engineering and Structural Dynamics, 2001. **30**(12): p. 1839-1856.
155. Liao, W.I., Loh, C.H., *Preliminary Study on the Fragility Curves for Highway Bridges in Taiwan*. Journal of the Chinese Institute of Engineers, 2004. **27**(3): p. 367-375.
156. Johnson, N., Saiidi, M., Sanders, D., *LARGE-SCALE EXPERIMENTAL AND ANALYTICAL SEISMIC STUDIES OF A TWO-SPAN REINFORCED CONCRETE BRIDGE SYSTEM*. 2006, Center for Civil Engineering Earthquake Research, Department of Civil and Environmental Engineering/ 258 University of Nevada Reno, Nevada 89557.
157. Kappos, A., Moschonas, I., Paraskeva, T., Sextos, A., *A METHODOLOGY FOR DERIVATION OF SEISMIC FRAGILITY CURVES FOR BRIDGES WITH THE AID OF ADVANCED ANALYSIS TOOLS*, in *First European Conference on Earthquake Engineering and Seismology, (a joint event of the 13th ECEE & 30th General Assembly of the ESC)* 2006: Geneva, Switzerland.
158. Lee, S., Kim, T., Kang, S. , *Development of Fragility Curves for Bridges in Korea*. KSCE Journal of Civil Engineering, 2007. **11**(3): p. 165-174.

159. Marano, G., Greco, R., Mezzina, M. , *Stochastic Approach for Analytical Fragility Curves*. KSCE Journal of Civil Engineering, 2008. **12**(5): p. 305-3012.
160. Zhang, Y., Conte, J. P., Yang, Z., Elgamal, A., Bielak, J., Acero, G., *Two-dimensional nonlinear earthquake response analysis of a bridge-foundation-ground system*. Earthquake Spectra, 2008. **24**(2): p. 343-386.
161. Banerjee, S., Shinozuka, M. , *Experimental verification of bridge seismic damage states quantified by calibrating analytical models with empirical field data*. Earthquake Engineering & Engineering Vibration, 2008. **7**: p. 383-393.
162. Kalantari, A., Karimi, K. , *Seismic vulnerability of highway bridges using fragility curves*. Research Bulletin of Seismology and Earthquake Engineering, 2009.
163. Azevedo, J., Guerreiro, L., Bento, R., Lopes, M., Proença, J., *Seismic vulnerability of lifelines in the greater Lisbon area*. Bull Earthquake Engineering, 2010. **8**: p. 157-180.
164. Ramanathan, K., DesRoches, R., Padgett, J.E. , *Analytical fragility curves for multispan continuous steel girder bridges in moderate seismic zones*. Transportation Research Record, 2010. **2202**(173-182).
165. Roy, N., Paultre, P., Proulx, J. , *Performance-based seismic retrofit of a bridge bent: Design and experimental validation*. Canadian Journal of Civil Engineering, 2010. **37**: p. 1-13.
166. Kibboua, A., Naili, M., Benouar, D., Kehila, F., *Analytical fragility curves for typical Algerian reinforced concrete bridge piers*. Structural Engineering and Mechanics, 2011. **39**(3): p. 411-425.
167. *Publication No. 511, The Guide Manual for the Seismic Vulnerability Assessment and Retrofit of Bridges*. 2011, Office of Deputy for Strategic Supervision Bureau of Technical Execution System, Iran.
168. Shirazian, S., Ghayamghamian, M.R., Nouri, G.R. , *Development of Fragility Curves for Two-Span Simply Supported Concrete Bridge in Near-Fault Area*. World Academy of Science, Engineering and Technology, 2011. **51**: p. 571-575.
169. Marano, G., Greco, R., Morrone, E. , *Analytical evaluation of essential facilities fragility curves by using a stochastic Approach*. Engineering Structures, 2011. **33**(1): p. 191–201.
170. Donatello, C., Giuseppe, P., Salvatore, S. , *A performance-based adaptive methodology for the seismic evaluation of multi-span simply supported deck bridges*. Bull Earthquake Engineering, 2011. **9**: p. 1463-1498.
171. El-Arab, I., *Analytical methodology of Seismic Fragility Curve for Reinforcement Concrete Pier Bridges in Egypt*. International Journal of Engineering and Advanced Technology (IJEAT), 2012. **2**(2).
172. Banerjee, S., Chi, C., *State-dependent fragility curves of bridges based on vibration measurements*. Probabilistic EngineeringMechanics, 2013. **33**: p. 116–125.
173. Avsar, O., Yakut, A., *Seismic vulnerability assessment criteria for RC ordinary highway bridges in Turkey*. Structural Engineering and Mechanics, 2012. **43**(1): p. 127-145.
174. Turkish Earthquake Code, *Specification for Structures to be Built in Disaster Areas*. 2007, Ministry of Public Works and Settlement Government of Republic of Turkey.
175. Mosleh, A., Varum, H., Jara, j., *A methodology for determining the seismic vulnerability of old concrete highway bridges by using fragility curves*. Journal of the Structural Engineering and Geotechnics, 2015. **5**(1): p. 1-7.

176. Zhu, L., Elwood, K.J., Haukaas, T., *Classification and Seismic Safety Evaluation of Existing Reinforced Concrete Columns*. Journal of Structural Engineering and Mechanics, 2007. **133**(9).
177. Nielson, B.G., DesRoches, R., *Seismic fragility methodology for highway bridges using a component level approach*. Earthquake Engineering and Structural Dynamics, 2007b. **36**: p. 823-839.
178. Ramanathana, K., Padgett, J., DesRoches, R., *Temporal evolution of seismic fragility curves for concrete box-girder bridges in California*. Engineering Structures, 2015. **97**(15): p. 29-46.
179. Jara, M., Jara, J.M. Olmos, B.A., *Seismic energy dissipation and local concentration of damage in bridge bents*. Structure and Infrastructure Engineering, 2013. **9**(8): p. 794-805.
180. Astaneh-Asl, A., *Lessons of the 1990 Manjil-Iran Earthquake*, in Tenth world conference 1994, Balkema, Rotterdam.
181. Manafpour, A.R., *Bam earthquake, Iran: lessons on the seismic behavior of building structures*, in *The 14th World Conference on Earthquake Engineering* 2008: Beijing, China.
182. Zahrai, S.M., Heidarzadeh, M., *DESTRUCTIVE EFFECTS OF THE 2003 BAM EARTHQUAKE ON STRUCTURES*. ASIAN JOURNAL OF CIVIL ENGINEERING (BUILDING AND HOUSING), 2007. **8**(3): p. 329-342.
183. AASHTO, *AASHTO LRFD Bridge Design Specifications* 2012, American Association of State Highway and Transportation Officials. Washington, D.C.
184. FHWA, *Seismic Retrofitting Manual for Highway Structures* 2006, Federal Highway Administration: Report No. FHWA-HRT-06-032.
185. Tubaldi, E., Barbato, M., Dall'Asta, A. , *Influence of model parameter uncertainty on seismic transverse response and vulnerability of steel-concrete composite bridges with dual load path*. Journal of Structural Engineering Structures, 2012. **138**(3): p. 363-374.
186. Manohar, C.S., Ibrahim, R.A., *Progress in structural dynamics with stochastic parameter variations*. Applied Mechanics Reviews, 1999. **52**(5): p. 177-197.
187. Li, J., Chen, J.B. , *Probability density evolution method for dynamic response analysis of structures with uncertain parameters*. Computational Mechanics, 2004. **34**(5): p. 400-409.
188. Schenk, C.A., Schueller, G.I. , *Uncertainty Assessment of Large Finite Element Systems*. Vol. 24. 2005: Springer Berlin Heidelberg.
189. Salcher, P., Pradlwarter, H., Adam, C. . *Reliability of high-speed railway bridges with respect to uncertain characteristics*. in *Proceedings of the 9th International Conference on Structural Dynamics, EURO-DYN 2014*. 2014.
190. Cameron, R.H., Martin, W.T. , *The orthogonal development of nonlinear functionals in series of fourier-hermite functionals*. Annals of Mathematics, 1947. **48**(2): p. 385-392.
191. Sepahvand, K., Marburg, S., Hardtke, H.J. , *Uncertainty quantification in stochastic system using polynomial chaos expansion*. Journal of Applied Mechanics, 2010. **2**(2): p. 305-353.
192. Sepahvand, K., Marburg, S. , *Stochastic dynamic analysis of structures with spatially uncertain material parameters*. International Journal of Structural Stability and Dynamics, 2014. **14**(8).